EXPLORING CATALYSIS IN THE MANDELATE RACEMASE SUBGROUP OF THE ENOLASE SUPERFAMILY: SUBTLE DIFFERENCES IN THE CATALYTIC MACHINERY

by

Christopher M. Fetter

Submitted in partial fulfilment of the requirements
for the degree of Master of Science

at

Dalhousie University
Halifax, Nova Scotia
August 2019

TABLE OF CONTENTS

LIST OF TABLES

LIST OF FIGURES

LIST OF SCHEMES

LIST OF EQUATIONS

ABSTRACT

The mandelate racemase (MR) subgroup of the enolase superfamily of enzymes (ENS) is mechanistically diverse but structurally similar. This work focused on conserved active site residues in subgroup members MR and L-fuconate dehydratase (FucD). The impact of a Tyr 137-Lys 164-Lys 166 triad on the pK_a of Lys 166 of MR was investigated. A Y137F mutation increased the pK_a of both Lys 166 and His 297 by 1-1.4 pK_a units. FucD was assayed for inhibition with tartronate and 3-hydroxypyruvate (3-HP), which bind the conserved Brønsted acid-base catalysts of MR. Tartronate was found to be a weak linear mixed-type inhibitor of FucD (K_i = 8.37 ± 0.72 mM, α = 7.53 ± 1.16) and 3-HP irreversibly inactivated FucD (k_{inact} = 1.49 ± 0.0058 × 10^{-4} s^{-1}, K_I = 7.94 ± 0.24 mM, k_{inact}/K_I = 0.0187 ± 0.0007 $M^{-1}s^{-1}$). Lastly, Trp 101 on the interdigitating loop of FucD was found to be critical for catalysis.

LIST OF ABBREVIATIONS USED

BSA	bovine serum albumin
BzH	benzohydroxamate
CD	circular dichroism
CHAPS	3-[(3-cholamidopropyl)dimethylammonio]-1-propanesulfonate
CHES	N-cyclohyxyl-2-aminoethanesulfonic acid
CoA	coenzyme A
E.C.	enzyme commission number
EDTA	ethylenediaminetetraacetic acid
ENS	enolase superfamily of enzymes
ESI	electron spray ionization
FPLC	fast protein liquid chromatography
FucD	L-fuconate dehydratase
GLH	glycolaldehyde
HEPES	4-(2-hydroxyehtyl)-1-piperazineethanesulfuonic acid
3-HP	3-hydroxypyruvate
HPLC	high-performance liquid chromatography
IPTG	isopropyl β-D-1-thiogalactopyranoside
ITC	isothermal titration calorimetry
LB	lysogeny broth
LC-MS	liquid chromatography-mass spectrometry
ManD	D-mannonate dehydratase
MES	2-(N-morpholino)ethanesulfonic acid
MOPS	3-morpholinopropane-1-sulfonic acid
MR	mandelate racemase
MS	mass spectrometry
MW	molecular weight

m/z	mass-to-charge ratio
NAD+	nicotinamide adenine dinucleotide – oxidized form
NADH	nicotinamide adenine dinucleotide – reduced form
NADP+	nicotinamide adenine dinucleotide phosphate – oxidized form
NMR	nuclear magnetic resonance spectroscopy
OD	optical density
PIPES	piperazine-N,N'-bis[2-ethanesulfonic acid]
PLP	pyridoxal phosphate
(*R*)-αPGA	(*R*)-α-phenylglycolate
(*S*)-αPGA	(*S*)-α-phenylglycolate
SDS-PAGE	sodium dodecyl sulfate polyacrylamide gel electrophoresis
TAPS	3-[[1,3-dihydroxy-2-(hydroxymethyl)propan-2-yl]propane-1-sulfonic acid
TarD	D-tartrate dehydratase
TFHTP	3,3,3-trifluoro-2-hydroxy-2-(trifluoromethyl)propanoate
TGD	L-talarate-galactarate dehydratase
TIM	triosephosphate isomerase
TS	transition state
UV	ultra-violet
WT	wild-type

ACKNOWLEDGEMENTS

I would like to thank Dr. Stephen Bearne for his continued support from the first day I stepped into his office. From when I had just started to consider graduate school, he has been generous with his time and patience. His passion for research is infectious, work ethic inspiring, and I am truly thankful for the insight into the world of science his tutelage has supplied.

I would like to thank my committee members: Dr. David Jakeman and Dr. David Langelaan for their support and expertise. Many of these experiments would not have been possible without their guidance, especially considering my frequent protein purification difficulties.

I would also like to thank past and present members of the Bearne Lab: Greg, Pooja, Himank, Amar, Nicole, Josh, Noa and Oliver who have all helped make my time as a MSc. student more productive and enjoyable. Particularly I would like to thank Dr. Amar Sharma for his help with the deuterium exchange experiments and Drs. Greg McCluskey and Himank Kumar for training me on DLS. I would also like to thank Dr. Mike Lumsden (NMR-3) for his help in ^{1}H NMR troubleshooting. I am also indebted to Drs. Alejandro Cohen and Abir Lefsay of the Biological Mass Spectrometry Core Facility, Dalhousie University for conducting the LC-MS/MS experiments and providing much data analysis expertise and general support over the last year. In addition, I would like to thank Dr. Alejandro Cohen for agreeing to serve on my examining committee.

There are many past members of the Bearne lab who have been instrumental in the progress of my research. I would like to thank Drs. Colin Douglas and Mitesh Nagar

for patiently responding to emails. Also, I would like to thank Zach Morrison who started the Y137F MR project and Minglu Gu who began the work with FucD.

I am very grateful for the funding sources of the Bearne lab (NSERC especially), particularly the NSERC-CREATE BioActives program for funding my research and the many opportunities the program has afforded. I am also thankful for the opportunities I've had to earn income as a teaching assistant and am truly grateful to Paul and Heidi who work tirelessly to provide quality content for the undergraduate program and support their TAs. I would also like to thank the Biochemistry and Molecular Biology Department office staff: Roisin, Brenda, and Barb who have all been exceedingly kind and supportive during my time at Dalhousie as well as providing excellent administrative support.

Lastly, I would like to thank my friends and family both in Halifax and Fredericton for their support as I've undertaken my studies, without which I know I would not have made it very far

CHAPTER 1 INTRODUCTION

1.0 ENZYMATIC ABSTRACTION OF PROTONS FROM CARBON ACIDS

Enzymes in the enolase superfamily (ENS) catalyze the abstraction of protons from carbon acid substrates with high pK_a values to create an *aci*-carboxylate intermediate (Scheme 1.1) (Babbitt et al., 1996; Gerlt, John A., Babbitt, Jacobson, & Almo, 2012). Mandelate racemase has been used as a model within this superfamily for studying this difficult step in enzymatic catalysis (Bearne, S. L. & St. Maurice, 2017). The pK_a of mandelate's α-proton is thought to be ~29 in solution (Chiang, Kresge, Pruszynski, Schepp, & Wirz, 1990). To facilitate this reaction, there are two options an enzyme can employ: reduce the pK_a of the substrate and/or increase the pK_a of the catalytic basic residues (Toney, 2019).

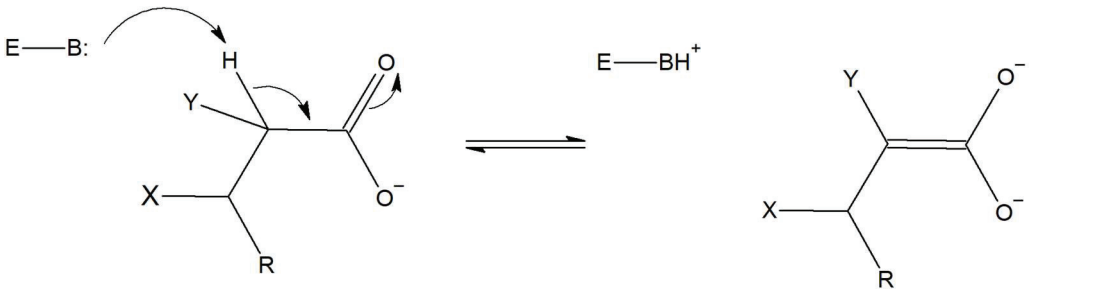

Scheme 1.1 Shared half-reaction of the ENS

An example of reducing the pK_a of the substrate is demonstrated by enzymes that use the co-factor pyridoxal phosphate (PLP) to couple an electron sink with the substrate that can delocalize and stabilize the negative charge created by abstraction of the proton of interest (Scheme 1.2) (Mozzarelli & Bettati, 2006). However, there are several

enzymes that do not employ PLP that still abstract protons with high pK_a values (Toney, 2019). Another common strategy is the use of significant electrostatic stabilization (Guthrie, J. P. & Kluger, 1993). This can involve a metal cation, which acts as a prominent electrophilic catalyst in the enzyme active site. Enzymes in the ENS, including MR, all catalyze the abstraction of an α-proton with a high pK_a value and require a divalent metal ion for catalysis. The positive charge of the metal ion presumably helps counteract the effect of the growing negative charge on the substrate at the transition state arising during the deprotonation reaction (Figure 1.1) (Babbitt *et al*., 1996).

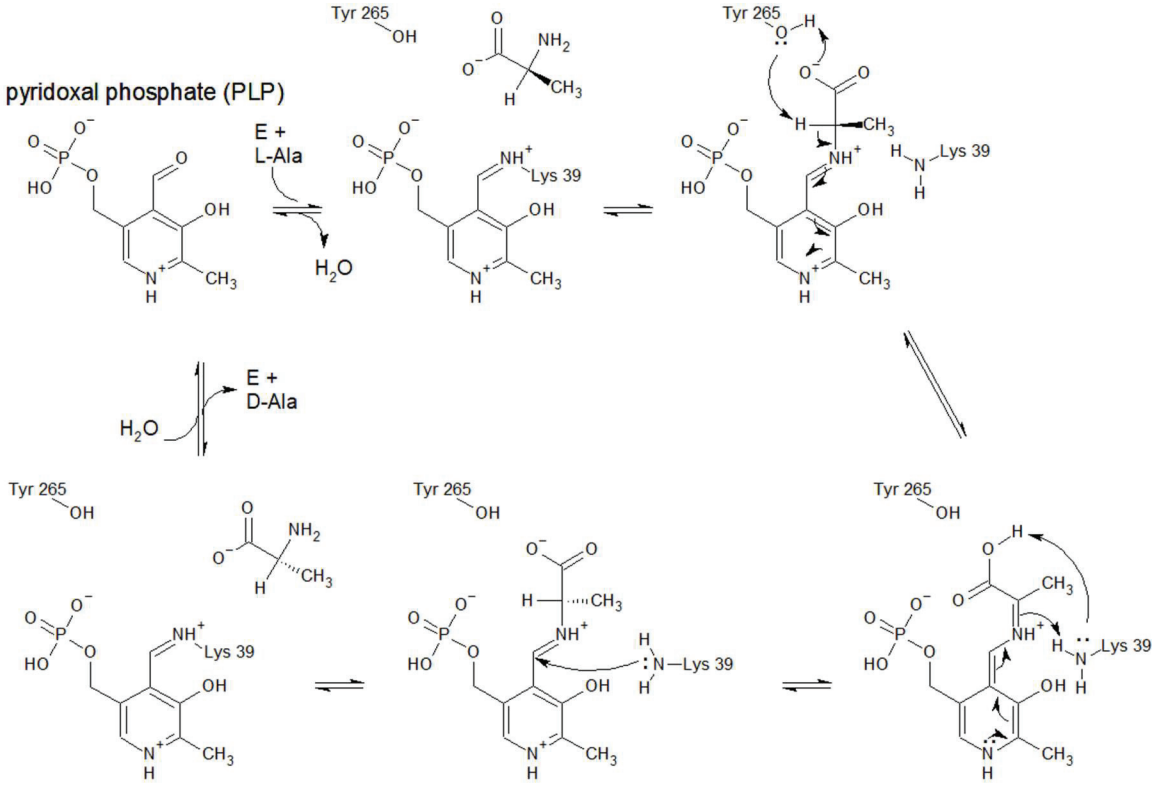

Scheme 1.2 Mechanism of *Bacillus stearothermophilus* alanine racemase. This enzyme provides an example where PLP is used to increase the acidity of a proton alpha to a carboxylate group. Modified from Yoshimura and Esaki (Yoshimura & Esaki, 2003).

The pK_a of mandelate in the active site of MR is further modulated by general acid catalysis where Glu 317 is in position to protonate the carboxylate of mandelate upon deprotonation of the α-proton (Figure 1.1) (Mitra *et al*., 1995). This creates the enol instead of the enolate which corresponds to a much more stable species.

The other strategy for facilitating enzymatic abstraction of high pK_a protons is, while stabilizing the deprotonated intermediate, to concomitantly increase the basicity of the catalytic basic residue. The strategy was shown to be carried out by triosephosphate isomerase (TIM) which increases the pK_a of Glu 165 at the transition state to 10 from 3 in the ground state (Zhai, Reinhardt, Malabanan, Amyes, & Richard, 2018).

While the above discussion focused on how an enzyme might facilitate the abstraction of a proton with a high pK_a, Marcus theory may be used to illustrate the challenges in deprotonating carbon acids in more detail. Marcus theory utilizes two main considerations: a thermodynamic barrier, represented by the unfavorable accumulation of negative charge on a carbon acid, and an intrinsic barrier which is independent of the energy inherent to species at different points during the reaction progress (Gerlt, J. A. & Gassman, 1992; Gerlt, John A., Kreevoy, Cleland, & Frey, 1997). It has been found that carbon acids with the same pK_a as heteroatom acids are deprotonated more slowly (Eigen, 1964; Guthrie, J. Peter, 1998). The rationale behind this intrinsic barrier is that it arises from the required rearrangement of electron density around the carbon acid and the subsequent reorganization of solvating water molecules (Bernasconi, 1992; Guthrie, J. Peter, 1998). Enzymes overcome this barrier by excluding water from active sites and specifically positioning solvating amino acids to selectively stabilize the transition state (Gerlt, John A. & Gassman, 1993; Gerlt, J. A. & Gassman, 1993).

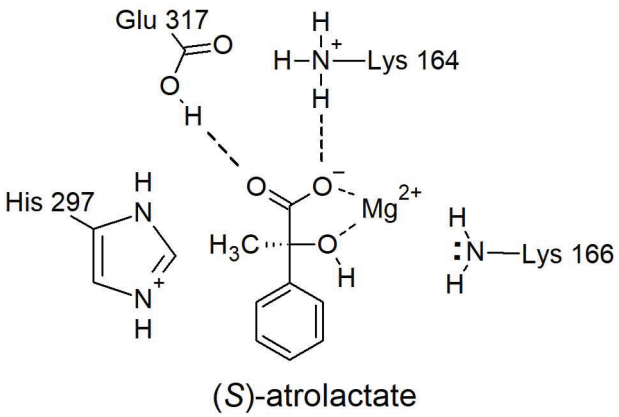

Figure 1.1 Binding of (*S*)-mandelate analogue (*S*)-atrolactate in the MR Active Site. Highlighting interactions with known or suspected positively charged elements and a hydrogen bond to Glu 317 implicated in general acid catalysis (pdb entry 1MNS).

1.1 MANDELATE RACEMASE

1.1.1 DISCOVERY AND METABOLIC ROLE

Mandelate racemase (MR, E.C. 5.1.2.2) was discovered by Stanier and colleagues when they observed that the *Pseudomonas putida* strain A.3.12 (ATCC 12633) was able to grow on minimal media with either enantiomer of mandelate as a sole carbon source (Gunsalus, Stanier, & Gunsalus, 1953). Operon analysis found the gene encoding mandelate racemase among several other genes for mandelate catabolism such as (*S*)-mandelate dehydrogenase, benzoylformate decarboxylase, NAD^+ dependent benzaldehyde dehydrogenase and $NADP^+$ dependent benzaldehyde dehydrogenase (Figure 1.2) (Hegeman, Rosenberg, & Kenyon, 1970; Kenyon, Gerlt, Petsko, & Kozarich, 1995). So far, MR is unique in its enzyme subgroup of the ENS given the primary reaction it catalyzes is racemization rather than β-elimination of a leaving group. Nevertheless, the observed genetic context and high activity with mandelate as substrate support this mechanistic classification. Furthermore, many enzymes in the MR subgroup catalyze epimerization reactions to some extent (Yew, W., Fedorov, Fedorov, Rakus et al., 2006; Yew, Ws, Fedorov, Fedorov, Almo, & Gerlt, 2007). Therefore, MR may be considered to represent one end of a spectrum between enzymes in the subgroup adapted to either racemization, racemization and epimerization, or elimination reactions.

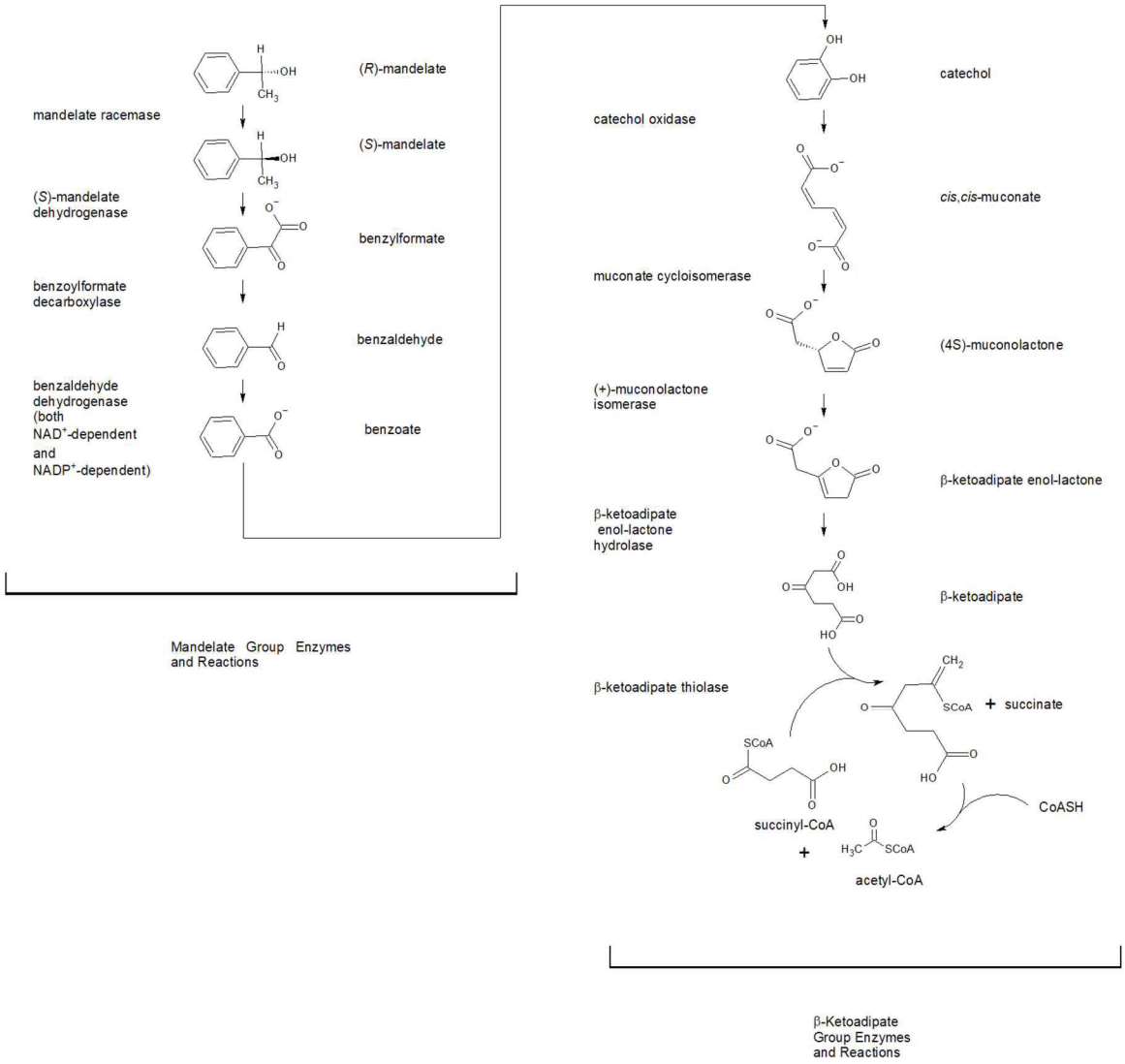

Figure 1.2 Catabolic pathway of (*R*)-mandelate in *P. putida* strain A.3.12 (ATCC 12633). Modified from Hegeman and colleagues (Hegeman *et al*., 1970).

1.1.2 STRUCTURE OF MR

The structure of MR is well conserved with other members of the ENS (Babbitt *et al*., 1996; Neidhart *et al*., 1991). The two major domains, the α+β capping domain and the modified triosephosphate isomerase (TIM) barrel, are conserved across all superfamily members. The α+β capping domain is comprised of residues from both the N and C-terminus and contains the 20s and 50s loops that interact with distal portions of the substrate away from the α-carbon. The modified TIM barrel contains the conserved glutamate and aspartate residues (Asp 195, Glu 221 and Glu 247) that chelate the essential magnesium ion as well as many other conserved residues essential for catalysis. The active site is found at the intersection of the capping and barrel domains (Neidhart *et al*., 1991) and aligns with the active sites for all known TIM barrel enzymes occurring at the C-terminal ends of the TIM barrel β-strands (Wierenga, 2001). The TIM barrel of enzymes in the ENS are modified such that one of the typical eight encircling α-helices is replaced with a less ordered loop such that it is a $(\alpha/\beta)_7\beta$ barrel (Wierenga, 2001).

Monomeric units of MR oligomerize into tight dimers as is illustrated by a structural feature of the MR subgroup, i.e., an interdigitating loop that emanates from the capping domain of one protomer and inserts into or near the active site of a neighboring protomer. In some MR subgroup members such as MR and FucD, the residue at the tip of this interdigitating loop appears to interact directly with the substrate in the neighboring protomer's active site (Leu 93 in MR, Trp 101 in FucD). However, in several other members of the MR subgroup residues on this loop don't appear to be directly involved with substrate binding but support other residues within the active sites of these enzymes to interact with the substrate (Bearne, S. L., 2017). The only other subgroup within the

ENS to contain an interdigitating loop is the D-mannonate dehydratase (ManD) subgroup where the residue at the tip of all known members contributes a binding determinant to the adjacent protomer's active site. In MR, dimeric units further oligomerize into tetramers of dimers such that in crystal structures MR is an octamer; however SDS-PAGE experiments do not clearly show whether it is an octamer or tetramer in solution (Fee, Hegeman, & Kenyon, 1974b; Tsou, Ransom, Gerlt, Powers, & Kenyon, 1989).

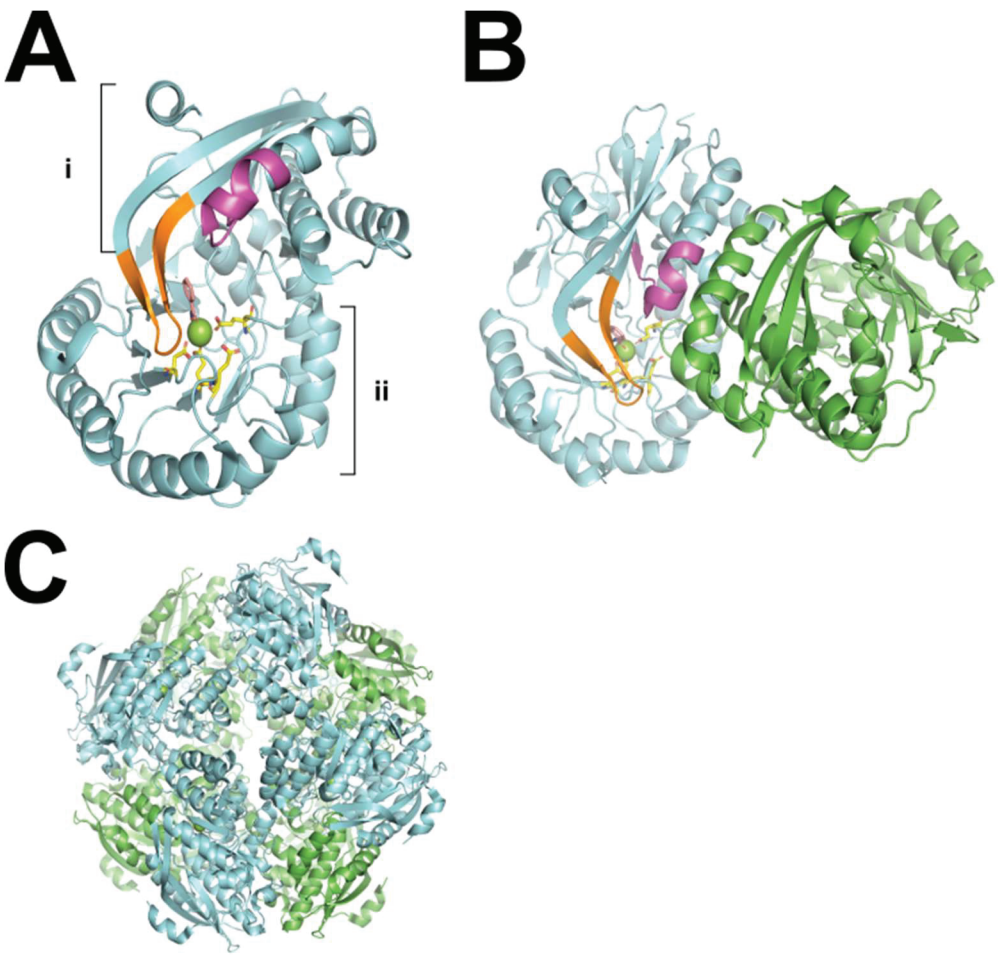

Figure 1.3 Structure of MR. MR monomer: i) α+β capping domain, ii) modified TIM barrel domain, 20s loop (orange), 50s loop (magenta), Mg^{2+} ion (green), Benzohydroxamate (salmon), conserved carboxylate containing residues chelating the Mg^{2+} ion (yellow) (A). MR tightly packed dimer (B). Octameric MR (tetramer of dimers) (C) (pdb entry 3UXK).

1.1.3 MECHANISM OF MR

Several experiments were conducted to elucidate the catalytic mechanism of MR including deuterium exchange, site-directed mutagenesis, and alkylation studies (Landro et al., 1994; Landro, Kallarakal, Ransom, Gerlt, & Kozarich, 1991; Powers, Koo, & Kenyon, 1991). From these experiments, it was determined that MR catalyzes the racemization of mandelate via a two base mechanism where His 297 abstracts the α-proton from (*R*)-mandelate and Lys 166 abstracts the α-proton from (*S*)-mandelate. It was also found that protonation of the *aci*-carboxylate intermediate to produce (*R*)-mandelate or (*S*)-mandelate is carried out by His 297 or Lys 166 respectively (Scheme 1.3).

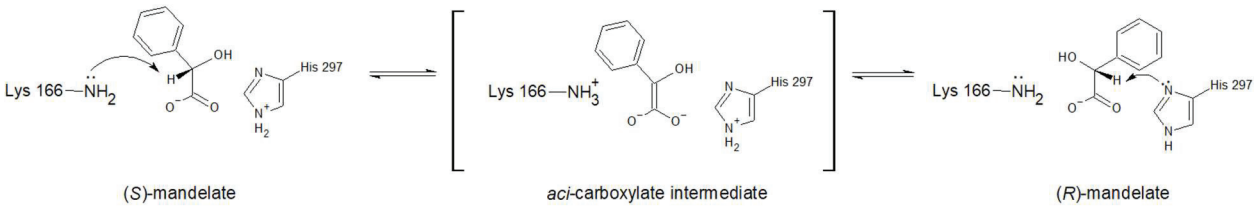

Scheme 1.3 General mechanism of racemization of mandelate by MR.

Deuterium exchange experiments alongside site-directed mutagenic studies played a large role in classifying the catalytic acid-base residues. It was found by Gerlt and colleagues that when MR catalyzed racemization of mandelate was conducted in D_2O for short times, there was little incorporation of deuterium into the substrate (*R*)-mandelate but full incorporation of deuterium into the product (*S*)-mandelate. In contrast, when (*S*)-mandelate was used as the substrate there was considerable deuterium present in the substrate (*S*)-mandelate as well as the product (*R*)-mandelate (Powers *et al*., 1991). This finding demonstrated there were two separate enantiospecific bases catalyzing the racemization of mandelate rather than one.

Upon crystallization of MR there were two residues that were observed to be poised in the active site to abstract a proton from a substrate mandelate, His 297 for the α-proton of (*R*)-mandelate and Lys 166 for the α-proton of (*S*)-mandelate (Neidhart *et al*., 1991). Classifying these two residues as the acid-base catalysts responsible for mandelate racemization was consistent with the deuterium exchange results where a polyprotic lysine acting as the *S*-specific base could rotate after abstracting the α-proton and present a deuteron two thirds of the time for incorporation into (*S*)-mandelate at the α-position. This mechanism was further confirmed when it was found the H297N variant, although unable to catalyze racemization, was able to incorporate deuterium at the α-position of (*S*)-mandelate (Landro *et al*., 1991) (Scheme 1.4). Added support for this mechanistic assignment was also generated when MR was treated with both *R* and *S* enantiomers of α-phenylglycidate (αPGA), which are analogues of mandelate where an epoxide replaces the α-proton. MR was irreversibly inactivated with (*R*)-αPGA where the epoxide replaces the α-proton of (*S*)-mandelate. However, MR inactivation by a solution of (*S*)-αPGA was found to be much less efficient and was attributed to contaminating (*R*)-αPGA (~10%) (Landro *et al*., 1994). Crystal structures of MR inactivated with (*R*)-αPGA found the adduct on the ε nitrogen of Lys 166. Interestingly, crystal structures show (*R*)-αPGA is almost superimposable with (*S*)-atrolactate, which is a substrate analogue of (*S*)-mandelate (Fig 1.4). This result is consistent with Lys 166 acting as the base to abstract the α-proton from (*S*)-mandelate (Landro *et al*., 1994).

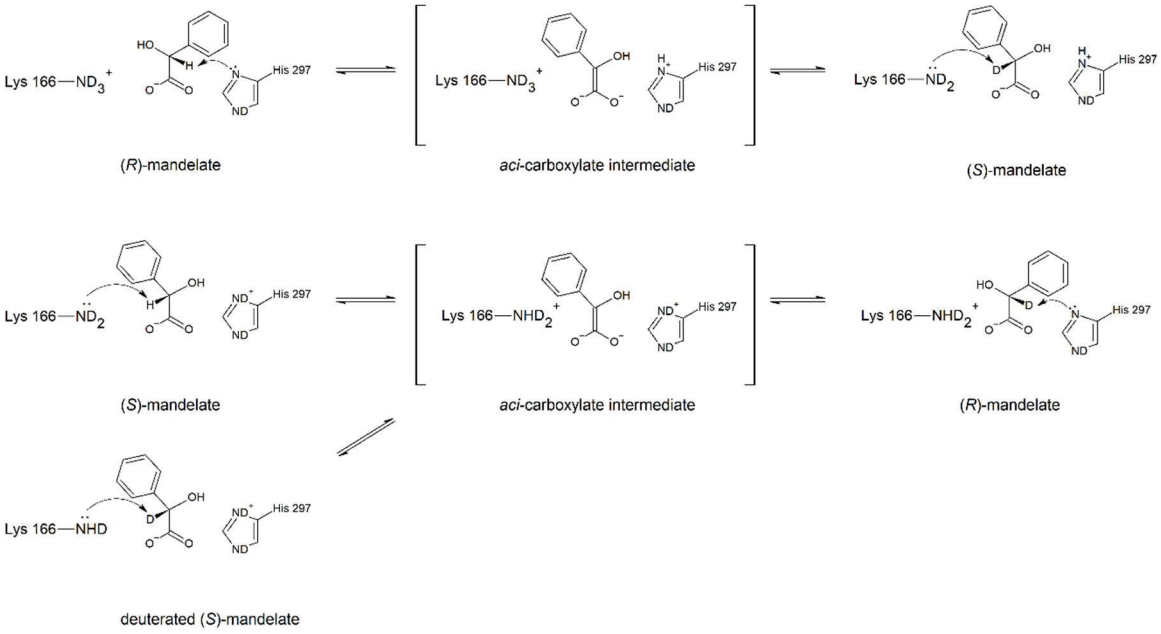

Scheme 1.4 Mechanism of incorporation of deuterium into mandelate enantiomers by MR. After generation of the aci-carboxylate intermediate the C-N$^{\varepsilon}$ bond of Lys 166 can rotate so that a deuterium can be incorporated at the α-position of substrate (*S*)-mandelate. Note that since His 297 is monoprotic, there is no mechanism of incorporating deuterium into (*R*)-mandelate via the back reaction.

1.1.4 SUBSTRATES AND STRUCTURALLY SIMILAR INHIBITORS OF MR

Initial crystal structures of MR were solved with substrate (*S*)-mandelate and the substrate inhibitor mimic (*S*)-atrolactate (Kallarakal *et al*., 1995; Powers *et al*., 1991). A crystal structure with (*R*)-mandelate or an *R* substrate analogue has not yet been able to be obtained. When an attempt to obtain a structure with (*R*)-mandelate was made using the K166R MR variant, conversion of (*R*)- to (*S*)-mandelate was observed (Kallarakal *et al*., 1995). The one crystal structure with (*R*)-mandelate bound in the active site had both enantiomers present and (*R*)-mandelate was bound in a non-productive conformation (Kallarakal *et al*., 1995). A conformational change of MR upon binding of the *R* substrate seems probable due to cracking of crystals, grown in the absence of substrate, upon soaking with (*R*)-atrolactate (Bearne, S. L. & St. Maurice, 2017). The binding pocket for the phenyl ring of (*R*)-mandelate was tentatively identified by use of benzilate, which contains two phenyl rings in order to mimic both (*S*)- and (*R*)-mandelate simultaneously (Fig. 1.4). The C92S/C264S/K166C enzyme variant was needed to obtain the crystal structure to allow sufficient space in the active site for binding (Nagar, Mitesh, Lietzan, St. Maurice, & Bearne, 2014).

There have been several transition state (TS) analogues for MR discovered by the Bearne group (Bourque, Burley, & Bearne, 2007; Burley & Bearne, 2005; Lietzan et al., 2012; Maurice, Bearne, Lu, & Taylor, 2003). These inhibitors were designed to mimic key electrostatic and geometric characteristics of the *aci*-carboxylate intermediate. Correlation of the enzyme efficiency (k_{cat}/K_m) of several mutant enzymes with the competitive inhibition constant (K_i) provides support these molecules are being

recognized as TS analogues. The two main characteristics of the *aci*-carboxylate intermediate that have been sought to be replicated by TS analogues have been the sp2 hybridization state of the carboxylate carbon and electron density in the molecule reminiscent of the enol/enolate transition state species. The negative charge of the carboxylate was replicated in a phosphonate transition state analogue although not the precise expected geometry. Nonetheless, α-hydroxybenzylphosphonate was found to act as a good inhibitor of MR with an affinity 100-fold greater than the substrate (St. Maurice & Bearne, 2000).

Benzohydroxamate (BzH) replicates the α-carbon-carboxylate carbon double bond of the presumed TS with a hydroxamate functionality. Although there is a missing atom where the second oxygen of the carboxylate would be expected (Lietzan et al., 2012; St. Maurice & Bearne, 2000). Given its commercial availability BzH has been the TS analogue used most predominantly when probing the effects of different mutations on MR catalysis.

In addition to these described reversible inhibitors, (*R*)-α-phenylglycidate represents an irreversible inhibitor of MR where the epoxide functionality replaces the α-proton (Fig 1.4). This ring was opened and formed a covalent link to Lys 166 (Landro *et al*., 1994). Propargylglycolate was also found to be an irreversible inhibitor of MR where the proposed mechanism involved a michael acceptor being generated from the deprotonated species. However, it was found that propargylglycolate predominantly acted

as a substrate for MR with a ratio of racemization to inhibition of ~17000:1 (Landro, Kenyon, & Kozarich, 1992).

Several other known substrates of MR have also been discovered and include para-substituted mandelate analogues, vinylglycolate, and trifluorolactate (Fig 1.4) (Felfer, Strauss, Kroutil, Fabian, & Faber, 2001; Li, Powers, Kozarich, & Kenyon, 1995; Nagar, M., Narmandakh, Khalak, & Bearne, 2011). An interesting substrate of MR is *p*-(bromomethyl)mandelate as after the α-proton is abstracted bromine is eliminated in contrast to other substrates which undergo racemization (Hegeman *et al*., 1970).

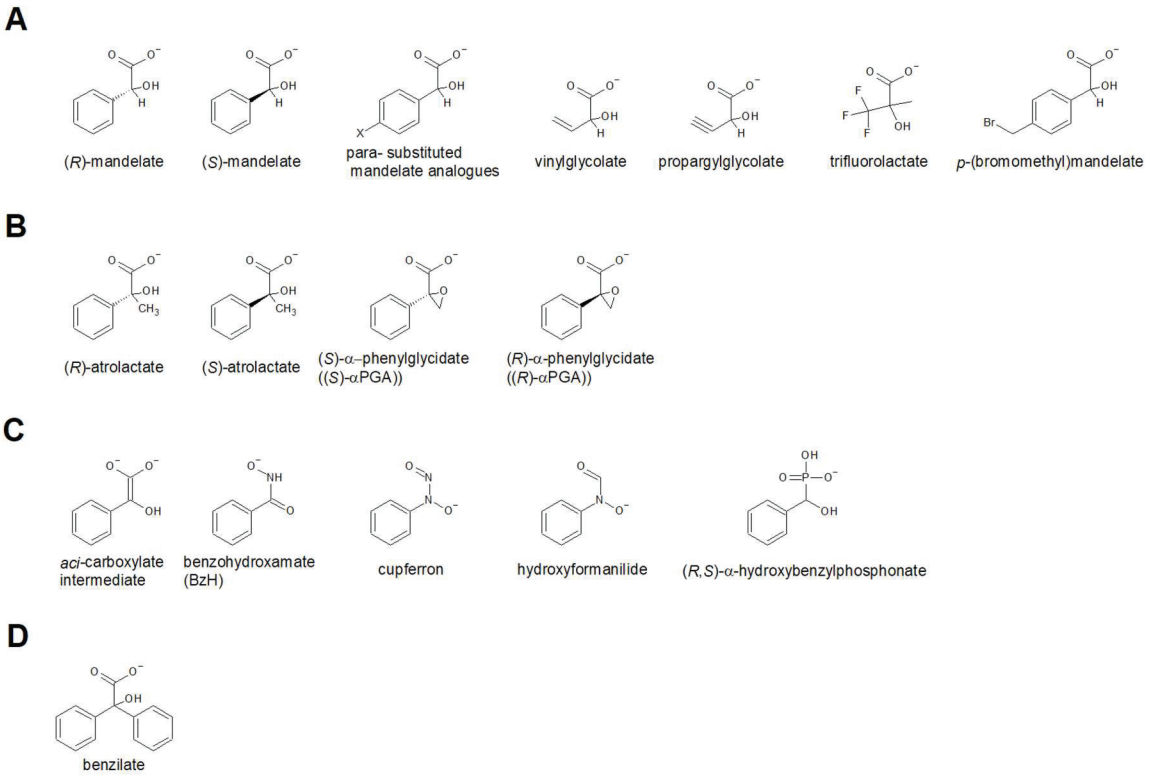

Figure 1.4 Substrates and inhibitors of MR designed from substrate mandelate molecules and the *aci*-carboxylate intermediate. Some substrates molecules of MR. For para substituted mandelate analogs X = Br, Cl, OH and OCH_3. Note that propargylglycolate was also found to be a mechanism-based inhibitor of MR but partitioned ~17000:1 for racemization over of inactivation (Landro *et al*., 1992). The reaction catalyzed by *p*-(bromomethyl)mandelate is elimination of bromide instead of racemization (Hegeman *et al*., 1970). (*R*) and (*S*) enantiomers of most substrates are not shown for brevity (A). (*S*)- and (*R*)-atrolactate as well as (*S*)-αPGA are reversible competitive inhibitors while (*R*)-αPGA is a mechanism-based inhibitor of MR (B). All transition state inhibitors of MR are reversible (C). Benzilate is a substrate-product analogue inhibitor of MR (D).

1.1.5 STABILIZATION OF THE *ACI*-CARBOXYLATE INTERMEDIATE BY GLU 317, LYS 164, AND THE Mg^{2+} ION

According to TS theory, enzymes mediate catalysis primarily by lowering the Gibb's free energy of the TS or high energy intermediate in the reaction pathway (Figure 1.5) (Wolfenden, 1972). From deuterium studies where exchange of a proton for a deuteron was possible into (*S*)-mandelate when it was used as a substrate it is evident that a deprotonated intermediate exists for at least the lifetime of the rotation of a single bond (40 ps for n-butane) (Landro et al., 1991; Zheng, Kwak, Xie, & Fayer, 2006). This intermediate must be stabilized in some way to account for the massive rate enhancement seen in the MR catalyzed reaction compared to the non-enzymatic reaction (Bearne, S. L. & Wolfenden, 1997).

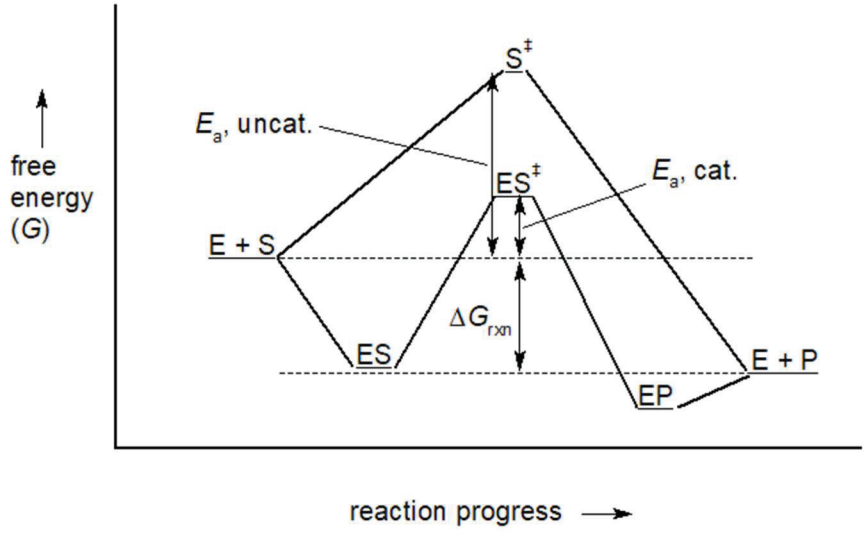

Figure 1.5 Transition state stabilization conferred by enzymes to facilitate catalysis. Enzymes are catalysts that increase the rate of chemical reactions by lowering the required activation energy (E_a) Where E = enzyme, S = substrate, ES = enzyme substrate complex, P = product, EP = enzyme product complex, uncat. = uncatalyzed, cat. = catalyzed, and ΔG_{rxn} = overall change in free energy. Modified from (Fersht, 1985).

Accumulation of negative charge due to deprotonation of the α-carbon to produce the *aci*-carboxylate intermediate is unfavorable. Given that all enzymes in the ENS catalyze the formation of an *aci*-carboxylate intermediate and require a divalent metal ion for activity, it seems intuitive that a function of the metal ion is, in part, to act as a balancing positive charge to stabilize the build-up of negative charge at the TS. Indeed, in crystal structures of known ENS members the divalent metal ion is chelated by at least one oxygen of the carboxylate where negative charge is presumed to accumulate during catalysis.

Another positive charge in the active site of MR and MR subgroup members that could help mitigate the energetic penalties of a buildup of negative charge on the carboxylate oxygens of the substrate is the Lys 164 analogue residue. In all MR subgroup members, a KXK motif exists where the second Lys acts as a basic residue in catalysis (Babbitt *et al*., 1996). In crystal structures of enzymes in the MR subgroup the Lys 164 analogue is found to be in hydrogen bonding distance to the carboxylate of the substrate and therefore could be acting to stabilize an accumulation of negative charge at this area of the molecule during catalysis (Neidhart *et al*., 1991; Yew, W. *et al*., 2006; Yew, W., Fedorov, Fedorov, Wood *et al*., 2006; Yew, Ws *et al*., 2007).

General acid catalysis has also been invoked as a method in which MR stabilizes the transition state of mandelate as it undergoes racemization. Deprotonation at the α-proton would normally produce an enolate ion, which is even more unfavorable when the carboxylate is already deprotonated as the molecule becomes doubly negatively charged. However, Glu 317 is positioned to be able to protonate the carboxylate oxygen upon

deprotonation of the α-carbon resulting in formation of an enol instead of an enolate ion. When Glu 317 is changed to a Gln residue catalysis is severely affected.

Two other residues bear mentioning at this stage for stabilization of the largely negatively charged *aci*-carboxylate intermediate in MR. Lys 166 and His 297, the active site Brønsted acid-base residues that facilitate abstraction and protonation at the α-carbon were also found to play an important role in substrate and TS analogue benzohydroxamate (BzH) binding through cation-π interactions with the phenyl ring (Nagar, Mitesh & Bearne, 2015). Particularly, Lys 166 was found to be important where changing it to a Met cause a 443-fold loss of affinity for the TS analogue BzH (Nagar, Mitesh & Bearne, 2015). Therefore, in addition to acting as Brønsted acid-base residues that mediate α-proton abstraction from mandelate, Lys 166 and His 297 can be presumed to aid in binding of the transition state through cation-π interactions to reduce the penalty of increased negative charge being isolated in the substrate during catalysis.

1.1.6 NON-TRADITIONAL INHIBITORS OF MR

Bearne and co-workers found that a resonance stabilization by a π-system was not essential for a mandelate analogue to be a substrate of MR (Nagar, M. *et al*., 2011). Although the potential to delocalize electrons into a π-electron system had been deemed a minimal requirement for substrates of MR in order to stabilize the negative charge generated upon formation of the *aci*-carboxylate intermediate (Li *et al*., 1995) Bearne and colleagues demonstrated that a mandelate analogue with the phenyl ring substituted for a trifluoromethyl group, (*R*)- and (*S*)-trifluorolactate, were both substrates of MR (Fig 1.4). This demonstrated that resonance stabilization of the *aci*-carboxylate intermediate was

not required for substrates of MR and inductive stabilization of the electron-rich intermediate was sufficient. Therefore, a substrate-product analogue of trifluorolactate with two trifluoromethyl groups in place of the α-proton and phenyl ring, comparable to benzilate, was assayed as an inhibitor of MR. Interestingly, 3,3,3-trifluoro-2-hydroxy-2-(trifluoromethyl)propanoate (TFHTP) had an affinity that was ~44-times greater than that of benzilate and the (*R*)- and (*S*)- trifluorolactate substrates (Nagar, Mitesh *et al*., 2014). A crystal structure of the complex showed a novel binding mode in which His 297 and Lys 166 were bridged by the carboxylate group of TFHTP (Fig 1.6).

This novel bridging binding mode suggested that tartronate might be an inhibitor of MR where His 297 and Lys 166 could be bridged by one carboxylate while the other carboxylate and the central hydroxyl group could chelate the Mg^{2+} ion similar to the binding mode observed for (*S*)-mandelate and (*S*)-atrolactate (Kallarakal *et al*., 1995; Neidhart *et al*., 1991). Tartronate was found to be a competitive inhibitor of MR, binding with a modest affinity of 1.8 ± 0.1 mM, similar to substrate (*R*)- and (*S*)-mandelate (Nagar, Mitesh *et al*., 2014). This finding was significant given that all MR subgroup members share these binding determinants in conserved orientations (Figure 1.7). Therefore, tartronate could possibly act as a general inhibitor for the MR subgroup enzymes.

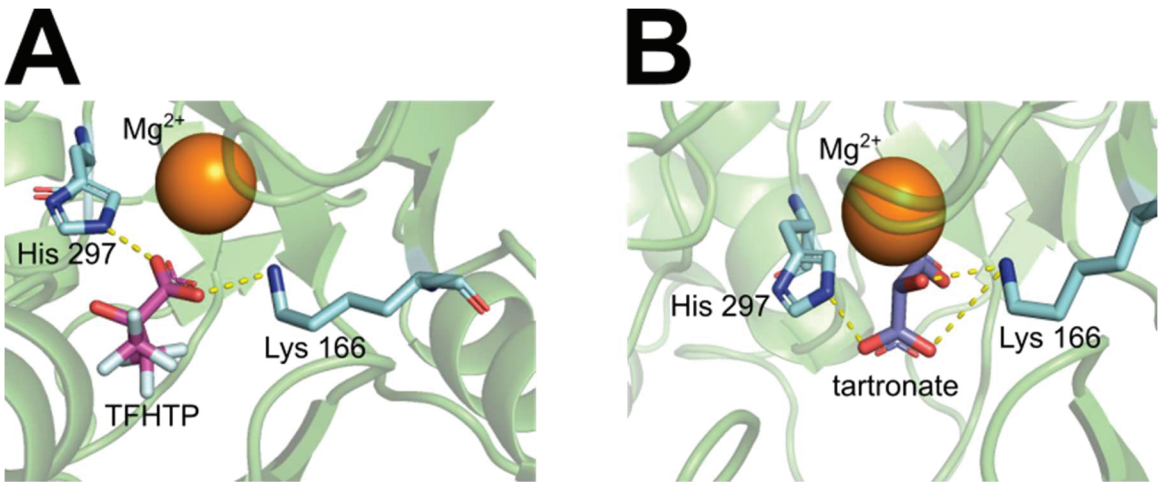

Figure 1.6 "Bridging" Inhibitors of MR. Binding of TFHTP (A, pdb entry 4FP1) and tartronate (B, pdb entry 4M6U) to the active site of MR depicting the 'bridging' binding mode.

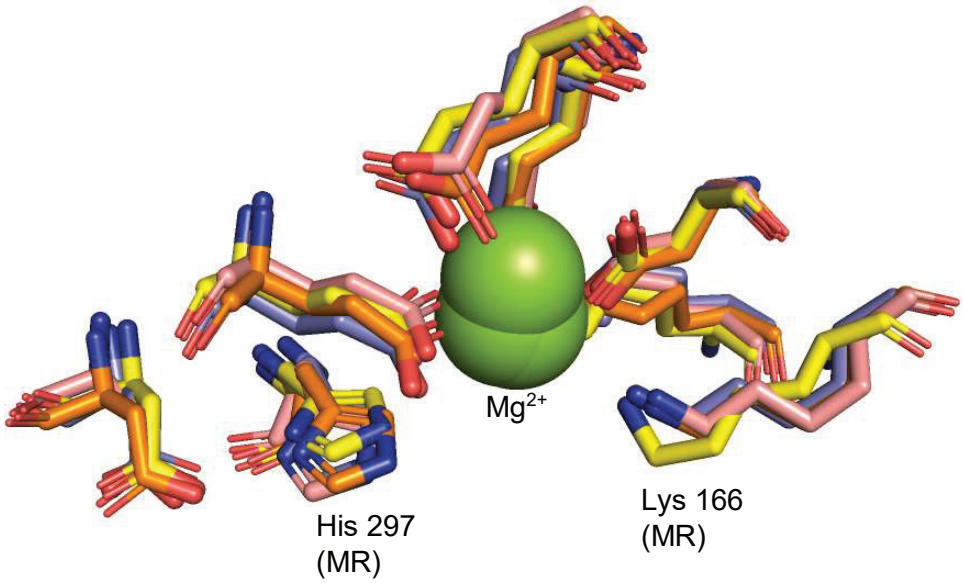

Figure 1.7 Conserved active site residues in members of the MR subgroup. The conserved metal binding and catalytic acid-base residues of MR (yellow, 3UXK), D-tartrate dehydratase (salmon, 2DW7), L-fuconate dehydratase (purple, 2HXT) and L-talarate/galacatarate dehydratase (orange, 2PP1) are superimposed. Numbering for the catalytic acid-base residues for MR is shown.

The other non-substrate, substrate-product or TS analogue inhibitor of MR of note is 3-hydroxypyruvate (3-HP) (Nagar, Mitesh, Wyatt, St. Maurice, & Bearne, 2015). Studied to investigate the effect 3-carbon α-keto acids as inhibitors of MR it was found that 3-HP was an irreversible inhibitor of MR. Co-incubation with the competitive inhibitor BzH protected MR from inactivation, indicating that the inactivation chemistry occurred at the active site. MS/MS analysis showed that Lys 166 was modified by an 86-Da adduct. X-ray crystal structure analysis of the enzyme-adduct revealed the presence of a deprotonated Schiff-base adduct in the E form to C-2 which indicated that tautomerization of 3-HP to tartronate semialdehyde did not occur (Fig. 1.8 and Scheme 1.5). Like tartronate, inhibition with 3-HP appeared to only involve elements of the MR active site that are conserved across the MR subgroup. Therefore, 3-HP could serve as an inhibitor of other MR subgroup members (Nagar, Mitesh *et al*., 2015).

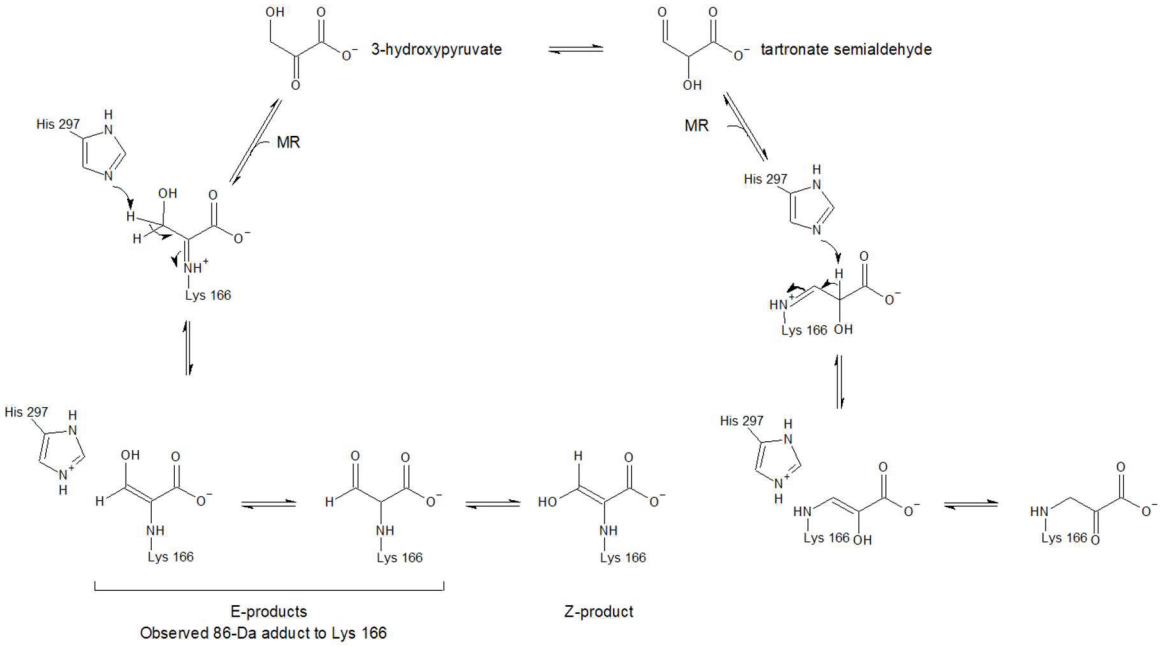

Scheme 1.5 Mechanism for formation of 86-Da adducts to Lys 166 of MR. Modified from Bearne and co-workers (Nagar, Mitesh *et al*., 2015).

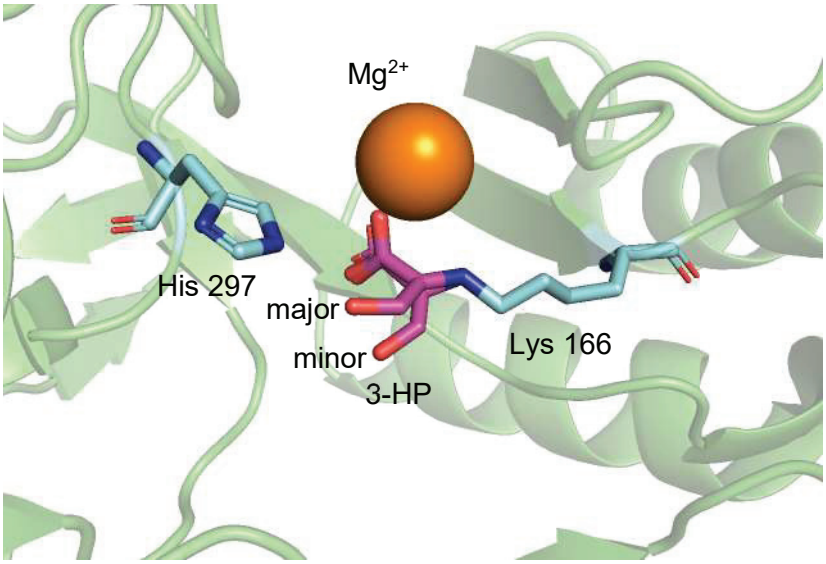

Figure 1.8 Adduct formed with Lys 166 of MR upon inactivation by 3-HP (PDB entry 4X2P).

1.1.7 ENOLASE SUPERFAMILY AND THE MR SUBGROUP

The ENS was the first mechanistically diverse enzyme superfamily to be described (Gerlt, John A. *et al*., 2012). All members share at least 35% sequence homology, significant structural homology and a conserved half-reaction (Babbitt *et al*., 1996). Named for the glycolytic enzyme enolase, the superfamily is comprised of ~49,000 members (Akiva *et al*., 2014).

Conserved structural elements include an α +β capping domain and modified TIM barrel domain as described earlier (Section 1.1.2). The conserved half reaction is abstraction of a proton alpha to a carboxylate group to create an *aci*-carboxylate intermediate (Scheme. 1.1). The Brønsted acid-base residues that carry out this abstraction and subsequent reaction steps (e.g. β-elimination, ketonization etc.) are varied within the superfamily and have been used to delineate seven subgroups including the enolase, MR, muconate lactonizing enzyme (MLE), β-methylaspartate ammonia lyase, D-glucarate dehydratase, D-mannonate dehydratase, and galactarate dehydratase subgroups (Akiva *et al*., 2014).

The MR subgroup is mechanistically diverse, but all discovered members facilitate catalysis that follows one of two reaction pathways. These pathways are broadly defined as β-elimination and racemization/epimerization. Most MR subgroup members follow the β-elimination pathway (Bearne, S. L. & St. Maurice, 2017).

Racemization/epimerization is the reaction catalyzed by mandelate racemase, to some extent L-talarate-galactarate dehydratase (TGD) when L-talarate is substrate, and L-fuconate dehydratase (FucD) when L-talonate or D-ribonate is the substrate (Yew, W. *et*

al., 2006; Yew, Ws *et al*., 2007). This pathway involves protonation of the *aci*-carboxylate intermediate directly by a Brønsted acid in the active site. The protonating amino acid is on the opposite side to the basic residue that abstracted the initial α-proton resulting in the enantiomer or epimer being produced.

The most common reaction mechanism of the MR subgroup is β-elimination of a hydroxyl leaving group from acid sugar substrates (Gerlt, John A. *et al*., 2012). Coupled with initial abstraction of the α-proton this reaction constitutes loss of water and so most MR subgroup members are sugar dehydratases. This reaction pathway typically involves abstraction of the α-proton by the conserved lysine residue and protonation of the hydroxyl leaving group by the conserved histidine residue. The orientation of the substrate within the active site is important given that without certain substrate-enzyme interactions, often far from the site of chemistry, catalysis can be severely impaired (Yew, W. *et al*., 2006).

What factors within a MR subgroup enzyme's active site promote the racemization/epimerization or β-elimination reaction pathway is an open question given the highly conserved nature of the catalytic acid-base residues. The answer may lie in whether the substrate has a leaving group available beta to the carboxylate carbon, whether it can be aligned in such a way to facilitate β-elimination or whether subtle differences in the reactivity exist between active site residues of different MR subgroup enzymes.

1.2 L-FUCONATE DEHYDRATASE

1.2.1 DISCOVERY AND METABOLIC ROLE

A gene annotated as a potential MR subgroup member from *Xanthomonas campestris* (GI:21233491; XCC 4069) was cloned and characterized by Gerlt and co-workers (Yew, W. *et al*., 2006). It was found in an operon that contained various genes presumed to encode enzymes involved in L-fucose metabolism, including a putative L-fucose permease, a mutarotase, a dehydrogenase, and a kinase (Fig. 1.9). Therefore, the unknown MR subgroup member was suspected to be a dehydratase or epimerase of L-fuconate consistent with the function of most characterized MR subgroup members. The gene encoding the putative L-fucose permease (XCC 4071) was annotated as an orthologue of the fucose permease in *Escherichia. coli* from literature annotation of that operon, therefore initial efforts were to determine whether the proposed MR subgroup member demonstrated activity with the corresponding acid sugar of L-fucose, L-fuconate. From testing a library of acid sugars, L-fuconate was found to be the substrate that showed the highest activity with k_{cat}, K_m, and k_{cat}/K_m values similar to other known sugar dehydratases (Yew, W. *et al*., 2006).

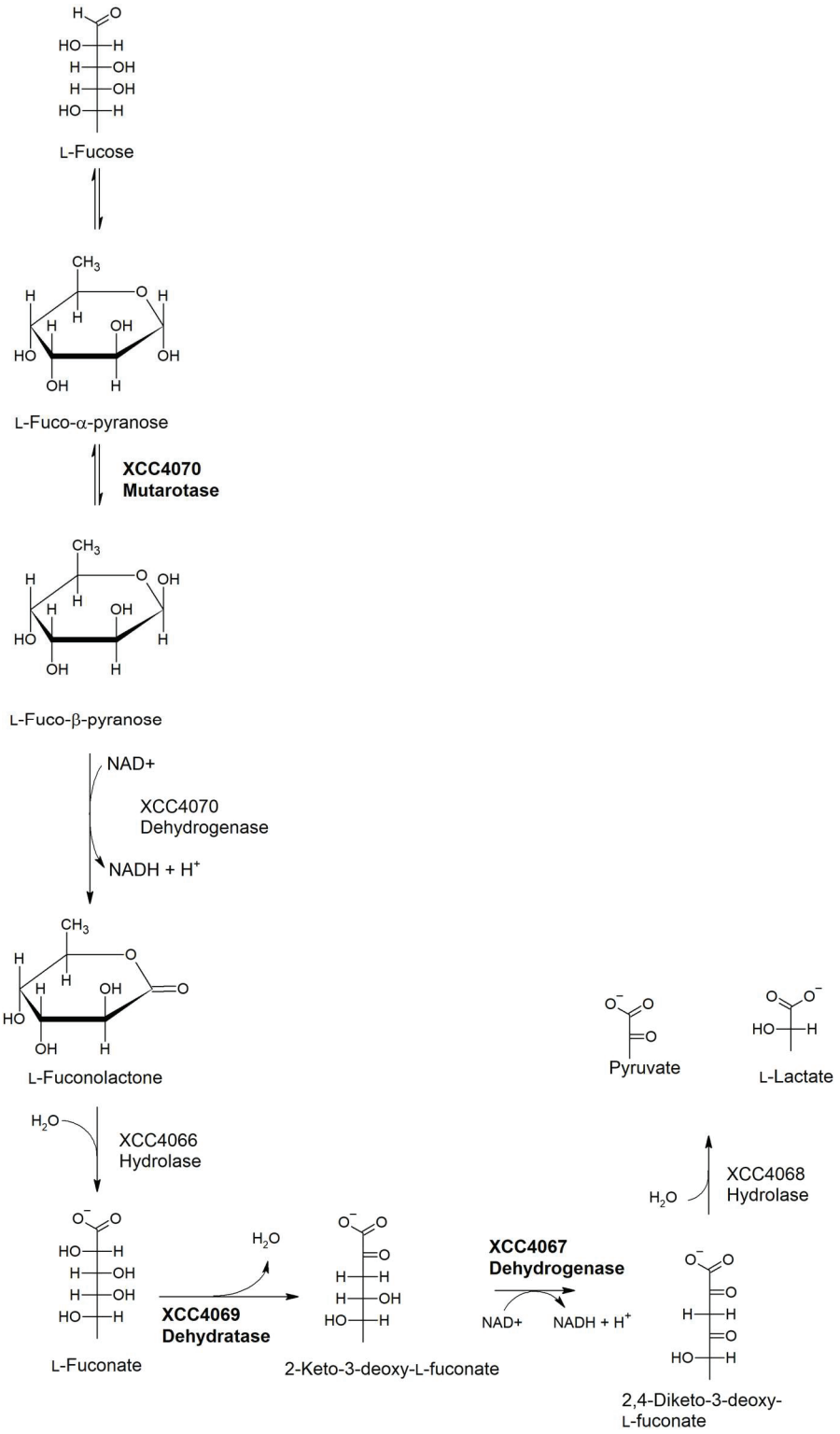

Figure 1.9 Catabolic pathway of L-fucose in *X. campestris* as inferred from homology to genes of known function. Bolded genes were expressed and functionally tested by Gerlt and colleagues (Yew, W. *et al*., 2006).

1.2.2 STRUCTURE OF FucD

The structure of FucD (E.C. 4.2.1.68) is characteristic of MR subgroup enzymes (section 1.1.7). The N and C terminal α+β capping domain and modified TIM barrel domains are as described for MR (Section 1.1.2). An interdigitating loop extends from the capping domain of one protomer into the active site of the neighboring protomer adding a Trp residue as a binding determinant. Trp 101 is within 4 Å of the terminal methyl group of L-fuconate and is presumed to bind with the substrate via hydrophobic interactions (Yew, W. *et al*., 2006). The neighboring protomer contributing a substrate binding determinant is similar to MR which has an analogous Leu residue to the Trp of FucD (Bearne, Stephen L., 2017).

This close association between protomers demonstrated by the interdigitating loop led Gerlt and co-workers to presume FucD is a dimer (Fig 1.10). However, all enzymes in the MR subgroup have a close dimer arrangement which often then dimerizes or tetramerizes to form functional tetramers or octamers in solution (Bearne, S. L. & St. Maurice, 2017). Unlike MR, extensive studies to determine the oligomeric state of FucD in solution have not been conducted (Fee *et al*., 1974b).

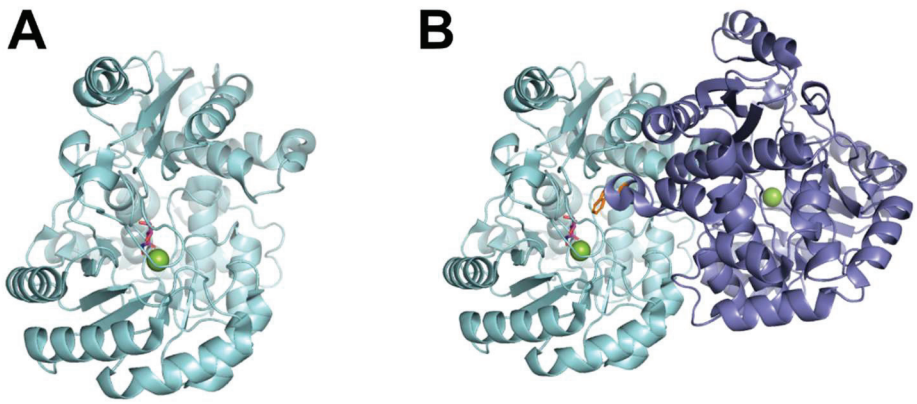

Figure 1.10 Monomeric and Dimeric FucD. Both monomer (A) and dimer (B) structures of FucD are shown, D-erythronohydroxamate is shown in magenta and the Mg^{2+} in green. Trp 101 (orange) is shown positioned in the active site of the neighboring protomer (B) (PDB entry 2HXT).

1.2.3 MECHANISM OF FucD

Through deuterium exchange experiments with several substrates, as well as analysis of the crystal structure, it was determined that Lys 220 abstracts the α-proton of L-fuconate to create the *aci*-carboxylate intermediate followed by elimination and protonation of the hydroxyl leaving group by His 351 (Scheme 1.6) (Yew, W. *et al*., 2006). The precise residues involved in ketonization are not conclusively known; however, the solvent derived deuterium comes from the side of the active site of Lys 220 leading to the proposed mechanism in scheme 1.6.

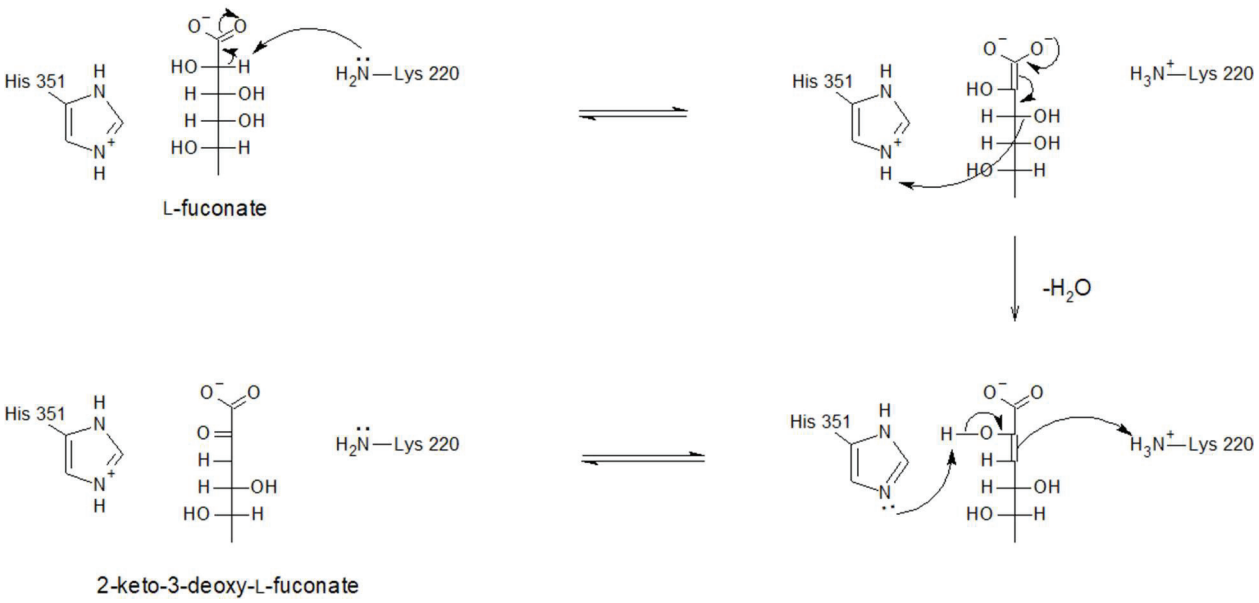

Scheme 1.6 Mechanism of L-fuconate dehydratase (FucD).

The primary substrate of FucD was determined to be L-fuconate by highest observed activity and operon context. However, significant dehydration of L-galactonate and D-arabinonate was also observed (Fig 1.11) (Yew, W. *et al*., 2006). Some dehydration of D-altronate was observed but much less than the above-mentioned substrates although significant exchange of the α-proton with solvent deuterium was observed indicating the *aci*-carboxylate intermediate was efficiently formed. Furthermore, epimerization of L-talonate and D-ribonate (epimers at C-2 of L-galactonate and D-arabinonate) was observed, although no back reaction was detected. There was no activity detected with D-fuconate as expected of a substrate when all binding determinant hydroxyl bearing carbons are of the opposite stereochemistry. The chirality of carbons 2 through 5 are identical for the best determined substrates of FucD L-fuconate, L-galactonate, and D-arabinonate (Fig 1.11).

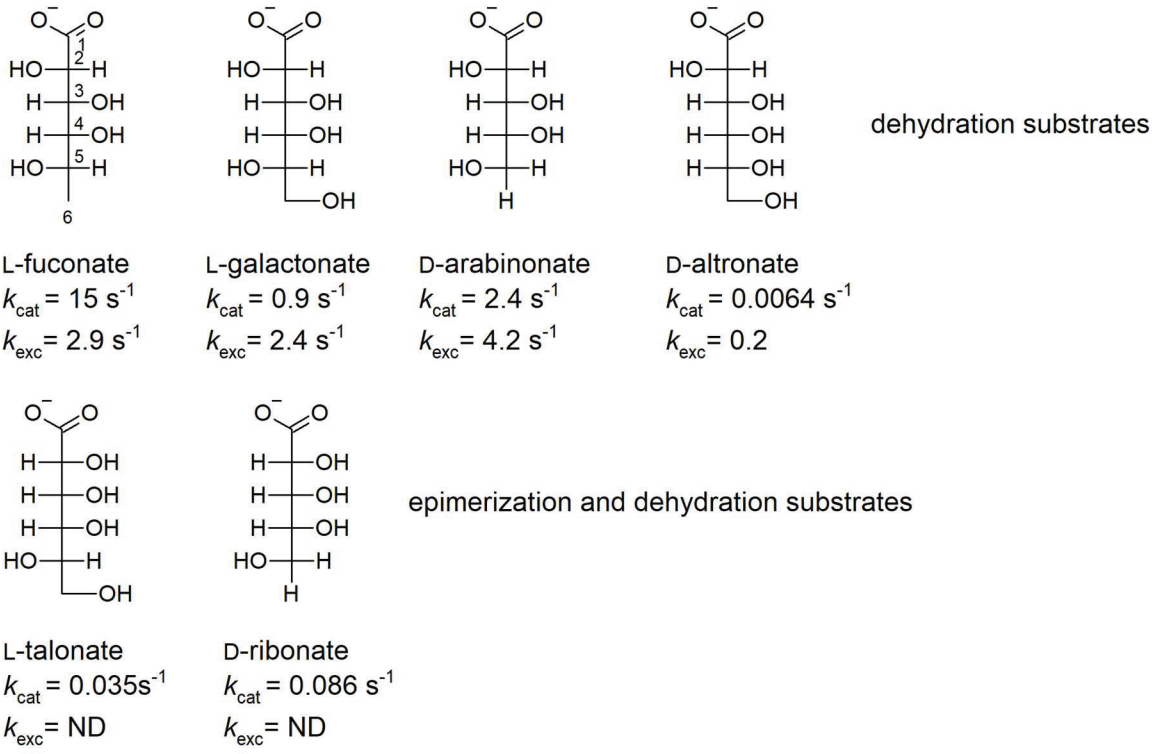

Figure 1.11 Substrates of FucD and kinetic parameters. Modified from Gerlt and co-workers (Yew, W. *et al*., 2006). Numbering scheme is shown on L-fuconate. k_{cat} = rate constant for dehydration, k_{exc} = rate constant for exchange of the α-proton with deuterium, ND = not detected.

Analysis of the crystal structures of both wild-type FucD with the intermediate analogue D-erythronohydroxamate and K220A FucD with L-fuconate bound reveal several hydrogen bonding interactions between L-fuconate/D-erythronohydroxamate and the active site. In brief, the 3-OH group is hydrogen bonded to His 351 and the backbone oxygen of Gly 353, the 4-OH group is hydrogen bonded to Asp 24 and the 5-OH group is hydrogen bonded to the backbone carbonyl of Gly 22 and the hydroxyl of Tyr 32. The 6-CH_3 group is enclosed in a hydrophobic pocket formed by Pro 30, Ile 56, and Trp 101 from the other protomer in the dimeric pair. The 2-OH group chelates the Mg^{2+} ion with one of the carboxylate oxygens. Similar to Lys 164 in MR, Lys 218 hydrogen bonds with the carboxylate oxygen on L-fuconate that is also coordinated to the Mg^{2+} ion while Lys 220 is positioned to abstract the α-proton (Figure 1.12).

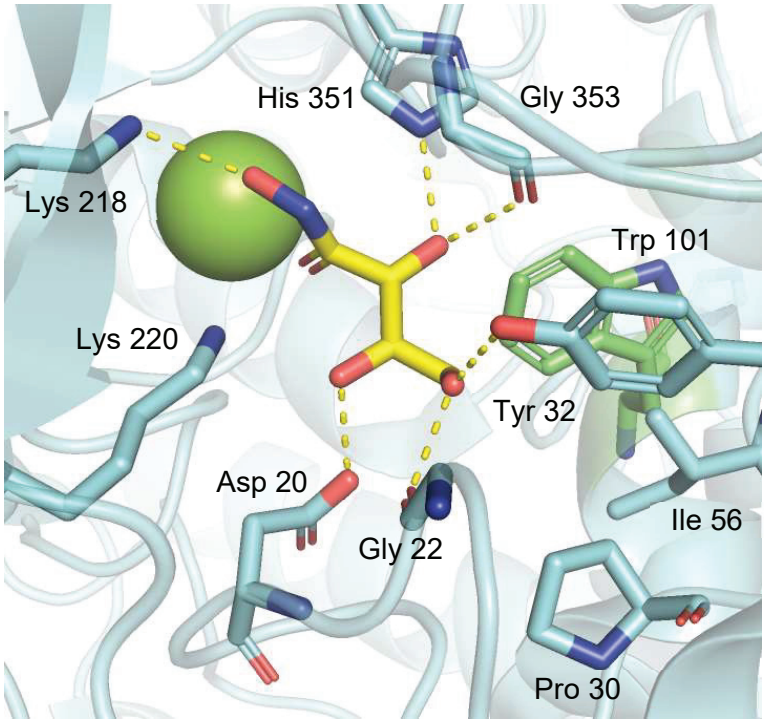

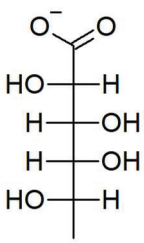

L-fuconate

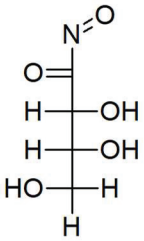

D-erythronohydroxamate

Figure 1.12 Binding of D-erythronohydroxamate in the active site of FucD with stated hydrogen bonding interactions. Trp 101 is coloured green to indicate that it is contributed from the neighboring protomer in the dimer. Polar contacts are indicated with yellow dashed lines, D-erythronohydroxamate is in yellow and the Mg^{2+} ion is in green (PDB entry 2HXT).

The hydrogen bonding interactions from hydroxyls 2 through 5 are important for substrate recognition but also for determining what kind of chemistry takes place and how efficiently. For example, D-altronate has identical stereochemistry at all carbons to L-fuconate except C-5 where the hydroxyl is facing the opposite direction. D-Altronate is a substrate of FucD, but deuterium exchange at the α-carbon was found to be much greater than the observed rate of dehydration. Therefore, although not critical for formation of the *aci*-carboxylate intermediate, it is likely that the interactions between a 5-OH and Gly 22 and Tyr 32 orients substrates to facilitate effective subsequent β-elimination.

It is also interesting that FucD can catalyze the epimerization of L-talonate and D-ribonate to L-galactonate and D-arabinonate, respectively. Since the stereochemistry at C2 is inverted for L-talonate and D-ribonate relative to L-fuconate, the α-proton is presented to His 351 rather than Lys 220. No incorporation of solvent deuterium was observed when L-talonate or D-ribonate were employed as substrates, reminiscent of no deuterium exchange occurring with the K166M MR variant and (*R*)-mandelate (Nagar, Mitesh & Bearne, 2015). These observations suggest that the α-proton of L-talonate and D-ribonate is being abstracted by the monoprotic base His 351. In addition to epimerization, L-talonate and D-ribonate undergo slow dehydration as substrates. This is intuitive given that the *aci*-carboxylate intermediate generated would be the same as for L-galactonate and D-arabinonate, although generation of the intermediate is slower using His 351 instead as the Brønsted base instead of Lys 220.

FucD also catalyzes the ketonization of the dehydrated product instead of releasing the enol to the bulk solvent like other mandelate racemase subgroup members

(Yew, W. *et al*., 2006). ^{1}H and ^{13}C NMR spectroscopy experiments indicated that protonation of the dehydrated enol product was stereospecific. Therefore, FucD catalyzes ketonization in the active site rather than releasing the enol product to solution for stereo-random solvent catalyzed tautomerization. This activity suggests further adaptation of FucD to its role as a dehydratase compared to other MR subgroup dehydratases given this added catalytic activity.

The range of reactions catalyzed by FucD demonstrates the premise of divergent evolution within the MR subgroup of enzymes. The core catalytic machinery responsible for abstracting a proton alpha to a carboxylate group remains constant, but the active site of each subgroup member is adapted to improve its efficiency in its particular role. This is demonstrated by FucD's optimization for anti-elimination shown by the essential 5-OH interaction with Gly 22 and Tyr 32 as well as its weak ability to abstract the α-proton of L-talonate and D-ribonate.

1.3 OVERVIEW OF THIS WORK

This work was undertaken to gather evidence to more fully understand the character of the conserved catalytic Brønsted acid-base His and Lys active site residues in MR subgroup members mandelate racemase (MR) and L-fuconate dehydratase (FucD). The importance of the residue at the tip of the FucD interdigitating loop (Trp 101) in FucD catalysis was also studied as well as the oligomeric state of FucD.

The most well studied MR subgroup member is MR. An interesting characteristic of MR that came to light in the work of Gerlt and colleagues in the 1990s is the decreased pK_a of Lys 166 of 6.4 from 10 (Kallarakal *et al*., 1995). I explored Tyr 137 as part of a

putative Tyr 137-Lys 164-Lys 166 triad as a mechanism for reducing the pK_a of Lys 166 of MR. I found Lys 164 was essential for substrate binding and catalysis by characterization of K164M and K164C MR variants. I investigated the role of Tyr 137 in catalysis by conducting pH studies with a Y137F MR variant. Not only was a change in the pK_a of Lys 166 observed but also His 297 which is 7 Å away from Tyr 137 in the active site. The results were consistent with the hypothesis that Tyr 137 and Lys 164 work in conjunction to reduce the pK_a of Lys 166 but also that there are long-range effects that arise from removing the hydroxyl from Tyr 137. It was also found that a cation-π interaction between Tyr 137 and Lys 164 is not crucial for catalysis.

FucD was studied to understand how the character of the conserved Lys and His residues behave in a MR subgroup member adapted to catalyzing β-elimination instead of racemization or epimerization. The catalytic residue targeting inhibitors tartronate and 3-hydroxypyruvate (3-HP) were employed to assess whether binding would occur given the Lys, His and Mg^{2+} ion that serve as binding determinants for these inhibitors are conserved between MR and FucD. Tartronate was found to be a weak linear mixed-type inhibitor of FucD. 3-HP was found to be an irreversible inhibitor of FucD with drastically reduced efficiency compared to what was found with MR (Nagar, Mitesh *et al*., 2015). Due to the slow nature of the inactivation, it was possible to determine the mode of inhibition and show 3-HP is a competitive inhibitor. Inactivation of FucD by 3-HP occurred through a different mechanism than was observed for the 3-HP-dependent inactivation of MR. MS/MS analysis showed a 58-Da adduct instead of a 86-Da adduct to Lys 220 in inactivated samples contrasting to what was found for MR (Nagar, Mitesh *et al*., 2015). Furthermore, there were multiple 58-Da adducts found at other sites instead of

only one 86-Da adduct indicating a reactive substrate was released into solution. Mapping of residues bearing a 58-Da adduct showed adducts on one face of the FucD dimer indicating the enzyme may exist as a higher oligomeric state in solution. This oligomeric state was investigated in solution via dynamic light scattering (DLS) and gel filtration HPLC (GF-HPLC). The diameter of the FucD species in solution was found to be 6.4 ± 0.4 nm from DLS and 114.5 ± 1.3 kDa from GF-HPLC consistent with a dimer and thus an alternate hypothesis for why 58-Da adducts are localized to one side of FucD had to be proposed.

Finally, the residue at the tip of the interdigitating loop of FucD (Trp 101) was mutated to investigate its role in substrate binding. X-ray crystal structures position Trp 101 4 Å from the 6-CH_3 group of L-fuconate. Therefore, mutation of Trp 101 to a positively charged amino acid was completed to promote binding of *m*-galactarate where the 6-CH_3 group is exchanged for a carboxylate. Mutation to an Arg or Lys residue did not allow FucD to catalyze dehydration of *m*-galactarate and eliminated catalysis with L-fuconate. Furthermore, mutation of Trp 101 to a Glu residue resulted in similar loss of activity with L-fuconate while even the more conservative W101Q variant was inactive. This finding suggests an important role for Trp 101 in catalysis or substrate binding. The possibility that mutating Trp 101 changed the oligomeric state of FucD was also investigated and all variants were found to be dimers.

CHAPTER 2 TYROSINE 137 IN MANDELATE RACEMASE CATALYSIS

Reproduced in part with permission from – Fetter, C., Morrison, Z., Nagar, M., Douglas, C., and Bearne, S. L. (2019) Altering the Y137-K164-K166 triad of mandelate racemase and its effect on the observed pK_a of the Brønsted base catalysts. Arch. Biochem. Biophys. ***666****, 116-126. Copyright Elsevier publishing*

2.1 INTRODUCTION

As discussed in chapter 1, MR catalyzes an acid-base reaction to convert the enantiomers of mandelate. Consequently, pH studies have been undertaken to gain understanding of the pK_as of the relevant catalytic residues (Kallarakal *et al*., 1995; Landro *et al*., 1991; Schafer *et al*., 1996). MR displays a bell-shaped pH dependence on k_{cat} and k_{cat}/K_m and two pK_a values can be ascertained by fitting eqn 2.1 to the data, which represents ionization states of the enzyme-substrate complex and the free enzyme, respectively (Scheme 2.1). The observed pK_as are not attributed to the substrate given that the pK_a of mandelate is well below the assayable pH range (3.41) (Jencks & Regenstein, 1968).

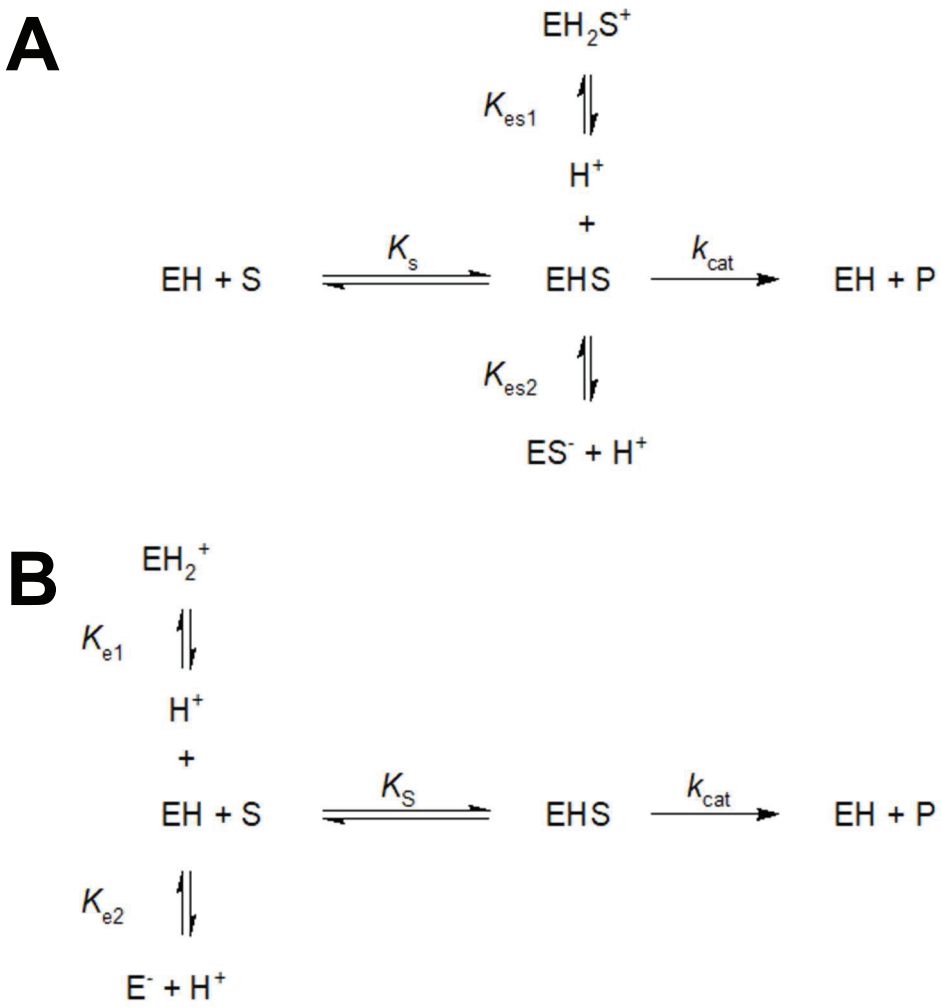

Scheme 2.1 Sample pH-dependent activity of an enzyme. Shown are schemes used to derive eqn 2.1 where the either the k_{cat} (A) or k_{cat}/K_m (B) data are analyzed (E = enzyme, S = substrate, H = hydrogen, K_e is the equilibrium constant for protonation of the free enzyme, K_{es} is the equilibrium constant for the protonation of the enzyme-substrate complex, K_s is the enzyme substrate dissociation constant ($K_s = K_m$ for MR (St Maurice, Martin & Bearne, 2002)), and k_{cat} is the turnover number.

$$\log y_{obs} = \log y_{max} - \log(1 + 10^{(pK_{a1} - pH)} + 10^{(pH - pK_{a2})})$$

Equation 2.1 Where y is k_{cat} or k_{cat}/K_m and pK_as either correspond to pK_es or pK_{es}s in Scheme 2.1.

Using (*S*)- or (*R*)-mandelate as a substrate gives pK_{es} values of 6.4 and 10 (Landro *et al*., 1991). Mutagenesis studies were completed by John Gerlt and co-workers in attempts to tie these pK_{es} values to specific active site residue pK_as. It was found that in the *S* to *R* reaction direction the pK_{es} of 6.4 corresponds to Lys 166 since changing this residue to an Arg increased this value to 8, consistent with the ~2 pK_a unit difference between Lys and Arg residues (Kallarakal *et al*., 1995). However, no change was observed in the descending limb when the reaction was carried out with (*R*)-mandelate where Lys 166 is known to act as the conjugate acid (Landro *et al*., 1991). Similarly, the pK_{es} of 6.4 found in the *R* to *S* reaction direction was determined to belong to His 297 given that when Asp 270, which hydrogen bonds to His 297, was mutated to an Asn the pK_{es} was drastically reduced so as to be unobservable (Schafer *et al*., 1996). However, similar to the K166R study, the pK_{es} of 10 was not perturbed when (*S*)-mandelate was used as a substrate during which His 297 acts to protonate the *aci*-carboxylate intermediate. Therefore, a pK_a of 6.4 was attributed to both Lys 166 and His 297 when they acted as a base but the residue responsible for loss of activity above pH 10 has yet to be identified.

Relevant to this work is the finding that the pK_a of Lys 166 was 6.4 in the active site of MR given this value is 4 pK_a units lower than the value of 10.5 commonly observed in folded proteins (Grimsley, Scholtz, & Pace, 2009). Therefore, there must be a mechanism in the active site of MR to favor a neutral deprotonated Lys reflected by this decreased pK_a. The mechanism postulated by which the neutral form of Lys 166 is stabilized stems from Lys 164 directly adjacent to Lys 166 in the active site. A positive Lys 164 would make a positive Lys 166 unfavorable by electrostatic repulsion and thus

promote the deprotonation of Lys 166 (Landro *et al*., 1991). This mechanism is similar to that initially postulated for acetoacetate decarboxylase given the proximity of Lys 116 and the catalytic Lys 115 with a determined pK_a of 6 in the primary sequence (Kokesh & Westheimer, 1971). However, when the X-ray crystal structure of acetoacetate decarboxylase was solved, this mechanism was found not to be true since Lys 115 and Lys 116 were pointed away from each other such that the amino groups could not interact. Therefore, the reduction of the pK_a of Lys 115 was attributed to its position in a hydrophobic pocket (Ho, Menetret, Tsuruta, & Allen, 2009).

To test the hypothesis that Lys 164 decreases the pK_a of Lys 166, the K164M and K164C MR variants were assayed for their activity and feasibility for pH studies. However, these MR variants were found to have very low activity and were not suitable for the assays at the suboptimal pH ranges that would be required. Tyr 137 hydrogen bonds to Lys 164 in MR crystal structures and could be acting to hold Lys 164 in a position such that it is available to interact with Lys 166 (Fig 2.1 and 2.2). Therefore, MR variants that eliminated this hydrogen bond (Y137F) and a possible cation-π interaction (Y137L) were investigated. Later, Y137S and Y137T MR variants were used to determine the effect of reintroduction of a hydroxyl group.

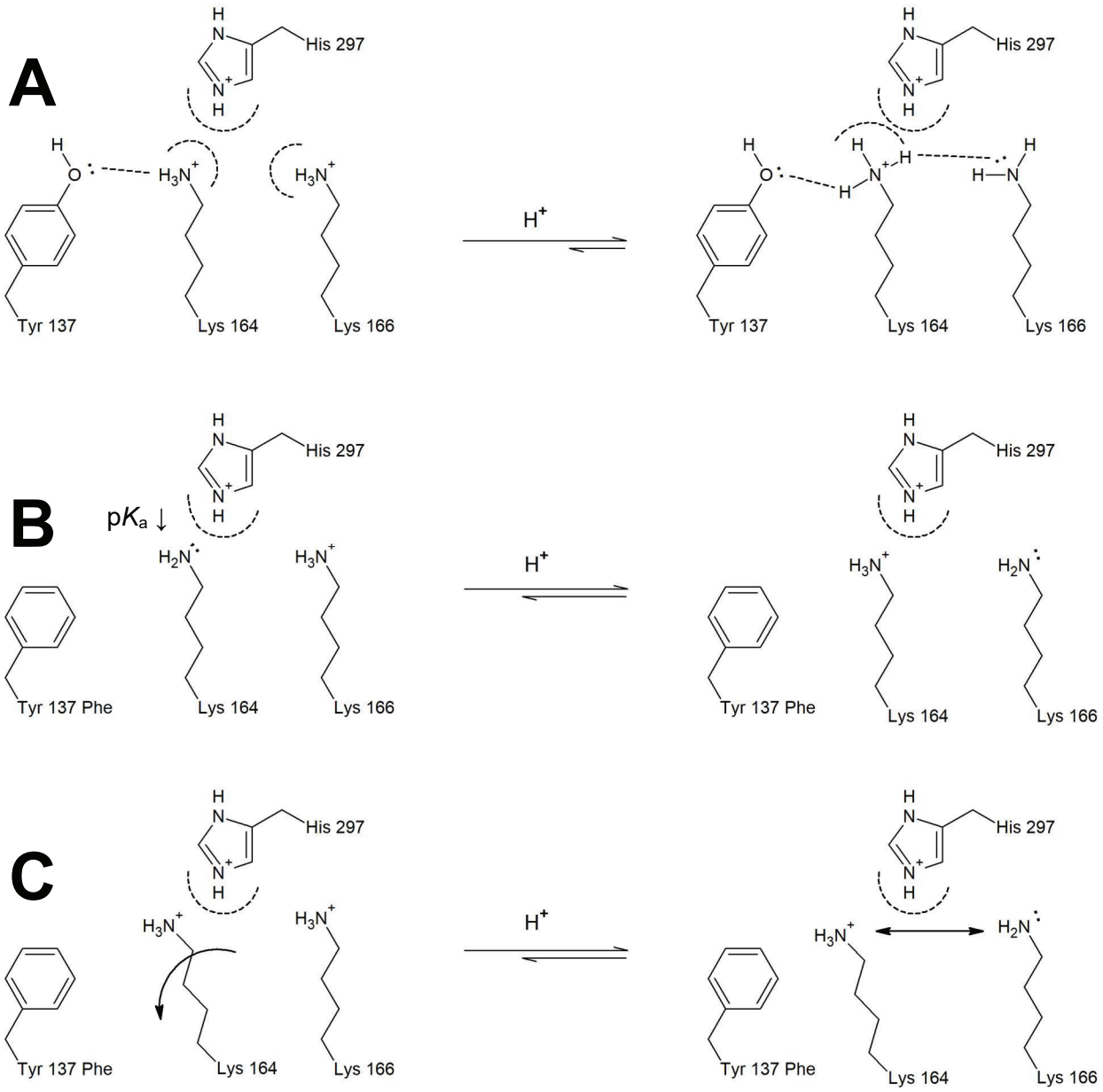

Figure 2.1 Mechanism by which Tyr 137 affects the pK_a of Lys 166. A) WT enzyme: Tyr 137 stabilizes Lys 164 in position to increase the favorability of a neutral Lys 166. B) Y137F variant: The lack of a Tyr 137-Lys 164 hydrogen bond decreases the pK_a of Lys 164, reducing its abundance as a positive species able to decrease the pK_a of Lys 166. C) Y137F variant: Without the tethering hydrogen bond, Lys 164 may move away from Lys 166 so that they no longer interact. Modified from Fetter *et al*. (Fetter, Morrison, Nagar, Douglas, & Bearne, 2019).

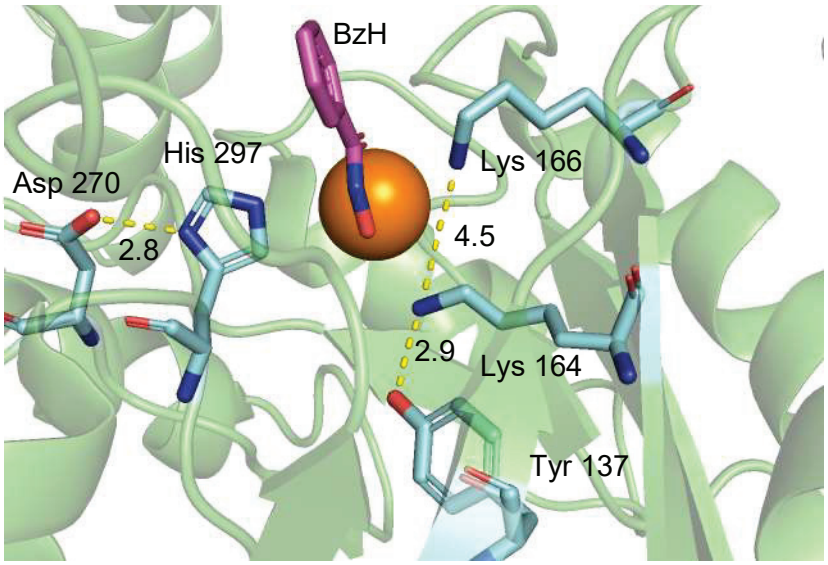

Figure 2.2 Active site of MR with Tyr 137-Lys 164-Lys 166 putative triad and His 297-Asp 270 Dyad. Distances are in Å. Orange sphere is the Mg^{2+} ion and BzH is shown in magenta. Distances (Å) unlabeled for clarity: Tyr 137-Mg^{2+} ion = 6.6, Tyr 137-His 297 = 7.0, and Lys 164-His 297 = 5.7 (pdb entry 3UXK).

2.2 MATERIALS AND METHODS

2.2.1 GENERAL

All reagents were purchased from Sigma-Aldrich Canada Ltd. (Oakville, ON, Canada) unless otherwise stated. Circular Dichroism (CD) spectra and time course experimental data were collected using a JASCO J-810 spectropolarimeter (Jasco Inc., Easton, MI). Proton nuclear magnetic resonance (^{1}H NMR) spectra were obtained using a Bruker AV 500 MHz spectrometer at the Dalhousie University Nuclear Magnetic Resonance Research Resource Center (NMR-3).

2.2.2 SITE-DIRECTED MUTAGENESIS

A pET52b (+) plasmid encoding wild-type MR from *Pseudomonas putida* bearing an N-terminal STREP II tag was extracted from *Escherichia coli* DH5α cells using a

Qiagen miniprep kit (Qiagen, Toronto, ON) according to manufacturer's instructions and used as template DNA for site-directed mutagenesis. The primers used for mutagenesis are listed in table 2.1 (Integrated DNA Technologies Coralville, IA). Phusion high fidelity polymerase was used for all amplification reactions according to manufacturer's instructions (New England Biolabs, Ipswich, MA). "PCR" conditions used were 98 °C for 30 s for initial denaturation followed by 16 cycles of 20 s at 98 ˚C for denaturation, 30 s at 66 °C for annealing, 5 min at 72 °C for elongation followed by storage at 12 °C. The reaction product was treated with DpnI overnight at 37 °C to remove wild-type methylated template DNA. PCR products were transformed into chemically competent DH5α cells using the standard heat shock method. DNA extracted via miniprep (Qiagen, Toronto, ON) from transformed colonies were sequenced to verify that only selected mutations to the MR gene were introduced (Robarts Research institute, London, ON). Verified plasmids were used to transform *E. coli* BL21 (DE3) cells, using the standard heat shock method, for protein expression.

Table 2.1 Primers for site-directed mutagenesis of MR variants. All primers are shown in the 5′ to 3′ direction. The altered codon is underlined and exchanged bases are in boldface. K164M and K164C variants were created by Mitesh Nagar, Y137F and Y137L MR variants by Zach Morrison, and Y137S and Y137T MR variants by Chris Fetter.

MR Variant	Primer type	Primer Sequence
K164M	F	GGATTCCGGGCGGTTA**T**GACCAAGATCG
	R	GCCGATCTTGGTC**A**TAACCGCCCGGAAT
K164C	F	GGATTCCGGGCGGTT**TGC**ACCAAGATCG
	R	GCCGATCTTGGT**GCA**AACCGCCCGGAAT
Y137F	F	CGACCAGTTCAGGCT**TT**TGACAGCCACAGCTTGG
	R	CCAAGCTGTGGCTGTCA**A**AAGCCTGAACTGGTCG
Y137L	F	CGACCAGTTCAGGCT**TTG**GACAGCCACAGCTTGG
	R	CCAAGCTGTGGCTGTC**CA**AAGCCTGAACTGGTCG
Y137S	F	CGACCAGTTCAGGCT**TC**TGACAGCCACAGCTTGG
	R	CCAAGCTGTGGCTGTCA**G**AAGCCTGAACTGGTCG
Y137T	F	CGACCAGTTCAGGCT**AC**TGACAGCCACAGCTTGG
	R	CCAAGCTGTGGCTGTCA**GT**AGCCTGAACTGGTCG

2.2.3 PROTEIN EXPRESSION, PURIFICATION, AND QUANTIFICATION

Wild type (WT), Y137L, and K164C MR variants were expressed and purified according to the protocol described by Narmandakh and Bearne for WT MR (Narmandakh & Bearne, 2010). Briefly, starter cultures of *E. coli* BL21 (DE3) cells were grown overnight from glycerol stocks in sterile LB media containing 100 μg/mL ampicillin. Expression cultures (2-L, LB media, 100 μg/mL ampicillin) were inoculated with overnight starter cultures (10-mL per L) and incubated at 37 °C with shaking (220 rpm) for 5 to 7 h without induction by isopropyl β-D-1-thiogalactopyranoside (IPTG). Cells were harvested by centrifugation (3795 × *g*, 10 min × 2, 4 °C,) and stored at −20 °C for future use. Frozen cell pellets were thawed and resuspended in ~30 mL cold wash buffer (100 mM Tris, 150 mM NaCl, 1 mM EDTA, pH 8.0). The cell solution was kept on ice and sonicated 6 × 30 s on a Branson Sonifier 250 with 1 min breaks (setting 5.5, 1-s bursts). The cell lysate was clarified by ultracentrifugation (146 550 × *g*, 35 min, 4 °C) and applied to a column containing Strep-Tactin Superflow affinity resin (10-mL) using an ÄKTA FPLC from GE Healthcare (Baie d'Urfé, PQ, Canada) kept at 4 °C. Protein was eluted with addition of wash buffer containing 2.5 mM desthiobiotin. Samples were dialyzed 3 × 8 h against storage buffer (100 mM HEPES, 3.3 mM $MgCl_2$, 150 mM NaCl, 10 % v/v glycerol), aliquoted in 1-mL portions and stored at −20 ˚C for future use. Storage buffer for Y137F MR was slightly different and included 10 mM $MgCl_2$ given initially Mg^{2+} affinity was unknown for this variant.

The Y137F, Y137S, Y137T, and K164M MR variants were expressed and purified as described above except expression cultures were grown for 3 h at 37 °C

followed by 24 h at ~25 °C (room temperature) following the procedure recently developed for *Salmonella typhimuriam* L-talarate/galactarate dehydratase (E.C. 4.2.1.42, TGD) by Bearne and colleagues (Easton, Aboushawareb, & Bearne, 2018).

Protein concentrations were obtained via Bradford assays conducted according to manufacturer's directions (Bio-Rad Laboratories, Mississauga, ON) with bovine serum albumin standards. Alternatively, UV absorbance at 280 nm with extinction coefficients calculated by the ExPASy ProtParam tool assuming all cysteines were reduced were used to determine protein concentration (Gasteiger *et al*., 2003) (WT, K164M, K164C = 53400 $M^{-1}cm^{-1}$; Y137F, Y137L, Y137S, Y137T = 51910 $M^{-1}s^{-1}$). Purity was verified by SDS-PAGE (10%) with Coomassie staining.

2.2.4 KINETIC ASSAYS

MR kinetic CD-basedassays were conducted as previously described (Narmandakh & Bearne, 2010; Sharp, Hegeman, & Kenyon, 1979). Briefly, purified MR was stored in assay buffer (100 mM HEPES, 3.3 mM $MgCl_2$) with 0.01 % w/v BSA on ice. At each assay point 100 µL MR was added to a 1900 µL solution of substrate ((*R*)- or (*S*)-mandelate) in a 1-cm pathlength quartz cuvette, mixed, and the transmittance of circularly polarized light at 262 nm was measured to track reaction progress from the substrate enantiomer of mandelate to a racemic mixture. Enzyme concentrations used were 3.64 nM, 100 nM, and 182-364 nM for WT, Y137L, and Y137F MR respectively. The Michaelis-Menten equation (eqn. 2.2) was fit to the initial velocity data to obtain K_m and k_{cat} ($V_{max}/[E]_T$) values using *KaleidaGraph* software (v. 4.02, Synergy Software, Reading, PA) for non-linear regression analysis. Experiments were conducted in triplicate

and data are reported as average values with errors corresponding to standard deviation values. Maximum velocity (V_{max}) values were divided by enzyme concentrations obtained via mg/mL data collected by Bradford assays divided by calculated molecular weights (Da): 41263.78 (wild-type), 41238.75 (K164C), 41266.80 (K164M), 41247.78 (Y137F), 41213.77 (Y137L), 41187.69 (Y137S), and 41201.71 (Y137T) obtained from the amino acid sequence using the ExPASy ProtParam tool (Gasteiger *et al*., 2003).

$$v_{\mathrm{i}} = \frac{V_{\mathrm{max}}[\mathrm{S}]}{K_{\mathrm{m}} + [\mathrm{S}]}$$

Equation 2.2

Assays with the K164M and K164C MR variants were conducted using a 0.5-cm pathlength cuvette and higher enzyme concentrations (520 μg/mL, 12.1 μM) than other MR variants (see above). Substrate concentrations were limited by CD instrument voltage constraints balanced against a required cuvette pathlength to observe activity (3 to 20 mM (*R*)- and (*S*)-mandelate for K164C MR and a fixed value of 20 mM for K164M MR). Values for k_{cat}/K_m were obtained as the slope of eqn 2.3 fitted to the initial velocity data.

$$v_{\mathrm{i}} = \frac{k_{\mathrm{cat}}}{K_{\mathrm{m}}}[\mathrm{E}]_{\mathrm{T}}[\mathrm{S}]$$

Equation 2.3

2.2.5 IC_{50} EXPERIMENTS

Concentrations of benzohydroxamate (BzH) giving 50% inhibition of Y137S and Y137T MR variants were determined using the CD-basedassay with 1 mM (*R*)-mandelate (at K_m). Eqn 2.4 was fit to data using *Kaleidagraph v. 4.02* software where *n* is the Hill coefficient. IC_{50} values were related to K_i constants assuming competitive inhibition by eqn 2.5 (Yung-Chi & Prusoff, 1973).

$$\frac{v_i}{v_o} = \frac{IC_{50}^n}{IC_{50}^n + [I]^n}$$

Equation 2.4

$$K_i = \frac{IC_{50}}{1 + ({}^{[S]}/_{K_m})}$$

Equation 2.5

2.2.6 pH STUDIES

Kinetic assays were conducted using the MR CD assay at pH values ranging from 5.5 to 10.25. The buffers used were MES (5.50, 5.75, 6.00 and 6.50), HEPES (7.00, 7.50, 8.00, 8.50), TAPS (8.50), CHES (9.00, 9.50 and 9.75) and CAPS (10.00, 10.25) at a concentration of 100 mM with 10 mM $MgCl_2$ for Y137F MR and 3.3 mM for WT MR. All buffers used had been used in previous pH studies with MR. This was done since effects due to changing buffer environments had been ruled out in previous studies (Kallarakal et al., 1995; Landro et al., 1991; Nagar, Mitesh, Kumar, & Bearne, 2018; Schafer et al., 1996; St Maurice, M. & Bearne, 2000). The enzyme and substrate concentration ranges used are listed in table 2.2 and needed to be varied due to changes in

activity and K_m observed for MR at the extreme pH regions. Eqn. 2.1 was fit to the initial velocity data using *Kaleidagraph v. 4.02* software.

Table 2.2 Conditions for pH-rate study assays

Buffer	pH	WT MR			
		$[E]_T$, μM	[(*R*)-mandelate], mM	$[E]_T$, μM	[(*S*)-mandelate], mM
MES	5.75	0.0036	0.25-15	0.0036	0.25-15
	6.00	0.0036	0.25-15	0.0036	0.25-15
	6.50	0.0036	0.25-15	0.0036	0.25-15
HEPES	7.00	0.0036	0.25-15	0.0036	0.25-15
	7.50	0.0036	0.25-15	0.0036	0.25-15
	8.00	0.0036	0.25-15	0.0036	0.25-15
TAPS	8.50	0.0036	0.5-15	0.0036	0.25-15
CHES	9.00	0.0036	1-20	0.0036	0.5-20
	9.50	0.0036	1-20	0.0036	0.5-20
	9.75	0.0036	1-20	0.0036	0.5-20
		Y137F MR			
MES	5.50	0.364	0.5-20	0.364	0.5-20
	5.75	0.364	0.5-20	0.364	0.5-20
	6.00	0.364	0.5-20	0.364	0.5-20
	6.50	0.182	0.5-20	0.182	0.5-20
HEPES	7.00	0.182	0.5-20	0.182	0.5-20
	7.50	0.182	0.5-20	0.182	0.5-20
	8.00	0.182	0.5-20	0.182	0.5-20
TAPS	8.50	0.182	0.5-20	0.182	0.5-20
CHES	9.00	0.182	1-20	0.182	1-20
	9.50	0.182	1-20	0.182	1-20
CAPS	10.00	0.364	1-20	0.364	1-20
	10.25	0.364	1-20	0.364	1-20

2.2.7 Mg^{2+} AFFINITY ASSAYS

The affinity for Y137F MR for Mg^{2+} was assessed using the assay developed by Fee and colleagues (Fee *et al*., 1974b). Y137F MR samples were dialyzed against HEPES buffer containing EDTA and glycerol (100 mM HEPES, 10 mM EDTA, 10 % v/v glycerol, pH 7.5) (2 mL sample per 250 mL buffer, 2 × 8 h, 4 °C). EDTA was then removed by dialysis against Mg^{2+} free storage buffer (100 mM HEPES, 200 mM NaCl, 10 % v/v glycerol, pH 7.5) with the same dialysis conditions used throughout all following steps in this section. These enzyme stocks were stored at –20 °C in 1 mL aliquots until needed. Prior to conducting assays, enzyme stocks were dialyzed against Mg^{2+} assay buffer (100 mM HEPES, pH 7.5) for immediate use and an assay stock was prepared to a concentration of 3.6 μM with 0.001% w/v BSA. At each assay point, enzyme was incubated with the desired [Mg^{2+}] (ranging from 0.05 to 2.5 mM) for 5 min at 25 °C prior to starting the reaction by addition of (*S*)-mandelate to a final concentration of 15 mM. Activity was measured using the CD-based assay and plotted against [Mg^{2+}]. The enzyme concentration used was 7.50 μg/mL (182 nM) with 0.00005% w/v BSA in the assay cuvette. The affinity of Y137F MR for Mg^{2+} in terms of K_A was estimated by fitting eq 2.6 to initial velocity data. Assays were conducted in triplicate where average K_A and standard deviations are reported.

$$v_i = \frac{V_{max}[Mg^{2+}]}{K_A + [Mg^{2+}]}$$

Equation 2.6

2.2.8 CIRCULAR DICHROISM

To assess whether the mutations had caused any large changes of secondary structure, CD spectra of all MR variants were collected and overlaid with the WT MR spectra. K164C, K164M, Y137S and Y137T MR were dialyzed overnight into sodium phosphate buffer (10 mM, pH 7.5) containing 3.3 mM $MgSO_4$ and the concentration was determined using a Bradford assay with BSA standards. Protein solutions of the same concentration 36 μg/mL (0.88 μM) were then added to a 0.1-cm pathlength quartz cuvette and CD spectra from 195 to 260 nm were recorded. The same procedure was carried out for Y137F and Y137L MR variants by the previous lab member Zach Morrison (Fetter *et al*., 2019). Spectra were recorded in triplicate and averaged. Buffer spectra in absence of protein were also recorded in triplicate, averaged, and subtracted from spectra including protein samples.

2.2.9 DEUTERIUM EXCHANGE

Deuterium exchange experiments were conducted for WT and K164C MR. HEPES buffer as well as (*R*)- and (*S*)-mandelate were dissolved in D_2O and lyophilized twice to replace all exchangeable protons with deuterons. Solutions (5 mL) in D_2O containing 100 mM HEPES buffer, 3.3 mM $MgCl_2$, 15 mM (*R*)- or (*S*)-mandelate at a pD of 7.5 were prepared. To initiate the reaction final concentrations of 1.5 μg/mL (36.4 nM) WT or 66.5 μg/mL (1.61 μM) K164C MR were added and 750 μL aliquots were taken at various timepoints where the reaction was stopped by acidification of each aliquot with 10 μL of concentrated DCl to a pD of ~1. All aliquots were analyzed using ^1H NMR and comparison of the relative integration between the α-^1H peak (singlet, ~5.37 ppm) to the

aromatic proton peak at ~7.37 ppm (5 protons) was used to determine reaction progress. The ^{1}H chemical shifts were determined in relation to the ^{1}H-OD peak at 4.79 ppm (Gottlieb, Kotlyar, & Nudelman, 1997).

2.3 RESULTS

2.3.1 LYS 164 MR VARIANTS

Both K164M and K164C MR exhibited extremely low activity compared to the WT enzyme. Affinity for (*R*)- and (*S*)-mandelate was drastically reduced as shown by the lack of saturation observed indicating a much increased K_m value possibly in excess of 20 mM (Fig 2.3). From the slope of the line shown in Fig. 2.3 a k_{cat}/K_m value could be estimated and was found to be five-orders of magnitude lower than that of WT MR (Table 2.3). Given the large amounts of enzyme required for kinetic studies, only the K164C variant was studied more extensively due to higher purification yields.

Table 2.3 Kinetic data for all tested MR variants. Values are from triplicate experiments and errors are standard deviations (WT = wild type). [a] Data collected by Zach Morrison.[b] ND = Not determined. [c] K_i values are derived from the Cheng-Prusoff equation (eqn. 3) (Yung-Chi & Prusoff, 1973) assuming competitive inhibition.[d] K_d value from ITC experiments carried out by Mitesh Nagar (Fetter *et al*., 2019).

MR variant	K_A (Mg^{2+}), mM	K_i (BzH), µM	$R \rightarrow S$			$S \rightarrow R$			K_{eq} ([*S*]/[*R*])
			K_m, mM	k_{cat}, s^{-1}	k_{cat}/K_m, $\times 10^5\ M^{-1}s^{-1}$	K_m, mM	k_{cat}, s^{-1}	k_{cat}/K_m, $M^{-1}s^{-1}$ $\times 10^5\ M^{-1}s^{-1}$	
WT	0.32 ± 0.02[a]	12.8 ± 1.2[a]	1.03 ± 0.05	1029 ± 8	10.0 ± 0.5	0.76 ± 0.03	775 ± 10	10.2 ± 0.5	1.0 ± 0.1
Y137L	0.20 ± 0.02[a]	162 ± 16[a]	1.79 ± 0.04	50 ± 2	0.28 ± 0.01	3.1 ± 0.1	84.0 ± 0.8	0.28 ± 0.01	1.0 ± 0.1
Y137F	0.27 ± 0.03	95 ± 12[a]	3.8 ± 0.5	150 ± 10	0.40 ± 0.07	4.0 ± 0.6	135 ± 2	0.34 ± 0.04	0.9 ± 0.1
Y137S	ND[b]	517± 24[c]	2.0 ± 0.2	9.0 ± 0.6	0.046 ± 0.03	2.9 ± 0.2	16.3 ± 0.4	0.057 ± 0.003	1.4 ± 0.2
Y137T	ND	753 ± 40[c]	1.7 ± 0.1	10.8 ± 0.2	0.064 ± 0.02	3.57 ± 0.09	23.1 ± 0.4	0.066 ± 0.003	1.2 ± 0.1
K164M	ND	ND	–	–	6.1 (± 0.1) × 10^{-5}	–	–	4.7 (± 0.4) × 10^{-5}	1.3 ± 0.1
K164C	ND	94.6 ± 9.6[d]	–	–	2.9 (± 0.1) × 10^{-5}	–	–	2.8 (± 0.2) × 10^{-5}	0.9 ± 0.1

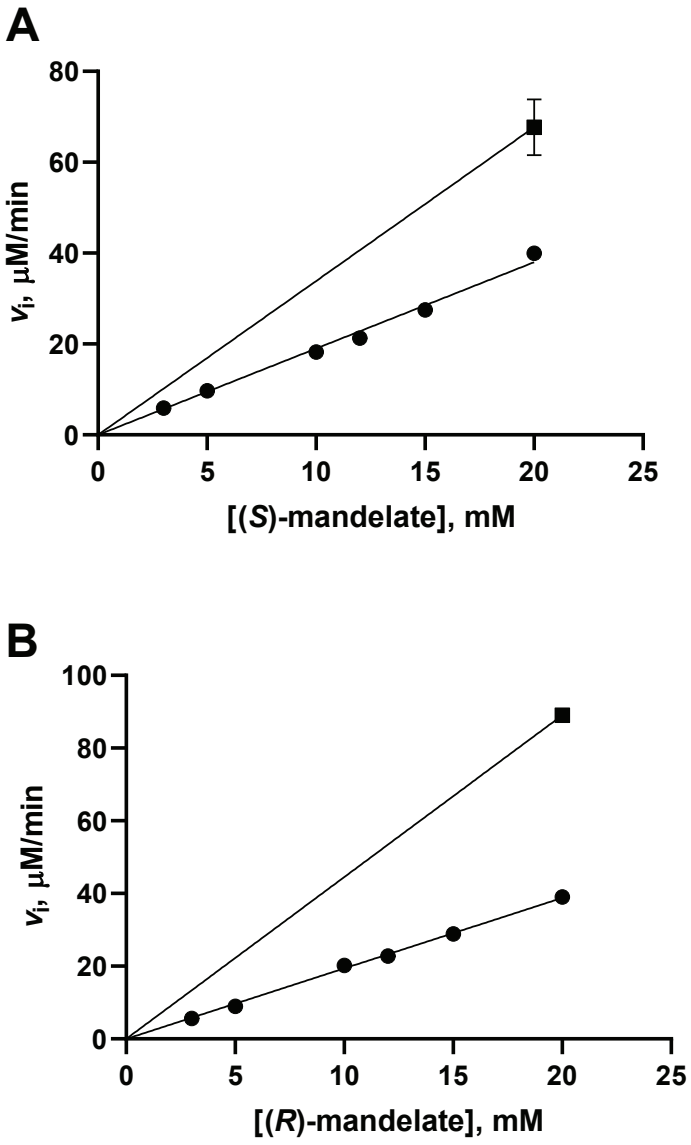

Figure 2.3 Estimation of k_{cat}/K_m for K164M and K164C MR. K164M MR (■), K164C MR (●). Data were collected at indicated substrate concentrations using a 5-mm pathlength quartz cuvette using the CD assay. $[E]_T$ was 520 μg/mL (12.1 μM). Only one point (20 mM) was determined in triplicate for the K164M MR variant due to its low purification yields, error bars (where visible) represent standard deviations.

To investigate the effect of Lys 164 on catalysis more thoroughly, deuterium exchange experiments were completed comparing WT and K164C MR (Fig 2.4). WT MR results were as reported in the literature (Landro et al., 1991; Nagar, Mitesh & Bearne, 2015), but no exchange was observed for K164C MR .

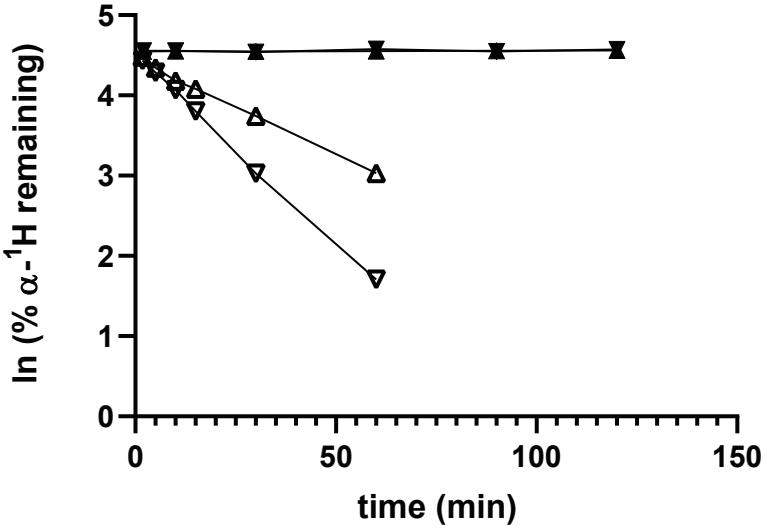

Figure 2.4 Deuterium exchange of wild-type (WT) and K164C MR variants. WT (*R*)-mandelate (△) WT (*S*)-mandelate (▽), K164C MR (*R*)-mandelate (▼), K164C MR (*S*)-mandelate (▲).

2.3.2 ACTIVITY OBSERVED FOR TYR 137 MR VARIANTS

Various Tyr 137 MR variants were assayed for activity to investigate the role of this residue in catalysis. All variants were found to have easily measurable activity that was reduced by ~1 to 3 orders of magnitude relative to WT MR (Table 2.3). Given the relative proximity (6.6 Å) of the Tyr 137 hydroxyl group to the Mg^{2+} ion in crystal structures, the metal binding affinity of the variants was assayed (Fig 2.5A). However, no change in Mg^{2+} affinity was detected with removal of the Tyr 137 hydroxyl group in the Y137F and Y137L MR variants (Fig 2.5B, Table 2.3).

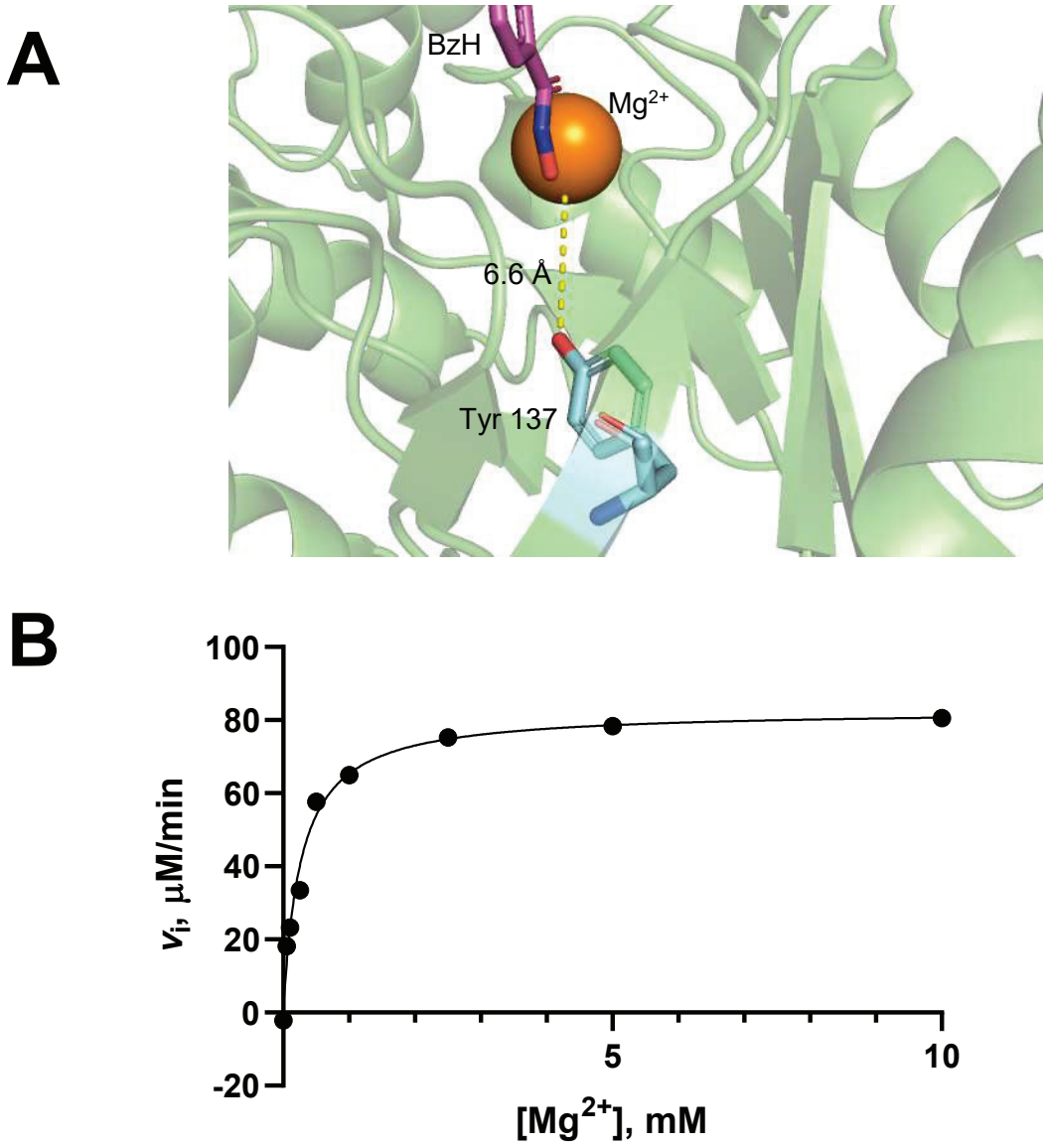

Figure 2.5 Mg^{2+} affinity of Y137F MR and active site structure showing the proximity of Tyr 137 to the Mg^{2+} ion. The X-ray crystal structure of the WT MR active site showing distance between Tyr 137 and the Mg^{2+} ion where Tyr 137 is cyan, Mg^{2+} is orange and the transition state analogue BzH is magenta (pdb entry 3UXK) (A). A representative Mg^{2+} affinity assay plot is shown for Y137F MR, analogous assays were conducted for WT and Y137L MR by Zach Morrison (Fetter *et al*., 2019) (B).

2.3.3 EFFECT OF THE Y137F MUTATION ON THE pK_aS OF MR

The effect of removing the hydroxyl group on Tyr 137 on the pK_as of the active site residues of MR was investigated via pH-rate profiles. The pK_as of the enzyme-substrate (ES) complex as well as the free enzyme (E) were probed via fitting eqn 2.1 to logk_{cat} or logk_{cat}/K_m vs. pH data (Table 2.4) as stated in the materials and methods (section 2.2.6). Given the pK_a of mandelate is below the assayed pH range (3.41) pK_as found by fitting logk_{cat}/K_m data represent pK_as of the free enzyme (E) and not substrate (S) (Jencks & Regenstein, 1968). Using (*S*)-mandelate as substrate, the pK_as shifted "inward" for the Y137F MR variant compared to WT MR giving a narrower curve for all Y137F MR pH-rate plots (Fig 2.6, Table 2.5). The same effect was observed when (*R*)-mandelate was used as substrate. Of note is that the pK_as corresponding to the ascending curve of all pH profiles was more affected than the descending curve pK_a. This is important given the pK_as of the ascending curve in the logk_{cat} vs. pH profiles have been assigned to active site amino acid residues and allow conclusions regarding the effect of the Y137F mutation on the pK_as of nearby residues to be drawn.

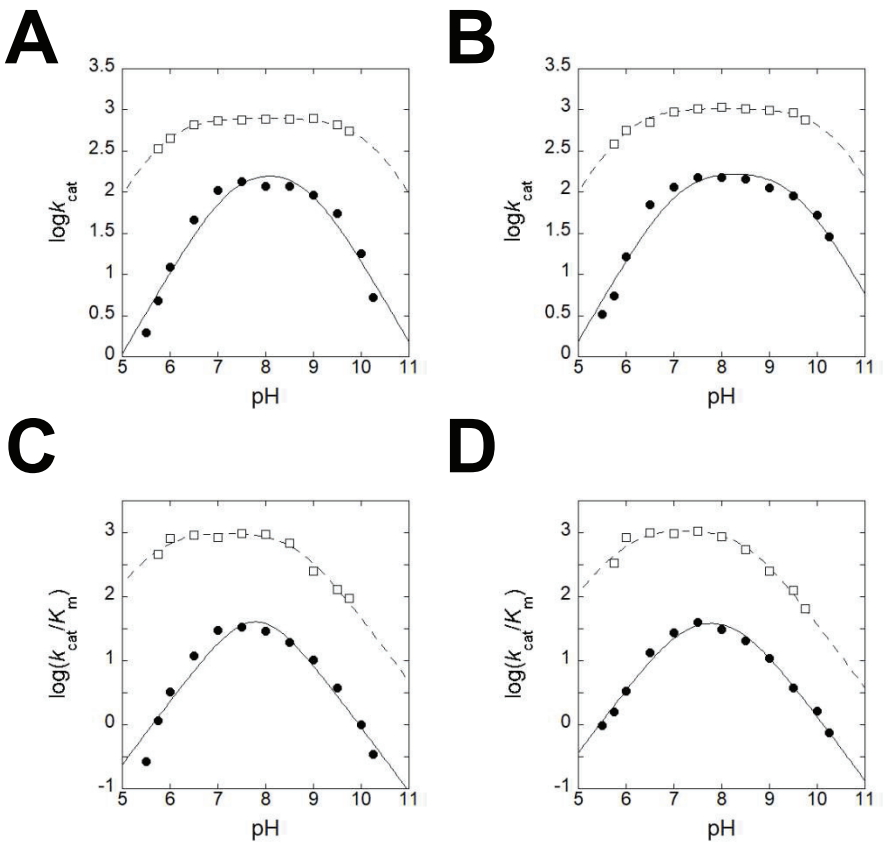

Figure 2.6 pH-rate profiles of Y137F and WT MR. A) (*S*)-mandelate log(k_{cat}) vs. pH profiles, B) (*R*)-mandelate log(k_{cat}) vs. pH profiles, C) (*S*)-mandelate log(k_{cat}/K_m) vs. pH profiles, D) (*R*)-mandelate log(k_{cat}/K_m) vs. pH profiles. WT MR (□), Y137F MR (●).

Table 2.4 k_{cat} and K_m data for WT and Y137F MR at indicated assayed pH values. [a] Errors from direct fitting of eqn 1 to initial velocity data. [b] Errors are standard deviations from triplicate experiments.

WT MR[a]					
		$R \rightarrow S$		$S \rightarrow R$	
		k_{cat} (s^{-1})	K_m (mM)	k_{cat} (s^{-1})	K_m (mM)
Buffer	pH				
MES	5.75	388.21 ± 5.81	1.15 ± 0.06	339.00 ± 3.91	0.73 ± 0.04
	6.00	570.26 ± 12.56	0.68 ± 0.06	453.32 ± 5.22	0.56 ± 0.03
	6.50	710.47 ± 12.56	0.70 ± 0.05	665.54 ± 12.29	0.72 ± 0.06
HEPES	7.00	938.11 ± 20.62	0.97 ± 0.08	731.06 ± 21.10	0.87 ± 0.10
	7.50	1031.23 ± 10.77	0.96 ± 0.04	759.94 ± 19.89	0.79 ± 0.09
	8.00	1075.61 ± 17.08	1.23 ± 0.08	767.64 ± 14.88	0.82 ± 0.07
TAPS	8.50	1034.99 ± 19.22	1.89 ± 0.11	776.68 ± 8.37	1.14 ± 0.05
CHES	9.00	980.93 ± 14.35	3.89 ± 0.17	786.17 ± 13.85	3.09 ± 0.19
	9.50	915.69 ± 30.40	7.22 ± 0.58	662.42 ± 16.37	5.08 ± 0.36
	9.75	762.60 ± 33.55	11.85 ± 1.04	556.51 ± 14.59	5.97 ± 0.42
Y137F MR[b]					
MES	5.50	3.26 ± 0.04	3.33 ± 0.55	1.94 ± 0.01	7.22 ± 2.27
	5.75	5.45 ± 0.25	3.46 ± 0.25	4.77 ± 0.24	4.08 ± 0.66
	6.00	16.60 ± 0.61	4.97 ± 0.28	12.15 ± 0.81	3.68 ± 0.29
	6.50	70.52 ± 5.13	5.22 ± 0.35	46.18 ± 2.04	3.85 ± 0.12
HEPES	7.00	116.17 ± 2.16	4.29 ± 0.20	106.15 ± 4.36	3.55 ± 0.41
	7.50	149.96 ± 9.63	3.79 ± 0.51	135.45 ± 1.76	4.04 ± 0.60
	8.00	150.03 ± 3.85	4.93 ± 0.69	118.99 ± 1.98	4.15 ± 0.15
TAPS	8.50	145.69 ± 3.95	7.01 ± 0.80	116.72 ± 3.68	6.01 ± 0.57
CHES	9.00	113.44 ± 3.48	10.49 ± 0.87	92.66 ± 8.22	9.08 ± 0.65
	9.50	89.67 ± 2.28	23.78 ± 1.45	55.11 ± 2.83	14.67 ± 0.52
CAPS	10.00	52.11 ± 1.48	32.18 ± 1.87	18.0 ± 0.63	18.00 ± 2.47
	10.25	28.5 ± 1.49	38.02 ± 4.78	5.2 ± 0.24	15.17 ± 1.74

Table 2.5 pK_e and pK_{es} values from from logk_{cat}/K_m and log(k_{cat}) vs. pH profiles in Fig. 2.6. [a] Values from literature reference (Landro *et al*., 1991).

MR variant	(*S*) → (*R*)-mandelate					
	pK_{e1}	pK_{e2}	log$(k_{cat}/K_m)^{max}$	pK_{es1}	pK_{es2}	log$(k_{cat})^{max}$
Y137F	7.2 ± 0.1	8.4 ± 0.1	4.76 ± 0.09	7.1 ± 0.1	9.5 ± 0.2	2.27 ± 0.09
Wild-type	6.0 ± 0.1	8.51 ± 0.08	6.07 ± 0.05	5.97 ± 0.04	10.2 ± 0.1	3.02 ± 0.01
Wild-type[a]				6.4	10.0	
	(*R*) → (*S*)-mandelate					
Y137F	7.6 ± 0.4	8.0 ± 0.4	5.0 ± 0.4	7.3 ± 0.2	8.9 ± 0.2	2.3 ± 0.1
Wild-type	5.8 ± 0.2	8.66 ± 0.08	6.03 ± 0.04	5.88 ± 0.02	10.14 ± 0.05	2.91 ± 0.01
Wild-type[a]				6.4	10.0	

It was evident that the K_m value remained largely constant until a pH of 8.5 was reached, which is near the descending curve of the profile (Table 2.4 and 2.5). This result is consistent with previous work that found that $K_m = K_s$ for MR at optimal pH (7.5) but adds that above pH 8.5 there appears to be additional processes that affect substrate binding (Cornish-Bowden, 1976; Knowles & Jencks, 1976; St Maurice, Martin & Bearne, 2002).

2.3.4 SUBSTITUTION OF TYR 137 BY LEU, SER, AND THR RESIDUES

In order to investigate the role of a potential cation-π interaction between a protonated amino group of Lys 164 and the phenyl ring of Tyr 137, a Y137L variant was kinetically characterized. No large changes in activity between the Y137F (which maintains potential for a cation-π interaction) and the Y137L MR variants was observed leading to the conclusion that a cation-π interaction at this position is not critical for catalysis (Table 2.3).

Given the impact of removing the Tyr 137 hydroxyl group on the observed pK_a values of MR, reintroduction of a hydroxyl group was attempted to assess whether activity could be regained. No activity was regained with the Y137S and Y137T MR variants (Table 2.3). However, it must be noted that the pK_a of Tyr phenol vs. Ser and Thr alcohol protons is significantly different (Grimsley *et al*., 2009). The general size difference between Tyr, Ser and Thr residues may also be at fault for not rescuing activity with these mutations. CD spectra of all mutants showed no gross alterations in secondary structure (Fig 2.7). Similarly, SDS-PAGE analysis showed all MR variants to be sufficiently purified (Fig 2.8).

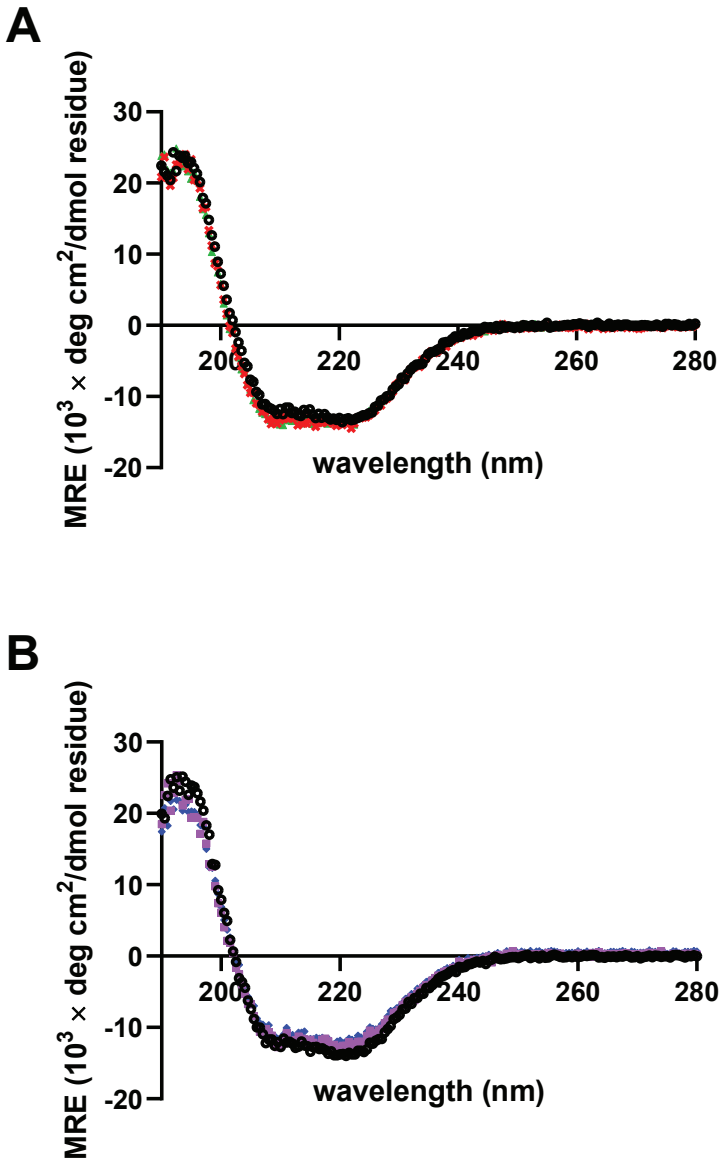

Figure 2.7 CD spectra of MR variants. A) Overlaid CD spectra of WT, Y137S and, Y137T MR variants B) Overlaid CD spectra of WT, K164M and, K164C MR variants. WT MR (○), Y137S MR (×), Y137T MR (▲), K164M MR (■), K164C MR (◆). For spectra of Y137F and Y137L MR variants collected by Zach Morrison see (Fetter *et al*., 2019). MRE = mean residue ellipticity.

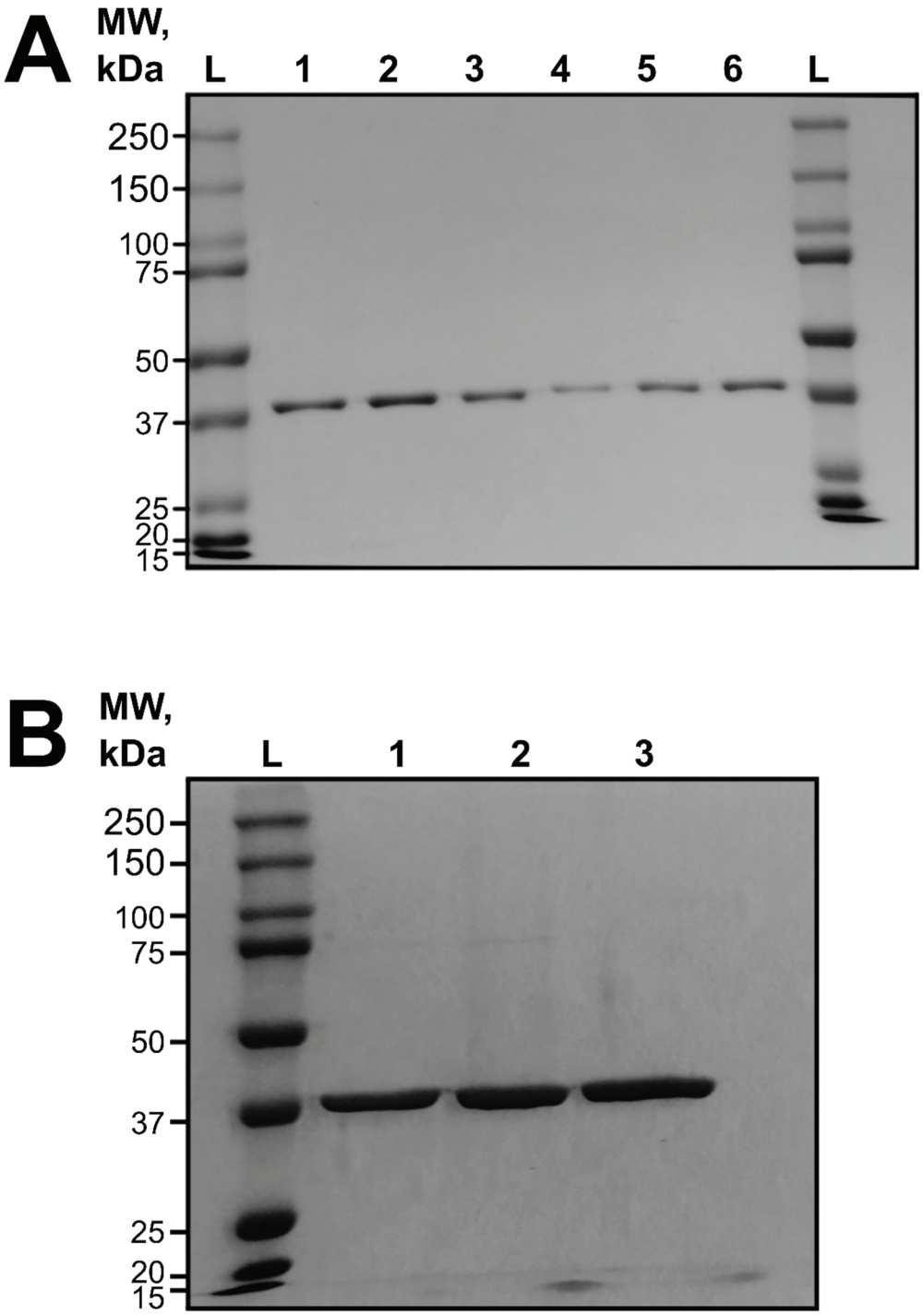

Figure 2.8 SDS-PAGE gels of MR variants. Shown are 10% SDS polyacrylamide gels of MR variants. The lanes correspond to ladder = L, wild type = 1 and 6, K164M = 2, K164C = 3, Y137S = 4, Y137T = 5 in (A). In figure (B) L = ladder, 1 = Y137L MR, 2 = Y137F MR and 3 = wild type MR. Sizes are in kDa, MW = molecular weight. Calculated MR variant MW: WT = 41.6 kDa, K164M = 42.6 kDa, K164C = 44.2 kDa, Y137S = 38.15, Y137T = 38.8 kDa, Y137L = 41.0 kDa, Y137F = 41.8 kDa.

Inhibition studies with the transition state analogue inhibitor BzH (St Maurice, M. & Bearne, 2000) were also carried out with all Tyr 137 MR variants. A linear free energy relationship (LFER) was found between the $\log(1/K_i)$ and $\log(k_{cat}/K_m)$ values found for each enzyme variant. Therefore, Tyr 137 plays a role in stabilization of the transition state. No LFER was found when comparing $\log(1/K_i)$ and $\log(1/K_m)$ values indicating Tyr 137 does not play a significant role in substrate binding (Fig 2.8).

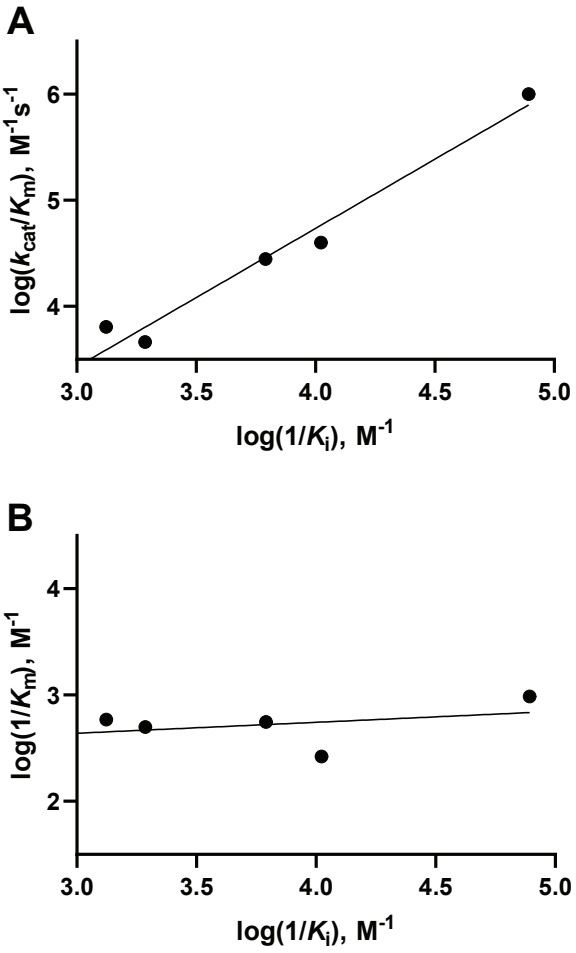

Figure 2.9 Inhibition of Tyr 137 MR variants by BzH yields a Linear Free Energy Relationship. A) Plotting k_{cat}/K_m vs. $1/K_i$ yields a LFER with a slope of 1.31 and a Pearson coefficient (R) of 0.985. Plotting K_m against K_i does not yield a LFER (slope = 2.33, R = 0.355)

2.4 DISCUSSION

2.4.1 THE ROLE OF LYS 164

Given the goal of this study was to investigate whether a positive Lys 164 decreases the pK_a of Lys 166 by electrostatic effects, initial studies centered on the K164M and K164C MR variants. However, the efficiency (k_{cat}/K_m) for both enzymes was severely reduced by approximately 5-orders of magnitude (Table 2.3). Furthermore, the affinity of the K164C variant was severely impacted such that saturation was not observed at even high concentrations of mandelate (20 mM) (Fig 2.3). This lack of activity made the rate of racemization of mandelate enantiomers difficult to detect via the CD-based assay without using high concentrations of enzyme (12.1 μM vs. 0.0036 μM for WT MR) even under optimal pH conditions. Therefore, pH profile studies that would necessitate measurements under non-optimal pH conditions were deemed unfeasible. Deuterium exchange experiments were also conducted as an alternative method to determine whether the K164C variant was able to abstract the α-proton of mandelate. No exchange was observed with either mandelate substrate enantiomer (Fig 2.4). Had enzyme concentrations been as high as those used for the CD assays, exchange might have been observed. Furthermore, increasing the time of the deuterium exchange experiment could have facilitated the detection of weaker activity; but this was not feasible because of the low stability of the enzyme at 25 °C over long periods.

Isothermal titration calorimetry experiments with the K164C MR variant and transition state analogue BzH were previously undertaken by Mitesh Nagar (Fetter *et al*., 2019). These studies found a K_d value of 94.6 ± 9.6 μM, indicating a ~26-fold drop in

affinity for BzH relative to WT enzyme (K_d = 3.7 μM). It was previously found that Lys 166 is critical for binding BzH given the K_d of the K166M and K166C enzyme variant were reduced most significantly of all assayed variants (K166M K_d = 1640 μM, K166C K_d = 3100 μM) (Nagar, Mitesh & Bearne, 2015). Therefore, although binding of BzH was severely impacted by the K164C mutation, it is apparent that Lys 166 is still able to interact with the inhibitor, likely through cation-π interactions. Should Lys 164 be acting to reduce the pK_a, it is possible that Lys 166 is more positively charged in the K164M and K164C variants, which would result in potentially stronger cation-π interactions between Lys 166 and the phenyl ring of BzH. However, this possibly stronger interaction could have been masked in the comparison of K_d values for K164C vs. WT MR for BzH given the additional loss of the interaction between Lys 164 and the hydroxamate oxygen of BzH (Fig 2.10).

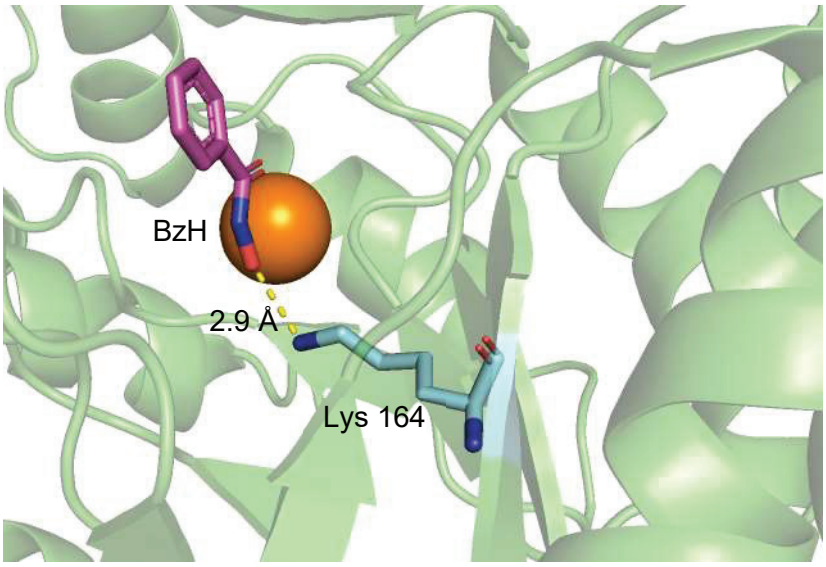

Figure 2.10 Interaction between Lys 164 and hydroxamate oxygen of BzH. (pdb entry 3UXK)

2.4.2 THE ROLE OF TYR 137

Given kinetic experiments with K164M and K164C enzyme variants were not practical under sub-optimal pH conditions, Tyr 137 was investigated as an alternative residue that could give information on the mechanism by which MR reduces the pK_a of Lys 166. In crystal structures of MR with BzH, (*S*)-mandelate and (*S*)-atrolactate bound Tyr 137 is positioned to hydrogen bond to Lys 164 (Fig 2.2) (Kallarakal *et al*., 1995; Lietzan *et al*., 2012; Neidhart *et al*., 1991). Notably, this feature is conserved across several enzymes in the MR subgroup (Fetter *et al*., 2019). We postulated that this interaction could be stabilizing Lys 164 as a positive charge proximal to Lys 166 and therefore assisting Lys 164 to modulate the pK_a of Lys 166 by electrostatic repulsion (Fig 2.1). There was also the possibility that a cation-π interaction between Tyr 137 and Lys 164 was mediating said effect or adding to the effect mediated by the hydrogen bond (Fig 2.10). Therefore, two MR variants to assess both interactions (Y137F and Y137L) were made by the previous lab member Zach Morrison. The activity of both the Y137F and Y137L variants were reduced from WT MR but acceptable for pH studies (Table 2.3). Notably, there was not a large change in activity between the Y137F and Y137L variants, indicating a potential cation-π interaction mediated by the Y137F but not the Y137L MR variant was not critical for catalysis (Fig 2.10). Enzyme variants where the hydroxyl group was reintroduced were also created to assess whether activity could be rescued with Y137S and Y137T enzymes. However, no rescuing of activity was observed (Table 2.3). This result can be rationalized by the difference in the size of Ser and Thr residues compared to Tyr which could impact whether a hydrogen bond to Lys 164 would be possible for distance reasons. Also, the pK_a of alkyl hydroxyl groups ~16 which is

significantly different than phenol hydroxyls (pK_a ~ 10) (Hornback, 2006) and so any hydrogen bond between Ser and Thr residues and Lys 164 could be of significantly different character and thus possibly mediate different effects on the position and/or charge of Lys 164. Inhibition studies with BzH revealed a linear free energy relationship between log(1/K_i) vs. log(k_{cat}/K_m) with a slope of 1.31 ± 0.13 and Pearson coefficient (r) of 0.985 for all the studied Tyr 137 enzyme variants (Fig 2.8). This relationship indicated Tyr 137 plays a role in stabilization of the *aci*-carboxylate intermediate, consistent with an effect on Lys 164 which directly interacts with the hydroxamate oxygen of BzH and carboxylate group of (*S*)-atrolactate in crystal structures (Fig 2.9). This K164-substrate carboxylate interaction could help reduce the unfavorable accumulated negative charge in this area of the molecule resulting from abstraction of the α-proton.

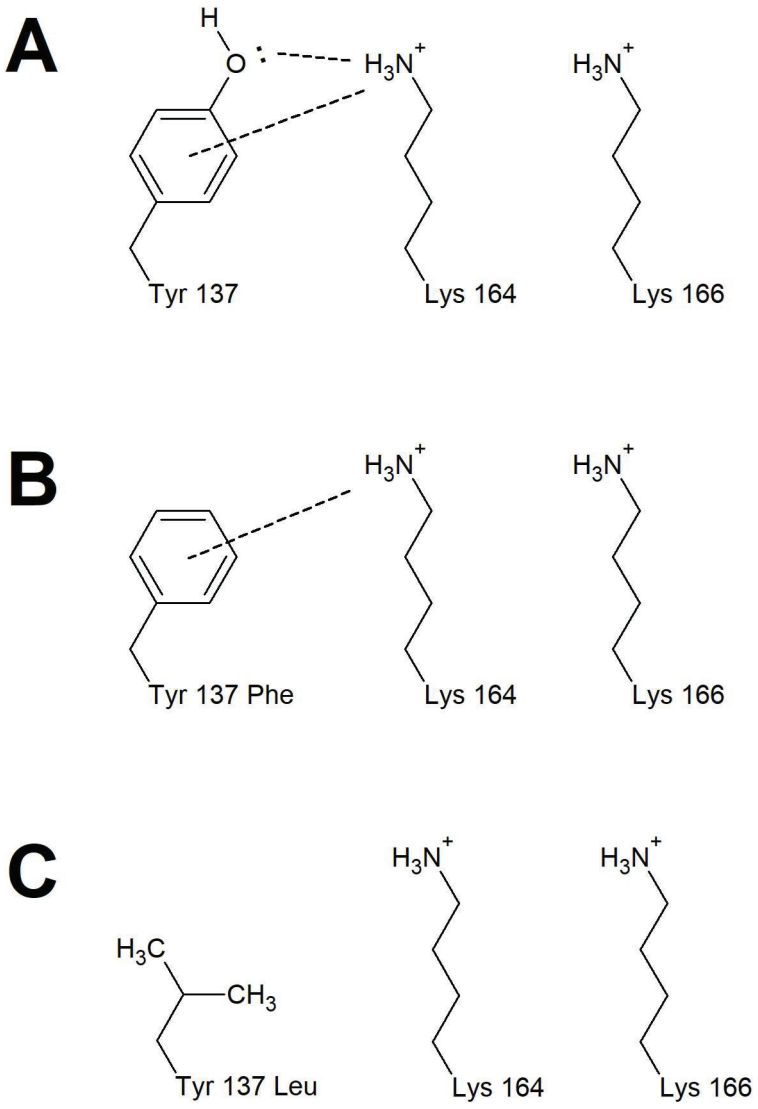

Figure 2.11 Possible interactions between Tyr 137 and Lys 164. MR variants used to assay their importance for catalysis A) WT MR, B) Y137F MR, C) Y137L MR

The Y137F MR enzyme variant was selected for pH-rate studies given its higher activity and the lack of evidence that a Tyr 137-Lys 164 cation-π interaction was crucial for catalysis (Table 2.3). As mentioned, studies undertaken by John Gerlt and colleagues ascribed the pK_a of the ascending limbs of logk_{cat} vs. pH profiles to the residue acting as the base to abstract the α-proton of the substrate mandelate enantiomer used (Lys 166 for (*S*)-mandelate, His 297 for (*R*)-mandelate) (Kallarakal *et al*., 1995; Schafer *et al*., 1996). Therefore, all discussion about the effect of the Y137F mutation on the pK_a values of specific active site residues will be limited to changes observed for the ascending limbs of pH-rate profiles.

It was observed that the Y137F mutation altered the pK_a values of MR compared to those values reported in the literature as well as in the present study for the WT enzyme (Kallarakal *et al*., 1995; Landro *et al*., 1991). When (*S*)-mandelate was used as the substrate the pK_a of the ascending limb shifted 1.4 units from 5.88 ± 0.02 to 7.3 ± 0.2 in the logk_{cat} vs. pH profile. This result corresponds to a ~15-fold greater proportion of protonated Lys 166 in the Y137F variant compared to the WT enzyme in the enzyme-substrate complex. This evidence is consistent with our model that Tyr 137 stabilizes Lys 164 in position to reduce the pK_a of Lys 166. Furthermore, the pK_a values of the ascending limb in the log(k_{cat}/K_m) vs. pH profile are similarly increased by ~1.8 units from 5.8 ± 0.2 to 7.6 ± 0.4. This result indicates that Tyr 137 also acts to reduce the pK_a of Lys 166 in the free enzyme. Interestingly, similar results were obtained when (*R*)-mandelate was used as the substrate and the pK_a of the ascending limb corresponds to His 297. The pK_a of the ascending limb of the logk_{cat} vs. pH and log(k_{cat}/K_m) vs. pH profiles increased 1.1 (5.97 ± 0.04 to 7.1 ± 0.1) and 1.2 (6.0 ± 0.1 to 7.2 ± 0.1) units, respectively.

A potential rationale for the observed increase in the pK_a of His 297 could be that the pK_a of His 297 might be reduced by the proximity of Lys 164 (~5.7 Å) and the Mg^{2+} ion and is brought to a "normal" pK_a by the influence of Asp 270 (Schafer *et al*., 1996). Therefore, when the positive character of Lys 164 is altered in the active site by the Y137F mutation, the pK_a of His 297 might be expected to increase as observed. Nonetheless, this finding was unexpected and suggests that the Y137F mutation has longer range effects on the electrostatic character of the active site than previously anticipated.

Although limited conclusions concerning findings about the descending limb of pH profiles can be made due to findings discussed above by John Gerlt and colleagues it is interesting to note that these pK_a values were also perturbed in the Y137F enzyme variant compared to WT MR. Specifically, in the *R* to *S* reaction direction, the pK_a of the descending limb shifted ~-0.1 units in the free enzyme (8. 51 ± 0.08 to 8.4 ± 0.1) and ~-0.7 units in the enzyme-substrate complex (10.2 ± 0.1 to 9.5 ± 0.2). In the *S* to *R* reaction direction, the pK_a is shifted ~-0.66 units in the free enzyme (8.66 ± 0.08 to 8.0 ± 0.4) and ~-0.7 units in the enzyme-substrate complex (10.2 ± 0.1 to 9.5 ± 0.2). There are several other residues important to MR catalysis that could be pH sensitive. For example the protonation state of Glu 317, which has been proposed to protonate the carboxylate of the *aci*-carboxylate intermediate (Mitra *et al*., 1995), could correspond to reduced activity in higher pH solutions. Therefore, the protonation state of Glu 317 could have been affected by the effect of the Y137F mutation on the electrostatic character of the active site resulting in the changes seen in the descending curve. However, a specific residue(s) responsible for the descending limb pK_a was not identified by this study.

MR is a pseudosymmetric enzyme where only close inspection of deuterium exchange experiments, inactivation by (*R*,*S*)-α-phenylglycidate, and X-ray crystallography data indicate that the base in the *R* to *S* and *S* to *R* reactions directions are different amino acid residues unlike cases like proline racemase where the enantiospecific bases are the same type of amino acid (two cysteines) (Buschiazzo *et al*., 2006; Landro *et al*., 1994; Powers *et al*., 1991). Therefore, one would expect there to be a normal and reverse protonated state on the enzyme corresponding to typical pK_as of the active site residues. In this case the "normal" protonation state would be that His 297 is deprotonated and Lys 166 is protonated, and the "reverse" protonation state would be where His 297 is protonated and Lys 166 is deprotonated. However, given the pK_as of His 297 and Lys 166 are the same in the ground state of MR, as ascertained by the pH studies discussed above, one could expect both states to be equally prevalent. However, this conclusion rests on the assumption that the pK_as of His 297 and Lys 166 do not change when either enantiomer of mandelate is bound. This assumption might not be safe given crystallography studies indicate MR undergoes a conformational shift upon binding since crystals of unliganded MR crack when soaked with (*R*)-atrolactate (Bearne, S. L. & St. Maurice, 2017). In fact, it could be that binding of one substrate might enforce a protonation state that would be most productive to catalysis of the bound enantiomer of mandelate and thus change the relative pK_as of His 297 and Lys 166 upon substrate binding. However, such claims would need supporting experimental evidence which is currently unavailable.

Perhaps the fundamental question concerning the reduced pK_a of Lys 166 in MR is what is the benefit of generating a less basic Lys residue to remove a very weakly

acidic proton (~29 in solution)? Part of the answer could be that abundance of a neutral Lys in the ground state is more important than its basicity. Guthrie and Kluger stated that electrostatic stabilization of the *aci*-carboxylate intermediate in MR could be sufficient to mediate observed rates of catalysis (Guthrie, J. P. & Kluger, 1993). Furthermore, John Gerlt and colleagues postulated that a short-strong hydrogen bond to the carboxylate of mandelate by Glu 317 represents general acid catalysis to protonate the intermediate from an enolate type species to an enol, which is a much more stable compound and would be reflected in a lower pK_a of the mandelate α-proton (Mitra *et al*., 1995). A neutral lysine in the ground state would allow for electron density to be available to remove the α-proton of (*S*)-mandelate whose pK_a in the active site is almost certainly much reduced than the solution value. Closing of the active site flap and exclusion of solvent could increase the basicity of an already neutral Lys 166 to favor the deprotonation of mandelate who's acidity has been increased via interactions with Glu 317, the Mg^{2+} ion and a positive Lys 164 as mentioned previously. In a study of triosephosphate isomerase (TIM) the pK_a of the base responsible for abstraction of the high pK_a substrate proton was indeed increased in the transition state compared to the ground state(Zhai *et al*., 2018). Therefore, it is possible that MR employs both mechanisms of facilitating the abstraction of high pK_a protons mentioned earlier: reduction of the substrate proton pK_a and increasing the basicity of the base responsible for said deprotonation. However, current evidence does not pertain to the transition state pK_as of MR and so further experiments would need to be completed to investigate whether the pK_as of MR active site bases increase at the transition state to help facilitate catalysis.

2.4.3 CONCLUSIONS

It was found that the Y137F mutation increased the pK_a values of Lys 166 and His 297. That the pK_a of Lys 166 was increased with this mutation is consistent with a proposed mechanism where Tyr 137 stabilizes Lys 164 in a position through a hydrogen bond where it can reduce the pK_a of Lys 166. The finding that the pK_a of His 297 was also increased by the Y137F mutation was surprising, but can be rationalized by the hypothesis found in previous literature sources that Lys 164 (along with the Mg^{2+} ion) is acting to reduces the pK_a of His 297 which is then brought to a "normal" value by an interaction with Asp 270 (Schafer *et al*., 1996). It was also found that, although a possibility for a Tyr 137-Lys 164 cation-π interaction exists due to proximity of the residues in the active site, that this interaction is not crucial for catalysis. A LFER was observed between the enzyme efficiency (k_{cat}/K_m) of Tyr 137 MR variants and their inhibition by BzH ($1/K_i$) but not relating substrate binding ($1/K_m$) and $1/K_i$. This finding shows that Tyr 137 plays an indirect role in transition state stabilization. Furthermore, Lys 164 was found to be critical for MR catalysis as indicated by low racemization efficiencies and lack of observed deuterium exchange.

In general, this study investigated the role of two active site residues (Tyr 137 and Lys 164) on the pH dependent catalysis of MR. The findings emphasize the important role of residues in creating a suitable electrostatic environment at the active site that maintains the correct protonation state of residues to facilitate efficient catalysis.

CHAPTER 3 L-FUCONATE DEHYDRATASE: INACTIVATION BY 3-HYDYROXYPYRUVATE AND INTERDIGITATING LOOP MUTANTS

3.1 INTRODUCTION

John Gerlt and colleagues identified the gene GI:21233491 in *Xanthomonas campestris str.* ATCC 33913 as encoding a member of the MR subgroup of the enolase superfamily based on sequence alignments correlating several well conserved residues in the enzyme subgroup (Yew, W. *et al*., 2006). Its natural substrate was ascertained as L-fuconate by analysis of the gene's operon context and highest observed activity after testing a library of acid sugars as substrates (Yew, W. *et al*., 2006). L-Fuconate dehydratase (E.C. 4.2.1.68, FucD) was found to first catalyze the dehydration of L-fuconate at the 2 position and then catalyze the ketonization of the dehydrated enol product (Fig 3.1). A continuum within the MR subgroup exists from enzymes that catalyze racemization or epimerization reactions to those that catalyze β-elimination reactions such as dehydration with or without subsequent enzyme-catalyzed ketonization. MR does not catalyze β-elimination of a known substrate (Bearne, S. L. & St. Maurice, 2017), L-talarate galactarate dehydratase catalyzes both epimerization and dehydration reactions (Yew, Ws *et al*., 2007), D-tartrate dehydratase catalyzes dehydration of D-tartrate but the product ketonizes non-enzymatically in solution (Yew, W. *et al*., 2006), and FucD catalyzes dehydration of L-fuconate and the stereo-specific ketonization of the enol product (Fig 3.1) (Yew, W. *et al*., 2006).

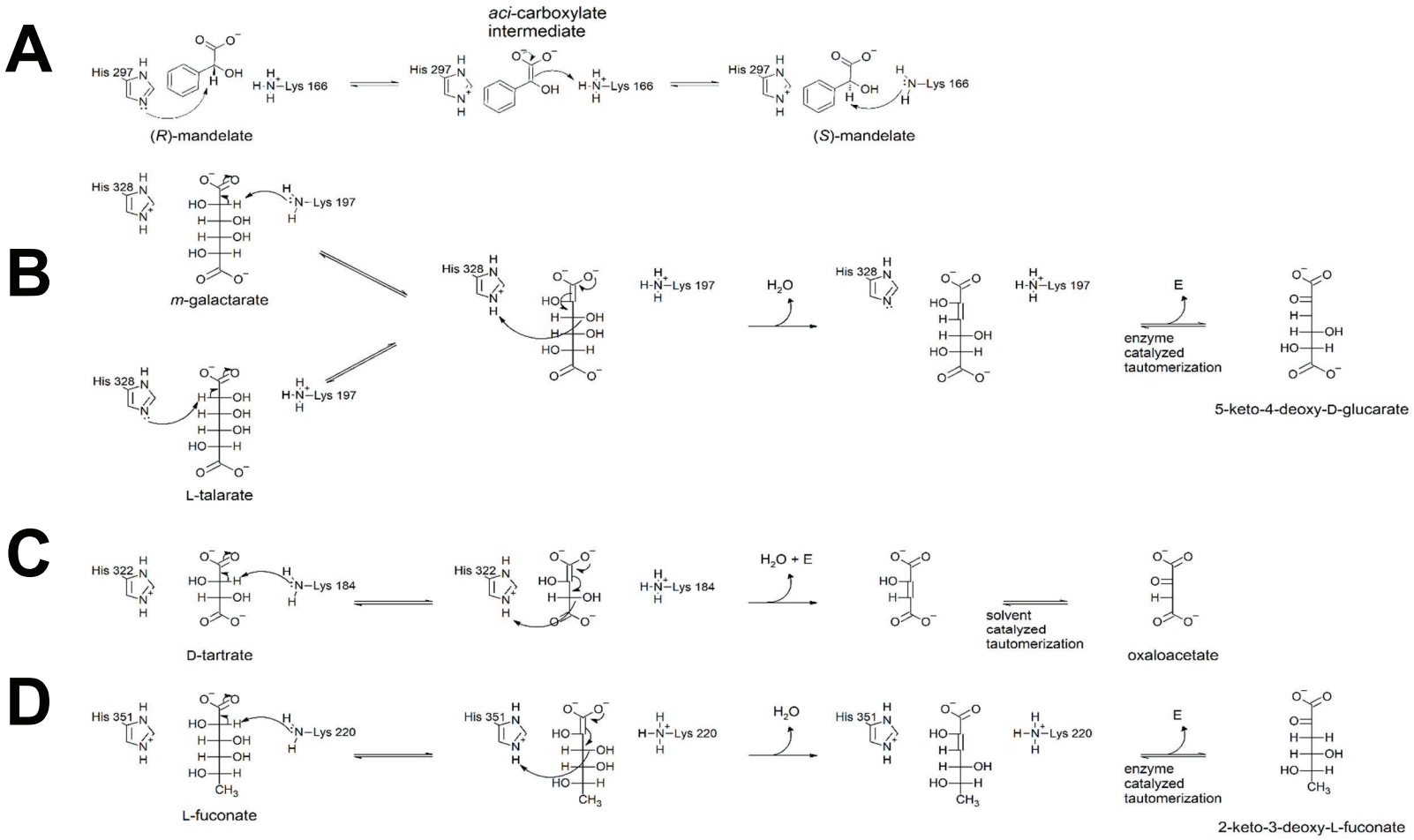

Figure 3.1 Examples of MR subgroup enzyme mechanisms. The catalytic mechanisms are shown for MR (A), TGD (B), TarD (C), and FucD (D) (E = enzyme). Precise enzyme tautomerization mechanisms are not shown due to some ambiguity in the literature as to which specific amino acids catalyze what steps (Yew, W. *et al*., 2006; Yew, Ws *et al*., 2007).

The active sites of all members of the MR subgroup have conserved positions of the catalytic His and Lys residues as well as other nearby binding determinants (Bearne, S. L. & St. Maurice, 2017) (Fig 1.7). Bearne and colleagues found that the catalytic His and Lys residues of MR (His 297 and Lys 166) act as the primary binding determinants (along with the bound Mg^{2+} ion) for the inhibitors tartronate and 3-hydroxypyruvate (3-HP) (Nagar, Mitesh *et al*., 2014; Nagar, Mitesh *et al*., 2015). Therefore, considering these binding determinants are positioned identically in all other MR subgroup members discovered so far (Bearne, S. L. & St. Maurice, 2017) these molecules might be general inhibitors of the enzymes of the MR subgroup.

Former Bearne lab members Nicole Easton and Sarah Aboushawareb found tartronate to be a reversible competitive inhibitor of TGD (Easton *et al*., 2018) and TarD (Easton, Aboushawareb & Bearne unpublished). Here, I show that tartronate is a linear mixed-type inhibitor of FucD with modest binding affinity (8.37 ± 0.72 mM, α = 7.53 ± 1.16).

As discussed in section 1.1.6, 3-HP was found to irreversibly inactivate MR via a Schiff base mechanism (Scheme 1.5 and Fig 1.8). The rate constant for inactivation k_{inact} could not be determined in the case of MR since inactivation occurred too quickly relative to the assay point timescale (3 min) to be able to assess 3-HP concentrations high enough to observe saturation (eqns 3.1 to 3.4) (Nagar, Mitesh *et al*., 2015). However, an efficiency of inactivation (k_{inact}/K_I) could be estimated from the linear k_{obs} vs. [3-HP] plots and was found to be 83 ± 8 $M^{-1}s^{-1}$. Furthermore, MR was protected from 3-HP-dependent inactivation by the competitive inhibitor BzH demonstrating that the

mechanism of inactivation occurs at the active site. An 86-Da adduct was observed at the active site on Lys 166 using MS/MS analysis and the mechanism of inactivation was supported by an X-ray crystal structure (Scheme 1.5, Fig 1.8). When the H297N MR variant was incubated with 3-HP, no adducts were observed by MS/MS analysis. However, when the H297N MR variant was incubated with 3-HP followed by reduction with sodium cyanoborohydride an 88-Da adduct was observed. These results indicated that His 297 is essential for formation of an 86-Da adduct on Lys 166 and the finding of a reduced 88-Da adduct upon treating MR with 3-HP and sodium cyanoborohydride was consistent with His 297 acting as the base to deprotonate a 3-HP imine adduct to Lys 166. Given that analogues of Lys 166 and His 297 are present in all studied MR subgroup members in identical positions (Fig 1.7), it was reasonable to suspect that 3-HP could inactivate other subgroup members as well.

$$\frac{v_{\mathrm{i}}}{v_{\mathrm{o}}} = \mathrm{e}^{-k_{\mathrm{obs}}t}$$

Equation 3.1

$$\ln(\%\mathrm{activity}) = 4.605 - k_{\mathrm{obs}}t$$

Equation 3.2

$$k_{\mathrm{obs}} = \frac{k_{\mathrm{inact}}[\text{3-HP}]}{K_{\mathrm{I}} + [\text{3-HP}]}$$

Equation 3.3

$$k_{\text{obs}} \approx \frac{k_{\text{inact}}}{K_{\text{I}}}[\text{3-HP}]$$

Equation 3.4 The equation used to determine a value for k_{inact}/K_I for MR inactivation by 3-HP since [3-HP] was small compared to K_I (Nagar, Mitesh *et al*., 2015).

Previous work with TarD and TGD by former Bearne lab members Nicole Easton and Sarah Aboushawareb found 3-HP to be a reversible competitive inhibitor of these enzymes (Easton, Aboushawareb and Bearne unpublished). Therefore, it was surprising when FucD displayed irreversible inhibition with 3-HP. Of further interest was that the inactivation of FucD by 3-HP occurred at a considerably lower efficiency of inactivation with a k_{inact}/K_I value of 0.019 ± 0.001 $M^{-1}s^{-1}$, which was ~4400-fold lower than what was observed for MR. Given a considerably slower rate of inactivation, a more thorough kinetic analysis of FucD inactivation by 3-HP could be carried out than that for MR thereby allowing determination of the k_{inact} and K_I values. However, protection experiments were not carried out due to the lack of a readily available, potent competitive inhibitor of FucD.

I then investigated the chemical mechanism of FucD inactivation by 3-HP using MS/MS experiments. Analogous to what was found with MR, an 86-Da adduct was found on Lys 220 of FucD (equivalent to Lys 166 of MR), but a 58-Da adduct was also found in equal or greater abundance at Lys 220. Furthermore, this adduct was found on other nucleophilic residues on the exterior of the protein.

A final study was undertaken to investigate the role of the interdigitating loop of FucD in substrate binding. An interdigitating loop emanates from the α + β capping domain of one protomer of FucD into the active site of its closest neighboring protomer.

This interdigitating loop is a structural characteristic of the MR subgroup and is only shared with the ManD subgroup in the enolase superfamily (Bearne, S. L., 2017). The Trp residue at the tip of the interdigitating loop in FucD (Trp 101) directly interacts with the terminal methyl group of L-fuconate. FucD variants where Trp 101 was substituted by a Lys or Arg residue were generated in order to investigate whether adding a positive charge at this position would allow *meso*-galactarate to be used as a substrate. These mutations were chosen because *m*-galactarate is identical to L-fuconate save the terminal methyl group is a carboxylate, and a facile CD-based assay had already been developed for detecting dehydration of *m*-galactarate (Easton *et al*., 2018). The W101K, W101R, W101Q, W101N and W101E FucD variants were generated. The W101Q mutation was selected as a potential conservative mutation where the general bulk and polar character of Trp was preserved, W101N was assayed also as a potential conservative mutation regarding polarity, whereas the W101E variant was selected to probe the impact of a negative charge at this position. The W101N variant could not be purified due to likely solubility issues but all other variants were expressed and purified. Unfortunately, all Trp 101 variants were inactive, which raised the question of whether the mutation to the interdigitating loop affected the oligomeric state of FucD. Gel filtration experiments were conducted to explore this possibility.

3.2 MATERIALS AND METHODS

3.2.1 GENERAL

Lithium 3-hydroxypyruvate (3-HP), mucic acid (*m*-galactarate), and all other reagents, unless otherwise mentioned, were purchased from Sigma-Aldrich Canada, Ltd. (Oakville, ON). Tartronic acid was purchased from Alfa Aesar (Ward Hill, MA, USA). Assays were conducted using a JASCO J-810 spectropolarimeter (Jasco Inc., Easton, MD, USA). Measurement of OD_{600} values were taken on a HP 8453 UV-visible spectrophotometer. Oligonucleotide primers were purchased from Integrated DNA Technologies (Coralville, IA, USA). Phusion and Q5 DNA polymerase kits, dNTPs, and DpnI were purchased from New England Biolabs (Ipswich, MA, USA). ^{1}H NMR spectroscopy was carried out at the Dalhousie Nuclear Magnetic Resonance Research Resource (NMR^{3}) using either a Brüker AV 300 or AV 500 spectrometer and chemical shifts (δ) were calibrated to the HOD peak at 4.79 ppm (Gottlieb *et al*., 1997). LC-ESI-MS/MS experiments were carried out at the Biological Mass Spectrometry Core Facility at Dalhousie University. An HPLC with nanoflow (UltiMate 3000, Dionex) was used for liquid chromatography and a hybrid ion trap-orbitrap high resolution tandem mass spectrometer (Velos Pro, Thermoscientific) was used for ESI-MS/MS experiments and run in data-dependent acquisition mode (DDA).

3.2.2 FucD EXPRESSION AND PURIFICATION

Gene GI:21233491 encoding wild-type FucD from *Xanthomonas campestris str.* ATCC 33913 was synthesized and inserted into a pET52b(+) vector by BioBasic Inc. (Markham, ON). An N-terminal STREP II tag was added to FucD as a product of insertion into the pET52b(+) plasmid. Chemically competent DH5α cells were transformed using the heat shock method. Plasmid DNA was extracted using a Qiagen miniprep kit (Toronto, ON) and used to transform BL21(DE3) cells for protein expression. The above steps were carried out by Minglu Gu.

To express FucD, BL21(DE3) cells, containing the WT FucD pET52b+ plasmid, from glycerol stocks were used to create 5-mL starter cultures (LB media, 100 μg/mL ampicillin) which were grown overnight (37 °C, 220 rpm). Starter cultures were used to inoculate larger expression cultures (5-mL starter culture per 1-L expression culture) of the same media composition. Expression cultures were grown at 37 °C (220 rpm) until an OD_{600} of ~0.6 was reached whereupon isopropyl β-D-1-thiogalactopyranoside (IPTG) was added to a final concentration of 0.1 mM to induce recombinant protein expression. Cultures were grown for an additional 24 h at 25 °C with shaking at 220 rpm before cells were harvested by centrifugation (3795 × *g*, 10 min × 3). Cell pellets were frozen at −20 °C for future use.

FucD was purified from cell pellets using a similar procedure to that described for MR (section 2.2.3). Briefly, cell pellets containing cells from 2 L of expression culture were resuspended in ~30 mL of cold sonication buffer (100 mM Tris, 5 mM $MgCl_2$, pH 7.5). Cells were lysed using sonication on ice with a Branson Sonifier 250 for 5 × 30 s with 1 min breaks in between (setting 5.5, 1-s bursts). The cell lysate was subjected to

ultracentrifugation (146 550 × *g*, 35 min) and applied to a Strep-Tactin Superflow affinity resin (10 mL) (IBA GmbH, Göttingen, Germany) using an ÄKTA Start FPLC from GE Healthcare Life Sciences (Baie d'Urfé, PQ, Canada) kept at 4 °C. The column purification procedure followed the manufacturer's instructions (IBA). Due to low yields of purified protein (~2.5 mg per liter of expression culture) typically 4 to 6 L of expression culture were purified simultaneously. Each pellet corresponding to 2 L of expression culture was processed independently but clarified lysate from two or three pellets were pooled for addition to the Strep-Tactin Superflow affinity resin at the same time such that obtained protein concentrations were sufficient for further studies. All FucD variants were expressed and purified in the same manner, although no W101N FucD could be purified likely due to solubility issues with the variant. Protein concentrations were determined by Bradford assays or UV absorbance at 280 nm where extinction coefficients were calculated from the primary sequence using the ExPASy protparam web tool as described in section 2.2.3 (ε = 64400 $M^{-1}cm^{-1}$ for WT, K220M and H351N FucD; ε = 58900 $M^{-1}cm^{-1}$ for W101K, W101R, W101E and W101Q FucD). The molecular weights of all FucD variants were also calculated from the primary sequence using the ExPASy protparam web tool (Gasteiger *et al*., 2003) as described in section 2.2.3 (WT = 50813.83 Da, K220M = 50816.85 Da, H351N = 50790.80 Da, W101K = 50755.79 Da, W101R = 50783.81 Da, W101Q = 50755.75 Da, W101N = 50741.72 Da, and W101E = 50756.73 Da). Purity of protein samples was assessed by SDS-PAGE (10%) with Coomassie staining.

3.2.3 SITE-DIRECTED MUTAGENESIS

PCR-based site-directed mutagenesis was carried out to construct the FucD variants using either Phusion (W101K, W101R, W101N) or Q5 (W101Q, W101E) high fidelity polymerases according to the manufacturer's instructions (NEB). The cycle temperatures and conditions were as follows: denaturation at 98 °C for 20 s, annealing at 67 °C for 30 s, elongation at 72 °C for 5 min with 15 cycles overall. Primers are listed in Table 3.1. After PCR, DNA constructs were subjected to agarose gel electrophoresis with visualization using ethidium bromide. For all variants except W101N FucD, strong bands were observed at the correct molecular weight and the PCR product was subjected to DpnI digestion before being used to transform chemically competent DH5α cells using the heat shock method. For W101N FucD, a diffuse band was observed and so the band was excised from the gel and the DNA was extracted using a Monarch DNA Gel Extraction Kit (NEB). This DNA was subjected to DpnI digestion and then used to transform DH5α cells in the same manner as the other PCR products. Plasmid DNA from all transformed DH5α cells was extracted using a miniprep kit (Qiagen) and sequenced commercially (Robarts Research Institute, London, ON).

Table 3.1 Primers used for site-directed mutagenesis. Bolded bases were changed from the WT sequence, underlined codons were changed to encode the desire mutation.

FucD Variant	Primer type	Primer Sequence
W101K	F	GGATTCCGGGCGGTTA**TG**ACCAAGATCG
	R	GCCGATCTTGGTC**AT**AACCGCCCGGAAT
W101R	F	GGATTCCGGGCGGTT**TGC**ACCAAGATCG
	R	GCCGATCTTGGT**GCA**AACCGCCCGGAAT
W101Q	F	GCTGCGC**CAG**CTGGGCCCGGAAAAG
	R	CTTTTCCGGGCCCAGC**TG**GCGCAGC
W101N	F	CAGCTGCGC**AAC**CTGGGCCCGGAAAAG
	R	CCTTTCCGGGCCCAG**GTT**GCGCAGCTG
W101E	F	CAGCTGCGC**GAA**CTGGGCCCGGAAAAG
	R	CTTTTCCGGGCCCAG**TTC**GCGCAGCTG
K220M[a]	F	GCACCATCAAGCTCA**TG**GTCGGCGCCAACG
	R	CGTTGGCGCCGACC**AT**GAGCTTGATGGTGC

[a] primer design and mutagenesis carried out by Dr. Himank Kumar

3.2.4 CD SPECTRA OF WT AND FucD VARIANTS

CD spectra of FucD variants were obtained using a protein concentration of 1.97 μM (100 μg/mL) in sodium HEPES buffer (10 mM, pH 7.5) with 3.3 mM $MgSO_4$. A 0.1-cm quartz cuvette was used, and spectra were collected from 195 to 300 nm where data collected below 200 nm was not used due to high voltage readings. Averaged buffer spectra collected in triplicate were subtracted from spectra of buffer containing protein samples also averaged from triplicate readings.

3.2.5 L-FUCONATE PREPARATION

L-Fuconate was synthesized by Minglu Gu using a protocol similar to Gerlt and colleagues (Yew *et al.,* 2006) and used for all following studies. Sodium L-fuconate was prepared by bromine oxidation of L-fucose (TCI chemicals). L-Fucose (1.5 g, 9.14 mmol) was dissolved in water (7.5 mL) in a round bottom flask (25 mL). A glass pipette was used to add Br_2 (0.5 mL, 9.4 mmol), the resulting solution was left to stir at room temperature for two days covered in aluminum foil and sealed with a stopper. After 48 h, air was blown into the reaction vessel to remove all colored species (excess Br_2) and the solution brought to a pH of 7 (pH paper) by dropwise addition of 6 M NaOH. Barium chloride (1.2 g, 5.76 mmol) was dissolved in a minimum volume of water and added to the reaction mixture to precipitate barium L-fuconate which was collected using suction filtration. Conversion to the sodium salt was completed by application of dilute sulfuric acid (2 mL, 5.76 mmol) to barium L-fuconate (2.65 g, 5.35 mmol) in water (5 mL). Precipitated $BaSO_4$ was removed by filtration through Celite. The filtrate was adjusted to pH 8 with addition of 6 M NaOH and the solvent evaporated under vacuum conditions. The product was a white powder which was further dried under a stream of air. Product

purity was assessed using ^{1}H NMR and a D_2O solution containing 25 mM sodium acetate and a known mass of sodium L-fuconate. Integration of the methyl peaks of each compound were compared for quantification.

3.2.6 KINETIC ASSAYS

A CD-based assay, analogous to the one used for MR (Sharp *et al*., 1979) and TGD (Easton *et al*., 2018) was implemented to measure FucD activity. Spectra were recorded of assay buffer (50 mM Tris-HCl, 10 mM $MgCl_2$, pH 7.5), L-fuconate (10 mM in assay buffer), and 10 mM L-fuconate with 19.8 ng/µL (0.340 µM) FucD were analyzed at 5-min intervals over 75 min from wavelengths 200 to 300 nm. This analysis was carried out by the previous lab member Minglu Gu. It was determined that the largest difference between the L-fuconate and the dehydrated product 2-keto-3-deoxy-L-fuconate CD spectra was at 216 nm (Fig 3.2). Therefore, a CD-based assay for measuring the change in ellipticity at 216 nm was developed.

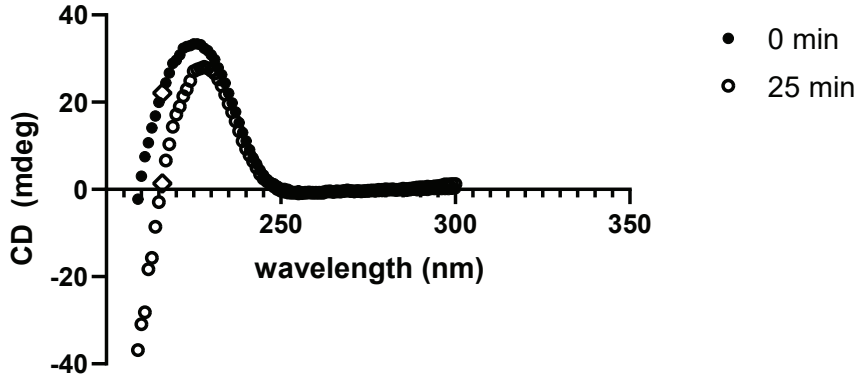

Figure 3.2 CD spectra of FucD assay solutions. solutions containing FucD (19.8 ng/µL, 0.340 µM), assay buffer (50 mM Tris, 10 mM $MgCl_2$, pH 7.5) and L-fuconate (10 mM) at 0-min (●) and after 25-min (○) of incubation at 25 °C. Diamonds (◇) label 216 nm as the chosen assay wavelength. Points at wavelengths less than 209 nm are excluded for clarity due to the high voltage at those wavelengths. Experiment was carried out by Minglu Gu.

The molar ellipticity change was determined so that the observed changes in mdeg ellipticity could be converted to units of concentration. The ellipticity of a solution containing L-fuconate (5 mM) and FucD (38 μg/mL, 0.75 μM) was measured over 50 min using a 0.5-cm pathlength quartz cuvette (total volume of 1000 μL) (Fig 3.3). Extrapolating to time zero allowed for estimation of the ellipticity of the solution with entirely reactant present and the final ellipticity of the levelled off curve was used as the ellipticity of the solution containing only product. A measure for the difference of molar ellipticity between the reactants and products ($[\theta]_{216}^{S}$–$[\theta]_{216}^{P}$) was determined to be 8985 ± 87 deg cm^2 mol^{-1}. This molar ellipticity change from reactants to products was used in eqn 3.5 to calculate reaction rates in units of concentration per unit time, where l is the pathlength, θ is the observed ellipticity (mdeg), and t is the time (s).

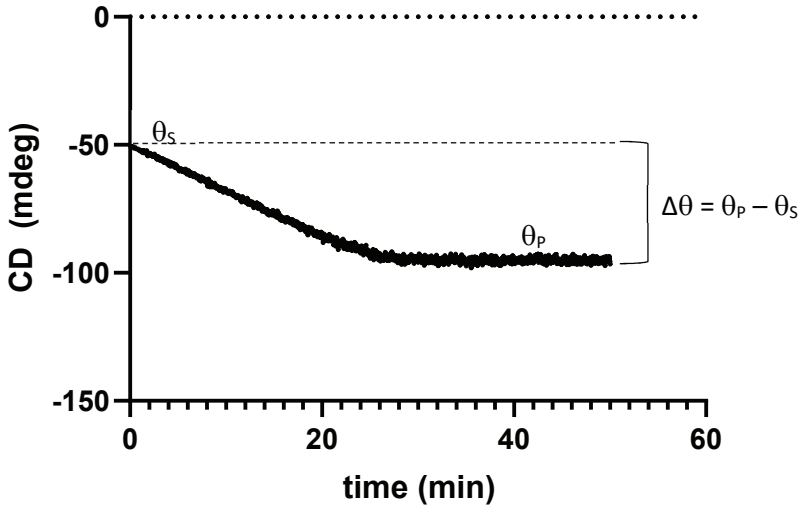

Figure 3.3 Determination of molar ellipticity for conversion of L-fuconate to 2-keto-3-deoxy-L-fuconate. θ_S = ellipticity of the solution containing 5 mM L-fuconate (extrapolated time 0 point = -64.3 ± 0.7 mdeg), θ_P = ellipticity of the solution containing 5 mM 2-keto-3-deoxy-L-fuconate (averaged final 10 min of reaction time = -42.1 ± 0.7 mdeg).

$$v_{\mathrm{i}}\{\text{in mM/s}\} = \frac{\Delta \mathrm{c}}{\Delta t} = \frac{\left(\frac{\Delta \theta}{\Delta t}\right)}{\left([\theta]^{\mathrm{S}}_{216} - [\theta]^{\mathrm{P}}_{216}\right) l} = 0.2226(\Delta\theta/\Delta t)\{\text{in mdeg/s}\}$$

Equation 3.5 Calculation for conversion of mdeg/s to dehydration of L-fuconate in mM/s with a 0.5-cm pathlength (l).

Kinetic assays used substrate concentrations ranging from 0.2 to 6.0 mM. Initial velocity values were obtained from the linear slopes of observed decreasing ellipticity (at 216 nm) with time. Reactions were initiated by addition of FucD to a final concentration of 9.5 µg/mL (0.19 µM) with a BSA concentration of 0.005 %. The reaction progress was monitored by following the ellipticity at 216 nm for 300 s. As before a 0.5-cm pathlength quartz cuvette was used with a final volume of 1000 µL. Data were plotted and *KaleidaGraph* software (v. 4.02, Synergy Software, Reading, PA) was used to fit eqn 2.2 to the initial velocity data (Section 2.2.4) using non-linear regression analysis. The turnover number (k_{cat}) was determined from V_{max} values divided by total enzyme concentrations measured by Bradford assays (mg/mL) converted to units of molarity using the molecular weight of WT FucD (50813.83 Da) calculated from the primary sequence by the ExPASy ProtParam tool (Gasteiger *et al*, 2003). All experiments were conducted in triplicate where reported data are average values with errors corresponding to standard deviation values.

3.2.7 INHIBITION STUDIES WITH TARTRONATE

IC_{50} values were determined using a procedure similar to the one for the inhibition of MR by BzH (section 2.2.5). Briefly, solutions containing 0.5 mM L-fuconate (at K_{m}) with varying concentrations of tartronate (1.0 to 11.0 mM) were assayed for activity using the CD-based assay. Eqn. 2.4 was fit to initial velocity data using non-

linear regression analysis and *KaleidaGraph* software (v. 4.02, Synergy Software, Reading, PA) as described in section 2.2.5.

FucD inhibition by tartronate was assessed using kinetic assays with 0.0, 4.0, 8.0 and 12.0 mM tartronate with a FucD concentration of 9.5 µg/mL (0.19 µM) in a 0.2-cm pathlength cuvette. Double reciprocal plots were fitted to collected initial velocity (v_i) data to assess the mode of inhibition. V_{max} and K_m values were obtained from eqn 3.6 fitted to observed v_i data from each inhibitor concentration curve. Replots of K_m/V_{max} vs. [I] and $1/V_{max}$ vs. [I] were used to determine K_i and α values in accord with equations 3.6 and 3.7 derived from the model in Fig 3.4 (Segel, 1975). Linear eqn 3.7 is derived from eqn 3.6 where plotting of K_s/V_{max} or $1/V_{max}$ against [I] allows determination of K_i or αK_i respectively.

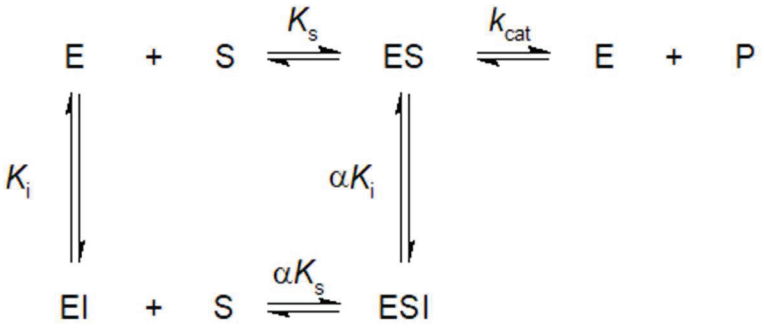

Figure 3.4 Model for linear mixed-type inhibition.
Modified from (Segel, 1975)

$$v_i = \frac{V_{max}[S]}{K_s\left(1 + \frac{[I]}{K_i}\right) + [S]\left(1 + \frac{[I]}{\alpha K_i}\right)}$$

Equation 3.6

$$\frac{1}{v_i} = \frac{K_s}{V_{max}}\left(1 + \frac{[I]}{K_i}\right) + \frac{1}{V_{max}}\left(1 + \frac{[I]}{\alpha K_i}\right)$$

Equation 3.7

3.2.8 INACTIVATION STUDIES WITH 3-HYDROXYPYRUVATE

Inhibition of FucD by 3-hydroxypyruvate (3-HP) was assessed initially using an IC_{50} assay analogous to that done with tartronate (section 3.2.7). Solutions containing L-fuconate (0.5 mM) and 3-HP (2.0 to 23.0 mM) were assayed until 50% inhibition was observed. The time dependence of inhibition was also assessed by incubating FucD (475 µg/mL with 0.05% w/v BSA) at 25 °C with concentrations of 3-HP ranging from 5.0 to 150.0 mM followed by a fifty-fold dilution (final [FucD] = 9.5 µg/mL (0.19 µM), BSA = 0.001%) and assaying for activity with 2.5 mM L-fuconate at 45-min time points. A control experiment was conducted concomitantly with the same composition but lacking 3-HP.

Time dependent inhibition of FucD by glycolaldehyde (GLH) was assessed in a similar manner. FucD (100 µg/mL) was incubated at 25 °C with GLH (50 mM) in assay buffer. Aliquots were diluted 10-fold and assessed for activity with 4 mM L-fuconate at 30-min time points. A control experiment was conducted concomitantly with solutions of FucD (100 µg/mL) in assay buffer where no GLH was added. No BSA was added to solutions given literature citing reactivity with GLH (Glomb & Monnier, 1995).

After observing time-dependent inhibition of FucD by 3-HP and GLH irreversibility was assessed by dilution of inhibitor molecules using extensive dialysis. Control (FucD incubated with buffer) and samples with FucD incubated with 3-HP until

no activity was observed (8 h with 50 mM 3-HP, or 1 h with 50 mM GLH) were dialyzed for 2 × 8 h at 4 °C in assay buffer (2 mL sample in 250 mL assay buffer). Samples were tested for activity the following day using the CD-based assay with an L-fuconate concentration of 4 mM to assess whether inactivation was reversible upon removal of the inhibitor by dialysis.

3.2.9 TIME-DEPENDENCE ASSAYS

To assess the kinetics of FucD inactivation by 3-HP, time-dependence assays were carried out. FucD (100 μg/mL, 1.97 μM) was incubated with 0, 5, 10, 20, 50 and 100 mM 3-HP in assay buffer containing 0.05 % BSA. Aliquots (20 μL) were diluted 50-fold and were assayed at 45-min intervals. Observed initial velocities were plotted as ln(% activity) vs. time and the slopes (k_{obs}) values were plotted against the concentration of 3-HP. The values of k_{inact}, K_I and k_{inact}/K_I were determined using eqns 3.1 to 3.3.

3.2.10 DETERMINING A MODE OF INHIBITION FOR 3-HP

Given that the inactivation of FucD by 3-HP was sufficiently slow so that no detectable loss of active enzyme occurred over the assay time of 5 min, a traditional inhibition study was conducted to determine the mode of inhibition. The study was completed as described for tartronate including the same enzyme and substrate concentrations (section 3.2.7) with 8.0, 16.0 and 24.0 mM 3-HP. Data were fit and analyzed as before (section 3.2.7).

3.2.11 MASS SPECTROMETRY SAMPLE PREPARATION

Samples of the FucD variants (WT, K220M, and H351N), at a concentration of 100 μg/mL (1.97 μM), were either inactivated with 3-HP (25 °C, 8 h, 50 mM 3-HP), GLH (25 °C, 1 h, 50 mM), or similarly incubated for the same time span without inactivating reagents present (buffer control). Aliquots (32 μL) were assessed for complete loss of activity after the indicated incubation times with 4 mM L-fuconate using the CD-based assay. After inactivation was complete, aliquots (20 μL) were subjected to electrophoresis using a 12 % SDS-polyacrylamide gel (visualized using Coomassie staining). Gel bands were excised, de-stained, and subjected to trypsinolysis (Promega, Madison, WI) and LC-MS/MS analysis. Reduction with DTT and alkylation with iodoacetamide were not used due to there being only two cysteines in the protein sequence and to avoid potential confounding formation of 58-Da adducts from possible iodoacetic acid contamination.

3.2.12 ^{1}H NMR of 3-HP IN REACTION SOLUTIONS

To test for the presence of aldehyde corresponding to possibly either tartronate semi-aldehyde or glycolaldehyde in 3-HP reaction solutions, ^{1}H NMR spectroscopic experiments were conducted. To test for non-enzymatic production of aldehyde a solution of 100 mM 3-HP in assay buffer was incubated for 6 h at 25 °C, lyophilized overnight, dissolved in D_2O, and subjected to ^{1}H NMR spectroscopic analysis. An identical solution of 100 mM 3-HP in assay buffer was also analyzed where the solution was not incubated at 25 °C for 6 h. Solutions of 100 mM 3-HP in assay buffer were also incubated with 100 μg/mL (1.97 μM) WT and K220M FucD for 6 h at 25 °C followed by removal of protein by centrifugation through a 10-kDa molecular weight cutoff filter, lyophilized overnight,

and dissolved in D_2O for ^1H NMR spectroscopic analysis. Peaks were calibrated to the H-OD peak at 4.79 ppm (Gottlieb et al., 1997) and relative integration of un-hydrated to hydrated 3-HP species are indicated in the legend of Fig 3.18.

3.2.13 ACTIVITY DETERMINATION OF FucD VARIANTS

W101X (X= K, R, Q, or E), K220M, and H351N FucD were assessed for activity with L-fuconate. A constant substrate concentration of 4 mM L-fuconate was used which gives an easily measurable initial velocity with WT FucD and is ~8 times higher than the K_m value (0.5 mM). The maximum assayed enzyme concentration was 300 μg/mL for all W101X variants and 100 μg/mL for K220M and H351N FucD. A 0.2-cm pathlength quartz cuvette was used to minimize voltage due to the absorbance at high enzyme concentrations. If no trend in activity was observed and velocity measurements at an enzyme concentration of 100 μg/mL or higher did not significantly vary from buffer controls, the enzyme variant was deemed to have activity too low to be measured by the CD-based assay.

The same process was repeated with *m*-galactarate as substrate (8 mM) with the W101K, W101R and WT FucD variants. Initial velocity values were found to be credible above ~40 μM/min; therefore, should a V_{max} of 100 μM/min be observed for an assay cuvette enzyme concentration of 300 μg/mL a k_{cat} of 0.3 s^{-1} should theoretically be able to be observed.

3.2.14 INHIBITION BY *m*-GALACTARATE

The IC_{50} value for inhibition of FucD by *m*-galactarate was determined in a similar manner as described for tartronate and 3-HP (Sections 3.2.7 and 3.2.8). L-Fuconate was kept at a concentration of 0.7 mM and the *m*-galactarate concentration was varied from 0 to 22 mM. The concentration of FucD was 9.5 μg/mL (0.19 μM) in the assay cuvette as with all other kinetic assays in this text. Higher concentrations of *m*-galactarate could not be assayed due to insufficient solubility. Eqn 2.4 was fit to initial velocity data to determine the IC_{50} value. All assays were done in triplicate where the average value is reported with errors as standard deviations.

3.2.15 GEL-FILTRATION HIGH PERFORMANCE LIQUID CHROMATOGRAPHY (GF-HPLC)

In order to determine the oligomeric state of FucD, gel-filtration HPLC (GF-HPLC) was carried out on WT and Trp 101 FucD variants (K, R, Q, and E) in sodium HEPES buffer (100 mM HEPES, 3.3 mM $MgCl_2$, pH 7.5). A Yarra 3 μM SEC-3000 LC column (300 × 7.8 mm) from Phenomenex (Torrance, CA, USA) was used with a flow rate of 0.5 mL/min. A Waters 510 pump and 680 controller were used for solvent delivery (100 mM HEPES, 3.3 mM $MgCl_2$, pH 7.5). Injections were made using a Rheodyne 7725i sample injector fitted with a 20-μL injection loop. Eluted proteins were detected by native protein fluorescence (λ_{ex} = 285 nm, λ_{em} = 335 nm). A calibration curve was prepared using bovine thyroglobulin (669 kDa), β-amylase (200 kDa), alcohol dehydrogenase (150 kDa), BSA (66 kDa), and carbonic anhydrase (29 kDa). The column void volume was estimated by the retention time of bovine thyroglobulin. Retention time

(min) of standard proteins was plotted against ln(molecular weight) and the linear regression line was used to estimate the molecular weight of the FucD variants.

3.2.16 DYNAMIC LIGHT SCATTERING (DLS)

To determine whether the non-equilibrium conditions associated with GF-HPLC affected the observed oligomeric state of FucD, DLS experiments were conducted. WT MR (monomer MW = 41263.78 Da) was used as a control given that GF-HPLC and previous cross-linking studies showed it to be at minimum a tetramer (Fee *et al*., 1974b) and its structure might be representative of a tetrameric FucD (monomer MW = 50813.83 Da) based on crystal structure analysis (Neidhart *et al.*, 1991; Yew, W. *et al.*, 2006). Experiments were conducted using a BI-200SM goniometer and laser light scattering system equipped with a Brookhaven Mini-L30 diode laser (637 nm, 30 mW) (Brookhaven Instruments, Holtsville, NY, USA). Sodium HEPES buffer (100 mM HEPES, 3.3 mM $MgCl_2$, pH 7.5) was filtered through a Anotop 10 Plus 0.02-µm nylon filter (GE Healthcare Life Sciences, Germany) and incubated at 25 °C prior to addition of WT FucD or WT MR to a concentration of 5.00 µM (206 µg/mL MR, 254 µg/mL FucD). The prepared sample was filtered using a 0.2-µM syringe filter (Chromatographic Specialties, Brockville, ON) into to a Suprasil quartz cuvette (75 × 10 mm, Hellma Analytics, Plainview, NY, USA). Samples were equilibrated at 25 °C for 10 min prior to measurement. Light scattering runs used an angle of 90 °, a first delay time of 2.0 µs, a last delay of 100 ms, and a total experiment time of 2 min. Viscosity measurements were taken using a RheoSense µVISC viscometer (San Ramon, CA, USA) and found to be 1.065 and 1.079 cP for the MR and FucD containing solutions, respectively. Refractive index measurements were taken using a Mettler Toledo Refracto 30GS refractometer

(Mississauga, ON) and found to be 1.338 for both the FucD and MR containing samples. Autocorrelation functions were fitted to collected DLS data using a non-negative least squares (NNLS) algorithm (Brookhaven Instruments DLS software v. 5.89) to determine the intensity and number weighted size distributions of FucD and MR proteins.

3.2.17 ROLE OF Mg^{2+} IN INACTIVATION OF FucD BY 3-HP

FucD was dialyzed against buffer containing EDTA (2 × 8 h, 50 mM Tris, 10 mM EDTA, pH 7.5) followed by dialysis against storage buffer containing no metal ions (2 × 8 h, 50 mM Tris, 10% v/v glycerol, pH 7.5). The resulting Apo-FucD was frozen at −20 °C until required for experiments. The role of Mg^{2+} in FucD inactivation by 3-HP was assessed using a time dependent assay analogous to that discussed in section 3.2.8. Four enzyme stocks were prepared as follows: Apo-FucD and 50 mM 3-HP, Mg^{2+} bound FucD and 50 mM 3-HP, Apo-FucD, and Mg^{2+} bound FucD. All FucD concentrations were 150 μg/mL (2.95 μM) and contained 0.05 % w/v BSA to increase stability of the samples over the experiment time span. The solutions were assayed for FucD activity at 30-min time points, by first incubating 32-μL aliquots with assay buffer containing 10 mM Mg^{2+} for 5 min prior to initiating the reaction with addition of L-fuconate to a final concentration of 4 mM. The final cuvette concentration of FucD in all cases was 9.5 μg/mL (0.19 μM). Initial velocity data were plotted against time to assess for the loss of activity.

3.3 RESULTS

3.3.1 STABILITY OF L-FUCONATE AND FucD VARIANTS

Different ellipticity values for solutions from subsequent assays were observed at the start and end for reactions for different trials; however, the same activity of FucD was observed regardless of the starting ellipticity, two examples are shown in Fig. 3.5A. To assess whether this change was due to changes in the L-fuconate between trials, ellipticity measurements of L-fuconate in solution with assay buffer or in distilled-deionized water (ddH_2O) were recorded in the absence of enzyme for three days. The L-fuconate solutions were stored at 4 °C in between measurements. No change in ellipticity was observed in the substrate solutions over three days (Fig 3.5B). Therefore, supposing the cause of the changed ellipticity was due to subtle changes in enzyme secondary structure content, especially since the CD-based assay was conducted at 216 nm where FucD exhibits an ellipticity (Fig 3.19), enzyme stocks were stored in smaller aliquots and thawed only once to avert changes that might be due to freeze thaw cycles; also, 10% v/v glycerol was added to the storage buffer (50 mM Tris, 10 mM $MgCl_2$). These pre-cautionary measures resulted in enzyme preparations that gave constant ellipticity values between assays conducted on different days (Fig 3.5C). Once enzyme and substrate stability had been assured, k_{cat} and K_m values for FucD were determined (Fig 3.6, Table 3.2).

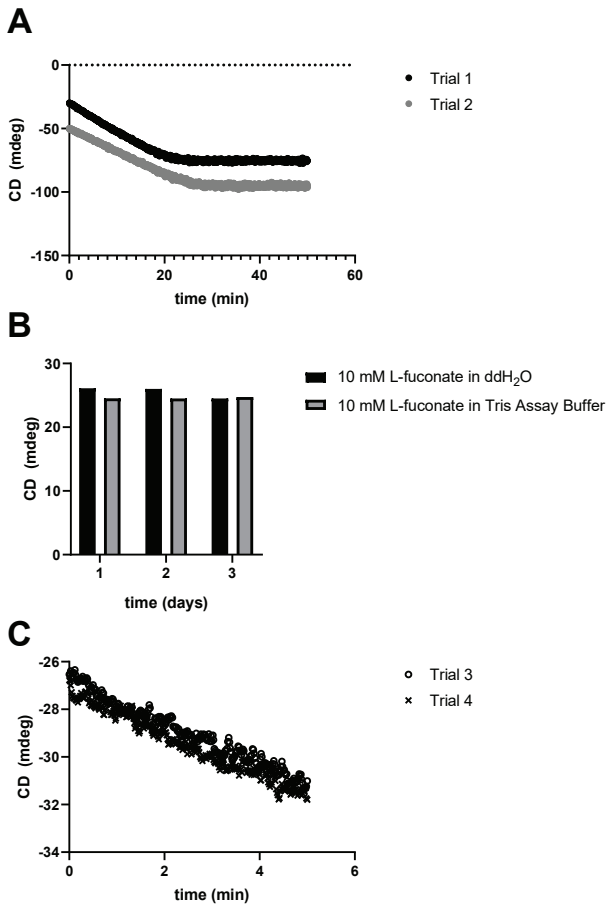

Figure 3.5 Change in assay solution ellipticity is due to protein stability and not substrate degradation. A solution of 38.5 μg/mL (0.758 μM) FucD with 10 mM L-fuconate was monitored for the change in ellipticity at 216 nm for 50 min on two consecutive days using the same enzyme stock solution. Dehydration of L-fuconate is shown by the decrease in ellipticity over the first 25 min. However, the starting ellipticity of the solution was consistently observed to decrease with each successive freeze-thaw cycle shown by the lower position of the gray curve (trial 2) relative to the black curve (trial 1).

B) CD readings of 10 mM L-fuconate in ddH_2O (black) or assay buffer (50 mM Tris, 10 mM $MgCl_2$, pH 7.5) (gray) stored at 4 °C did not change the observed ellipticity of the solution over three consecutive days.

C) Changes in ellipticity of solutions of 9.5 μg/mL (0.19 μM) FucD with 6 mM L-fuconate in assay buffer. The change in ellipticity of the assay solution at 216 nm between assay days is eliminated by removal freeze-thaw cycles of the protein solutions and by addition of 10% v/v glycerol to enzyme storage buffer. Trial 3 and Trial 4 were conducted on two consecutive days using separate protein aliquots stored at −20 °C in assay buffer with glycerol, each aliquot was only thawed once prior to conducting the assay.

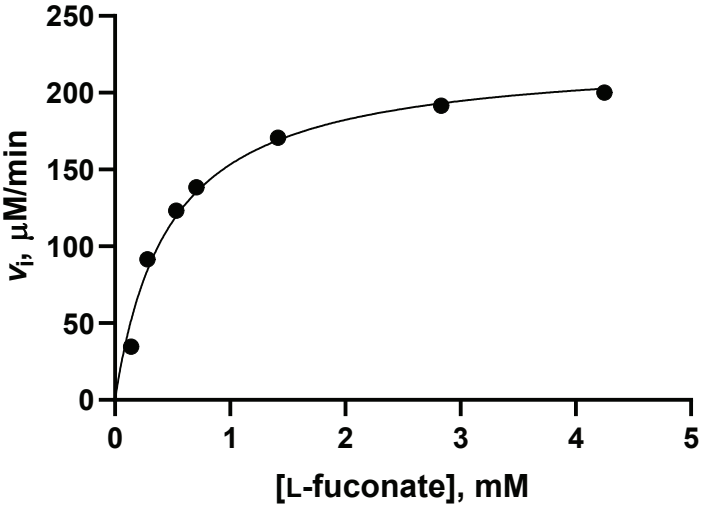

Figure 3.6 Representative Michaelis-Menten plot for FucD-catalyzed turnover of L-fuconate. Assay solutions contained 9.5 μg/mL (0.19 μM) FucD and L-fuconate concentrations ranging from 0.2 to 4.3 mM.

Table 3.2 Kinetic parameters of FucD

	This work	**Literature[a]**
k_{cat} **(s^{-1})**	19.48 ± 0.64	15 ± 0.2
K_m **(mM)**	0.48 ± 0.02	0.33 ± 0.06
k_{cat}/K_m **($M^{-1}s^{-1}$)**	40840 ± 1237	45000

[a] (Yew, W. *et al*., 2006)

3.3.2 INHIBITION OF FucD BY TARTRONATE

Assays with tartronate revealed that the IC_{50} value was 8.30 ± 0.15 mM (error from direct fitting of eqn 3.3 to initial velocity values) which indicated that inhibitor concentrations of 0.0, 4.0, 8.0 and 12.0 mM would be appropriate for steady-state inhibition assays. Note the assay cuvette pathlength needed to be reduced to 0.2 cm in order to bring the high-tension voltage values below 700 V for accurate readings. Tartronate was found to be a linear mixed-type inhibitor of FucD activity with a K_i value of 8.37 ± 0.72 mM and an α value of 7.53 ± 1.16, obtained from triplicate experiments (Fig 3.7).

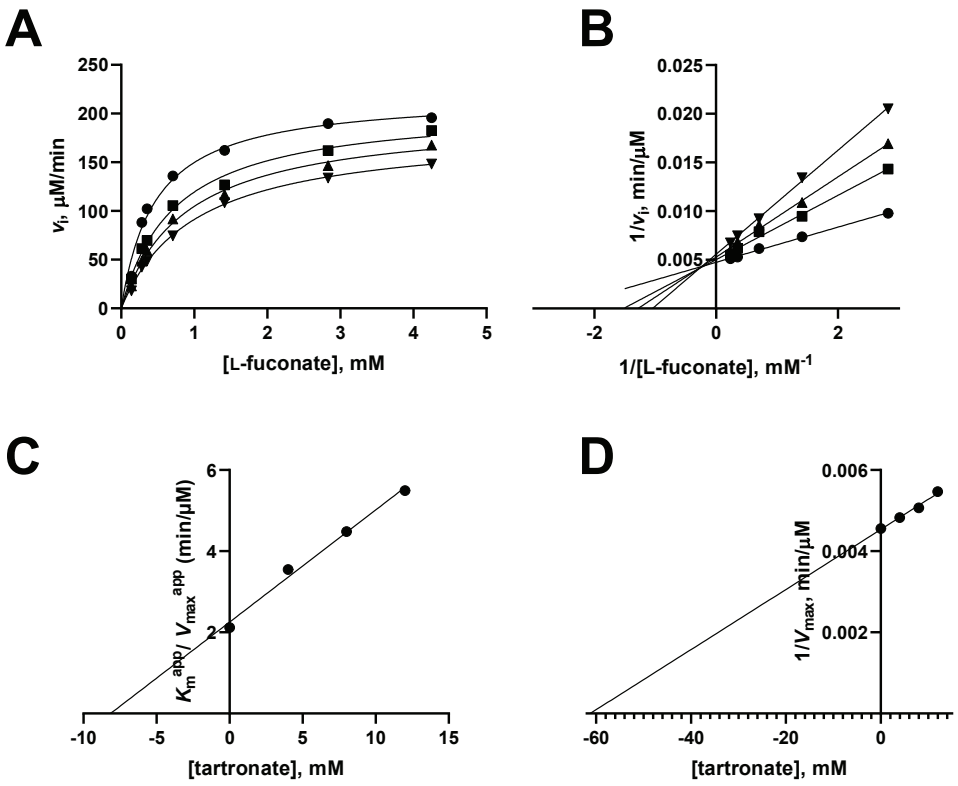

Figure 3.7 Inhibition of FucD by tartronate. Representative Michaelis-Menten plots of FucD with varying concentrations of tartronate (● = 0 mM, ■ = 4 mM, ▲= 8 mM, ▼ = 12 mM) are shown (A), along with the corresponding double reciprocal plots (same labelling scheme) (B). Replots of K_m^{app}/V_{max}^{app} (C) and $1/V_{max}$ (D) against the concentration of tartronate are also shown.

3.3.3 TIME-DEPENDENT INHIBITION OF FucD BY 3-HP

Inhibition of FucD by 3-HP was found to be time-dependent (Fig 3.8A and B) and not reversible after extensive dilution of inhibitor through repeated dialysis against assay buffer (Fig 3.8 C). Kinetic characterization of the inactivation of FucD by 3-HP was carried out using 3-HP concentrations ranging from 5.0 to 150.0 mM. Eqn 3.4 was fitted to the k_{obs} data obtained at different concentrations of 3-HP and the values of k_{inact}, K_I, and k_{inact}/K_I were estimated using non-linear regression analysis (Fig 3.7B, Table 3.3). Inactivation of FucD by 3-HP was found to be 4400-fold less efficient (k_{inact}/K_I) than

what was observed with MR although other parameters could not be compared due to lack of saturation observed for the inactivation of MR by 3-HP (Nagar, Mitesh *et al*., 2015). The role of Mg^{2+} was also assessed in FucD inactivation by 3-HP and found that inactivation did not proceed in the absence of Mg^{2+} (Fig 3.8D).

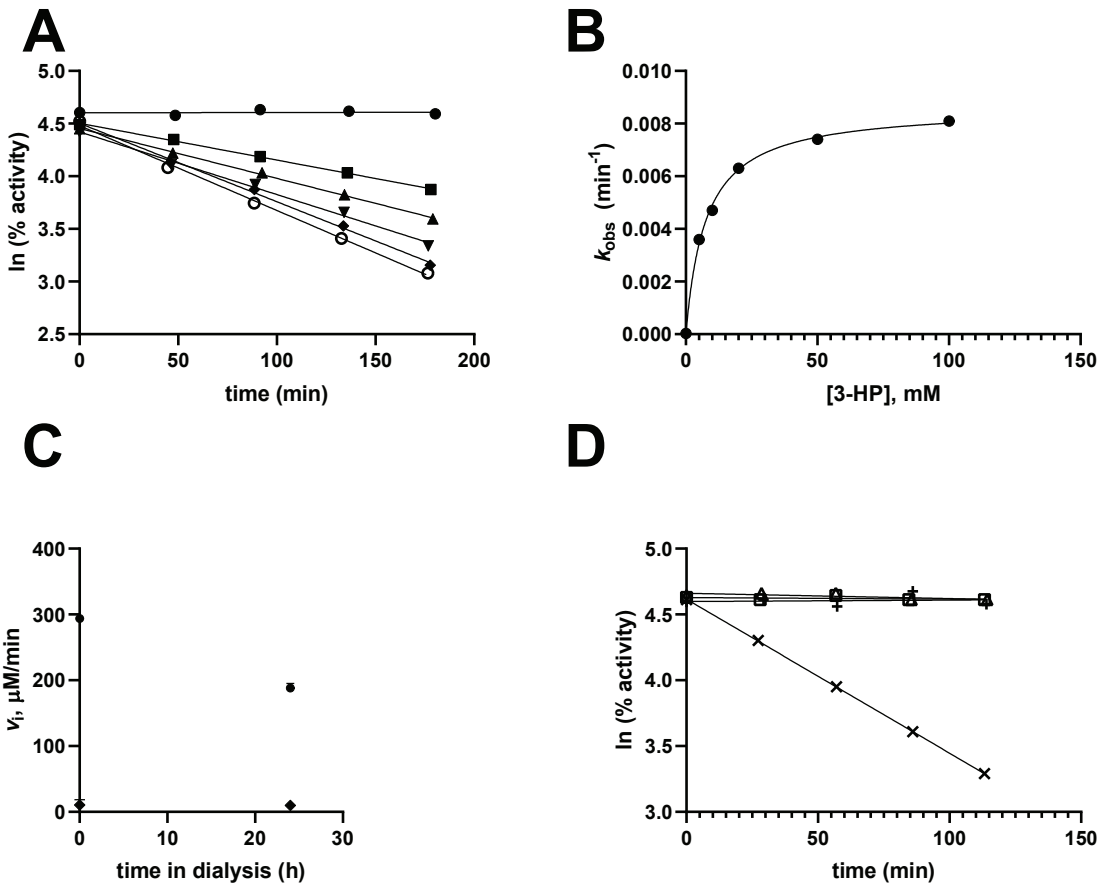

Figure 3.8 Time-dependent inhibition of FucD by 3-HP. Various concentrations of 3-HP (● = 0 mM, ■ = 5 mM, ▲ = 10 mM, ▼ = 20 mM, ◆ = 50 mM, ○ =100 mM) were incubated with FucD (475 µg/mL) (A). The k_{obs} values obstained from the slopes of Fig. 3.8 A were plotted against [3-HP] to estimate k_{inact} and K_I (B). Activity of FucD, incubated with 50 mM 3-HP for 8 h, is not regained after 24 h dialysis (● = 0 mM, ◆ = 50 mM), although some loss of activity occurs during dialysis (C). FucD inactivation by 3-HP requires Mg^{2+} (□ = Apo-FucD with 50 mM 3-HP, × = Mg^{2+} bound FucD with 50 mM 3-HP, + = Mg^{2+} bound FucD, △ = Apo-FucD) (D).

Table 3.3 Kinetic parameters of 3-HP-dependent FucD inactivation

	FucD	MR[a]
k_{inact} (s^{-1})	$1.49 \pm 0.0058 \times 10^{-4}$	-
K_I (mM)	7.94 ± 0.24	-
k_{inact}/K_I ($M^{-1}s^{-1}$)	0.0187 ± 0.0007	83 ± 8

[a] (Nagar *et. al.,* 2015)

Due to the lack of a readily available competitive inhibitor, protection studies were not carried out to determine if inactivation was due to reaction of 3-HP at the active site. However, given inactivation was so slow such that less than ~7% of enzyme could be expected to be inactivated during the 5 min required to make an initial velocity measurement (Fig 3.8A), kinetic inhibition studies were carried out to determine the mode of inhibition (Fig 3.9). 3-HP was found to be a competitive inhibitor with a K_i of 12.6 ± 0.4 mM, which is similar to the value obtained from the time-dependence studies ($K_I = 7.9 \pm 0.2$ mM).

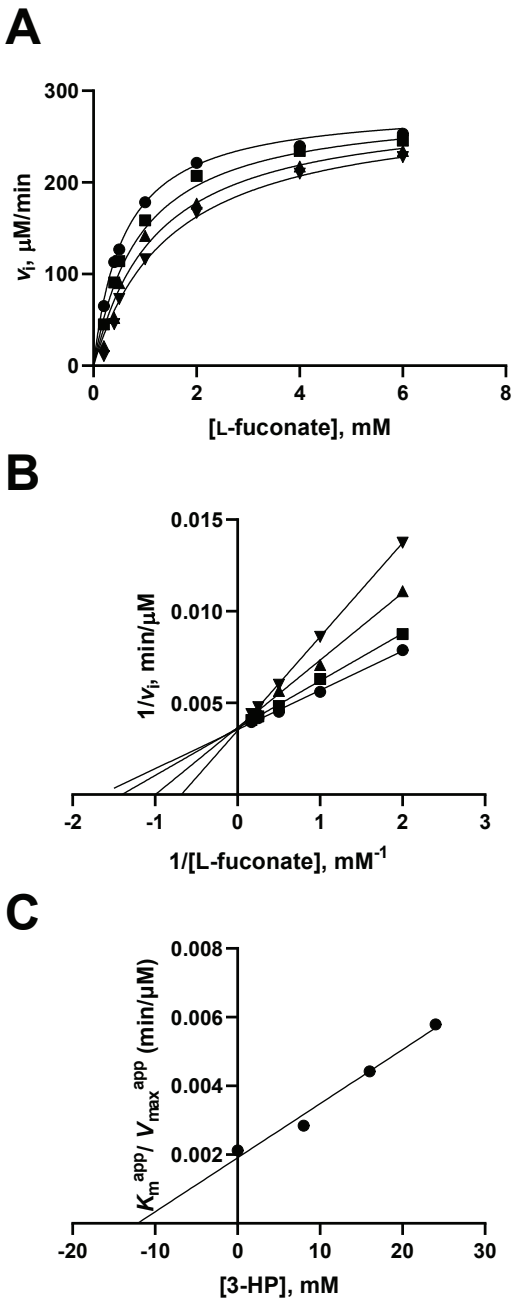

Figure 3.9 Competitive inhibition of FucD by 3-HP. Representative Michaelis-Menten plots of FucD with 0 (●), 8 (■), 16 (▲) and 24 (▼) mM 3-HP are shown (A). Double reciprocal plots for the inhibition of FucD by 3-HP (same labelling scheme as A) are shown in (B). The replot of K_m^{app}/V_{max}^{app} vs. [3-HP] yields a K_i value of 12.6 ± 0.4 mM (C).

An intermediate in the proposed inactivation scheme for FucD (see Discussion section 3.4.3) is glycolaldehyde (GLH). Hence GLH was also assessed as a time-dependent inhibitor of FucD. Time-dependent irreversible inactivation of FucD by GLH was observed (Fig 3.10), as was anticipated based on the relevant literature (Glomb & Monnier, 1995).

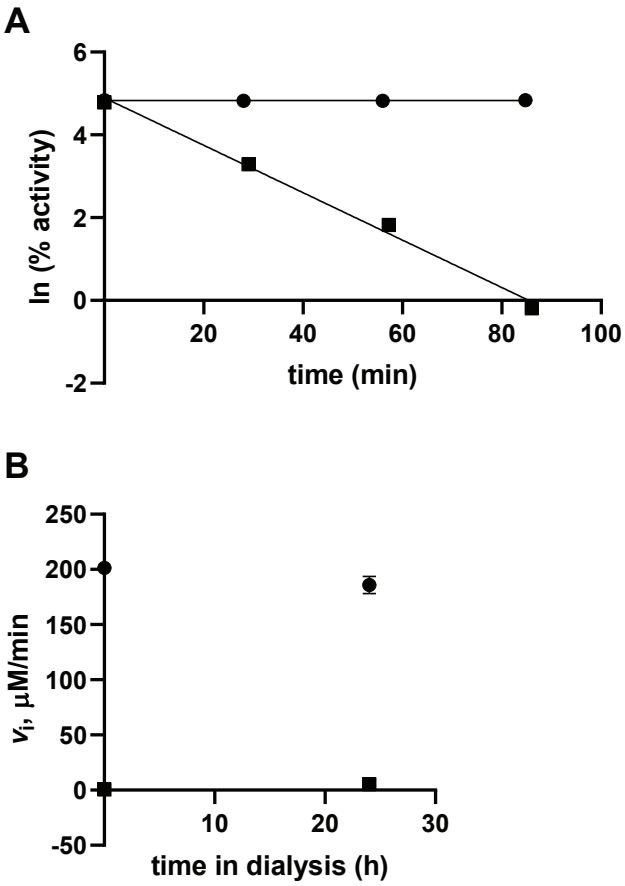

Figure 3.10 Glycolaldehyde-dependent inactivation of FucD. A plot of ln(% activity) vs. time shows that GLH inactivates FucD in a time-dependent manner (● = 0 mM GLH, ■ = 50 mM GLH) (A). Solutions containing 100 µg/mL FucD and either 50 mM GLH or an equivalent volume of buffer were tested for activity by addition of 4 mM L-fuconate and monitoring ellipticity at 216 nm. FucD incubated with GLH showed loss of activity over time. Overnight dialysis in FucD assay buffer to remove free GLH in solution did not restore activity to FucD (B).

3.3.4 MASS SPECTROMETRY ANALYSIS OF FucD TREATED WITH 3-HP OR GLH

Mass spectrometry experiments with WT FucD (100 μg/mL, 1.97 μM) treated with 3-HP (50 mM), showed the presence of an 86-Da adduct on Lys 220 as well as a 58-Da adduct, which was also found on several other polar surface residues (H, K, S). These adducts were not found on FucD in the buffer treated control solutions that lacked 3-HP (Fig 3.11-3.14). The H351N FucD variant also showed a 58 Da adduct on Lys 220 as well as surface residues with the same pattern as WT FucD (Fig 3.15).

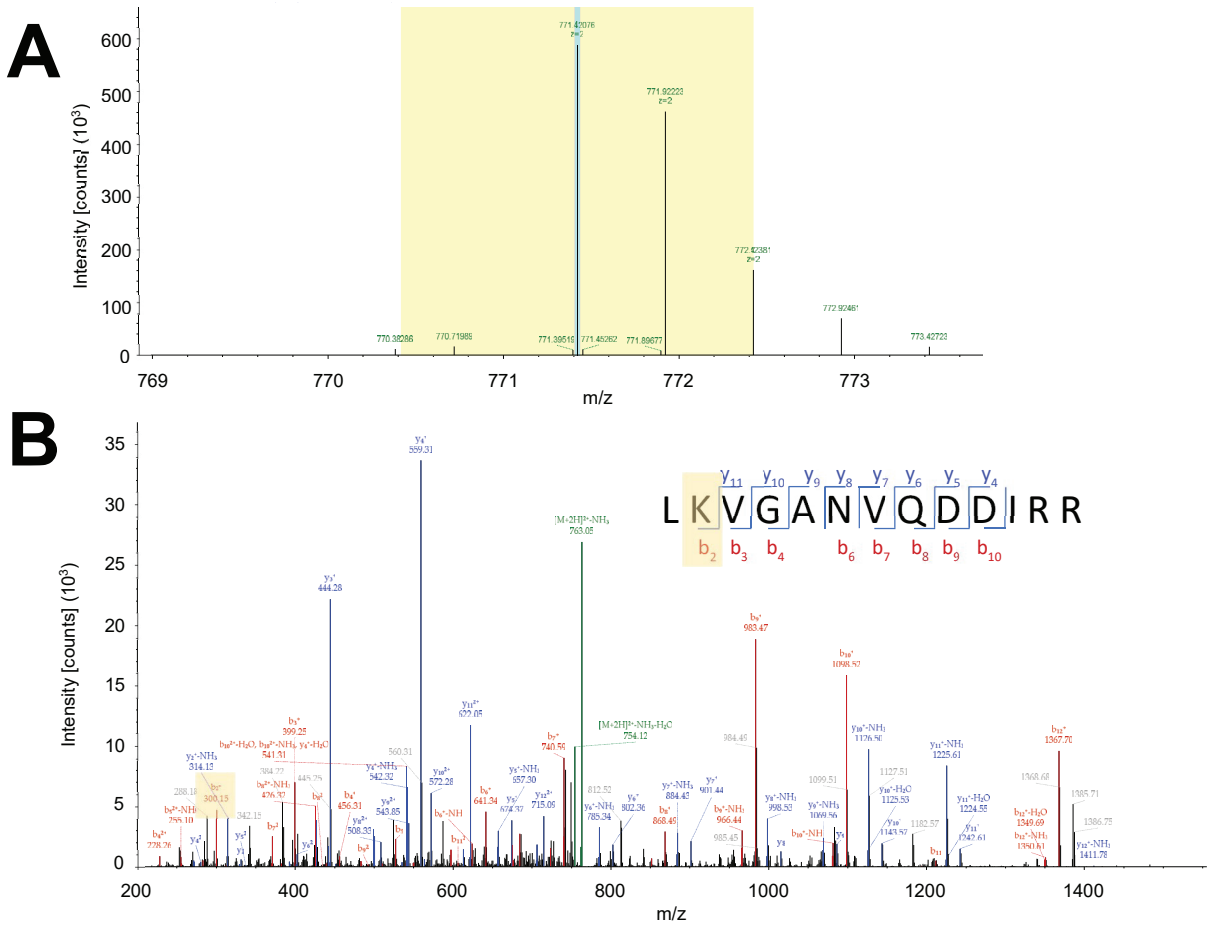

Figure 3.11 MS/MS evidence of a 58-Da adduct with Lys 220. The precursor isotope pattern spectrum (MS1 spectrum) for the LK peptide from FucD inactivated with 3-HP showing a 58 Da adduct ($[M+2H]^{+2}$, monoisotopic m/z: 771.421 Da) (A). MS/MS spectrum depicting the 58-Da adduct on the b_2^+ ion corresponding to Lys 220 (highlighted in orange) (B).

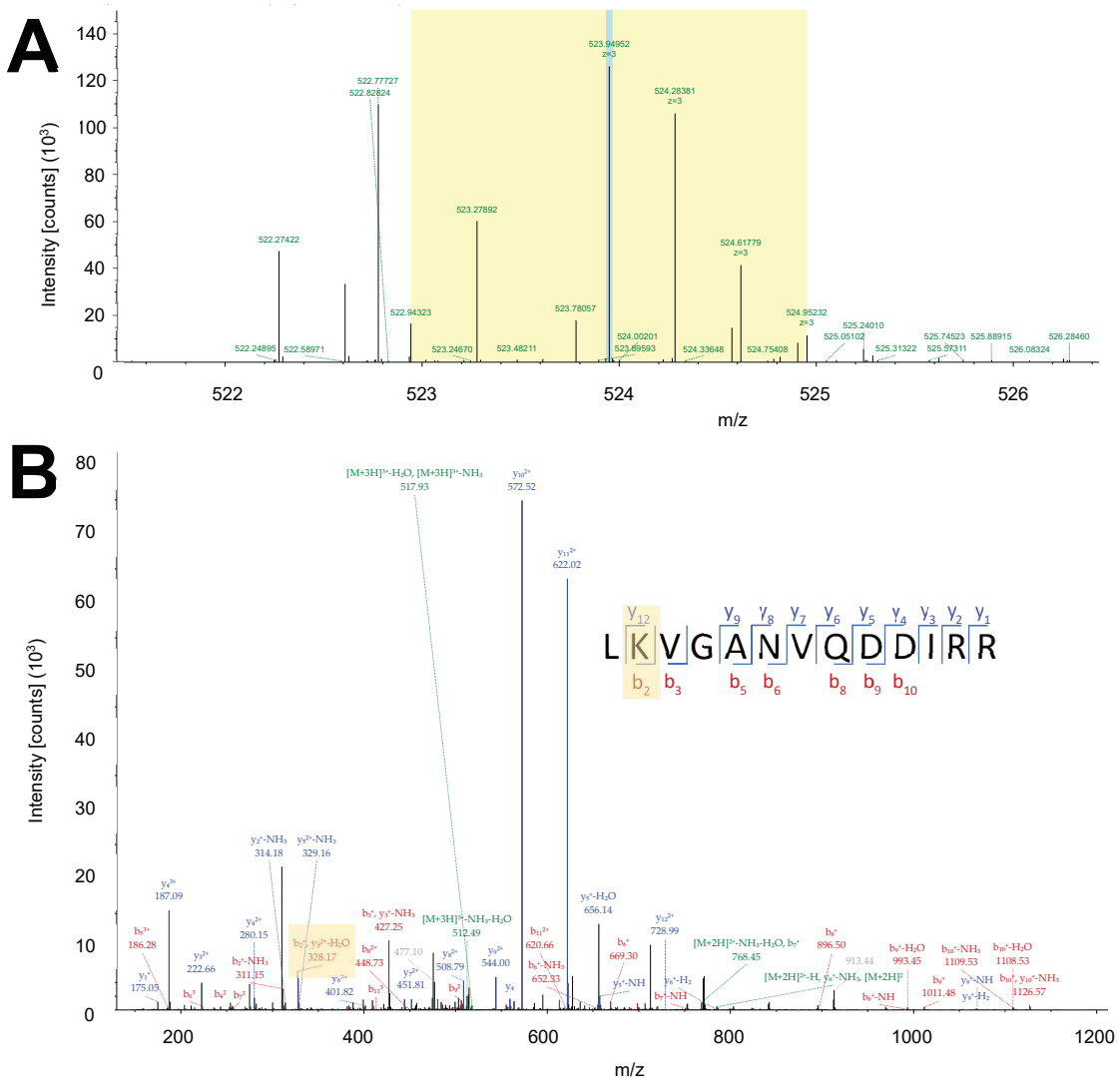

Figure 3.12 MS/MS evidence of an 86-Da adduct with Lys 220. The precursor isotope pattern spectrum (MS1 spectrum) for the LK peptide from FucD inactivated with 3-HP showing an 86-Da adduct ($[M+3H]^{+3}$, monoisotopic m/z: 523.950 Da) (A). MS/MS spectrum depicting the 86-Da adduct on the b_2^+ ion corresponding to Lys 220 (highlighted in orange) (B).

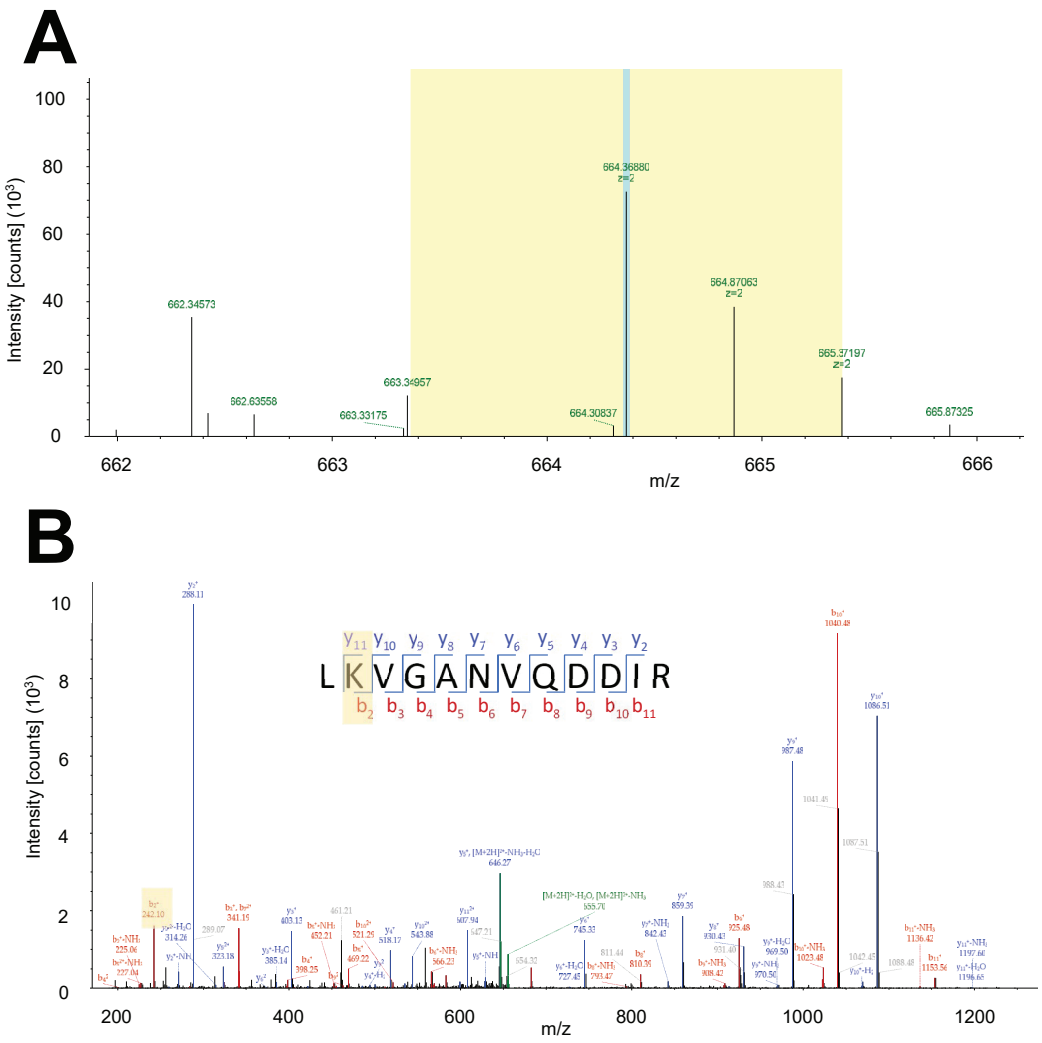

Figure 3.13 MS/MS data showing no adducts to Lys 220 in absence of 3-HP treatment. The precursor isotope pattern spectrum (MS1 spectrum) for the LK peptide from FucD incubated without 3-HP showing no adducts ($[M+2H]^{+2}$, monoisotopic m/z: 664.369 Da) (A). MS/MS spectrum depicting the LK peptide without adducts to Lys 220 indicated by the lower m/z value of the b_2^+ ion (highlighted in orange) (B).

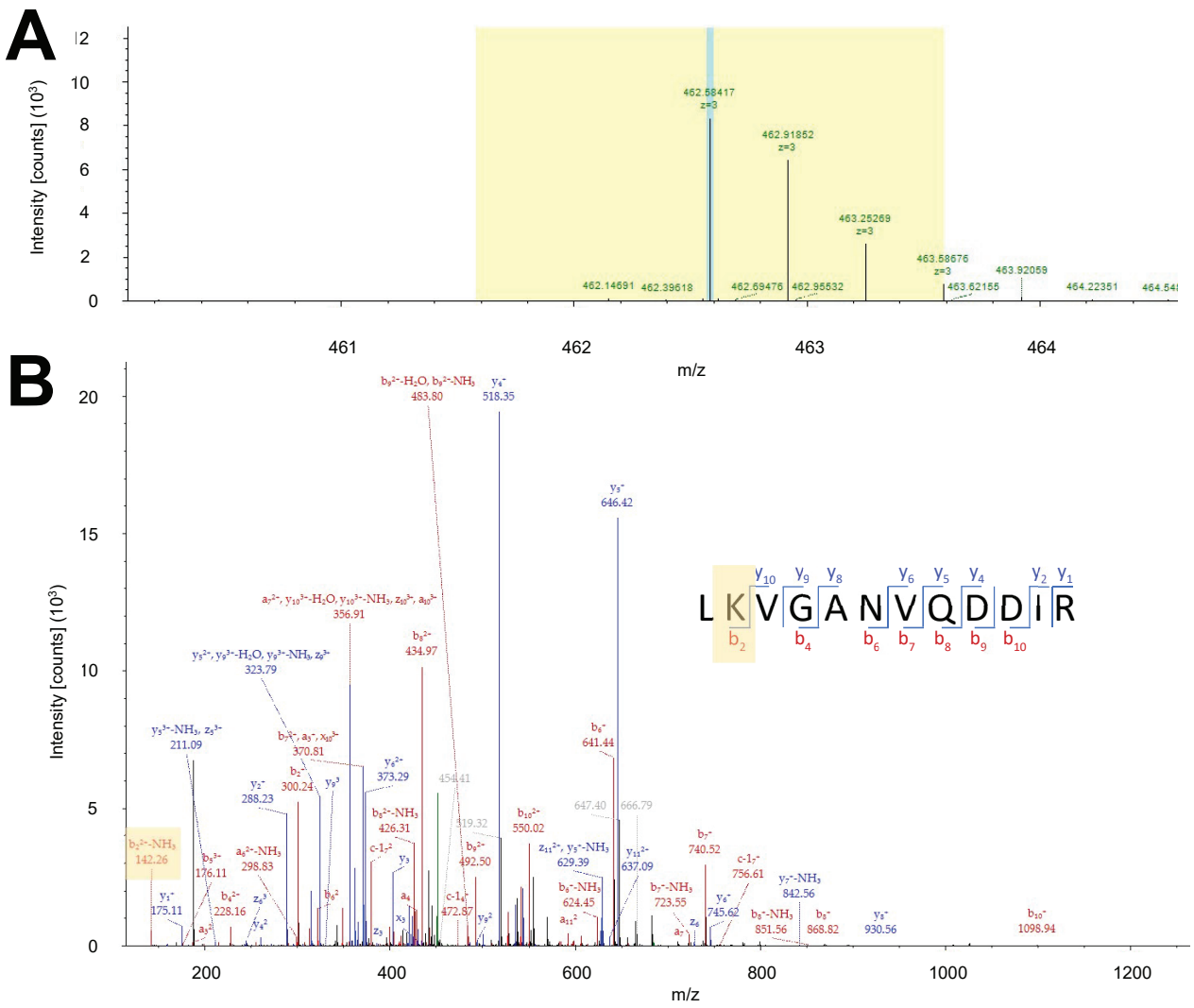

Figure 3.14 MS/MS data showing a 58-Da adduct to Lys 220 in H351N FucD treated with 3-HP. The precursor isotope pattern spectrum (MS1 spectrum) for the LK peptide from H351N FucD incubated with 3-HP showing a 58 Da adduct ($[M+3H]^{3+}$, monoisotopic m/z: 462.584 Da) (A). MS/MS spectrum depicting the LK peptide with a 58 Da adduct to Lys 220 indicated by the m/z value of the b_2^+ ion (highlighted in orange) (B).

I

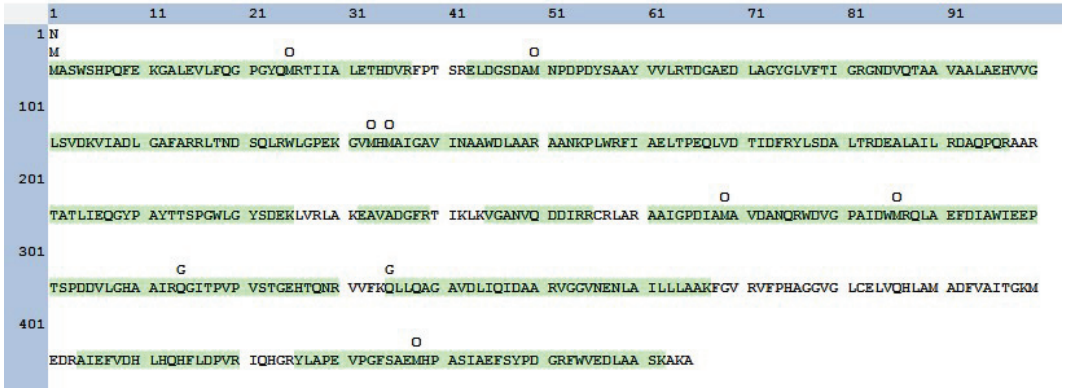

II

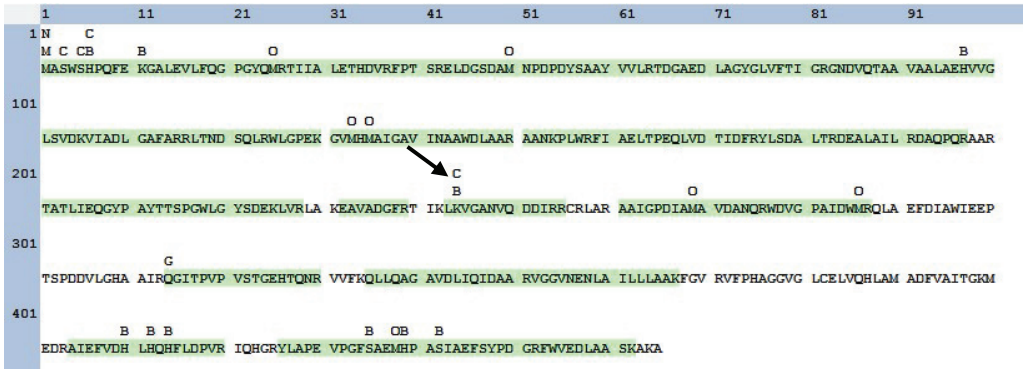

Figure 3.15 58- and 86-Da adducts are present in the 3-HP-treated FucD sample (II) but not the control (I). FucD (100 µg/mL, 1.97 µM), incubated without 3-HP, showing no 58- or 86-Da adducts (B = 58-Da adduct, C = 86-Da adduct, O = oxidation, M = N-terminal Met loss, N = N-terminal Met loss + Acetyl, G = Gln to pyro-Glu) (A). FucD (100 µg/mL, 1.97 µM) incubated with 50 mM 3-HP showed both 58- and 86-Da adducts on Lys 220 (indicated by the arrow), but also several 58-Da adducts on other polar residues. The distribution of 58-Da adducts is 6 His, 2 Ser, 2 Lys. The distribution of 86-Da adducts is 1 His, 2 Ser, 1 Lys (II). Sequence coverages were 84.52% and 81.08% for control (I) and 3-HP-treated samples (II).

Because the proposed mechanism for generation of 58-Da adducts involved formation of a Schiff base with Lys 220 (Discussion section 3.4.3, Scheme 3.1), I sought to assess the role of Lys 220 in generation of adduct between 3-HP and FucD. Treatment of the K220M FucD variant with 3-HP under the same conditions as WT FucD showed that 58-Da adducts were still present in roughly equivalent proportions to the WT enzyme (Fig 3.15). The H351N variant was also assessed for ability to form adducts with 3-HP given the role of His 297 determined in 3-HP mediated MR inactivation (Nagar *et al.,* 2015). No 86-Da adduct was observed on Lys 220 of H351N FucD incubated with 3-HP; however, 58 Da adducts were present to the same degree as seen in the WT trials (Fig 3.16).

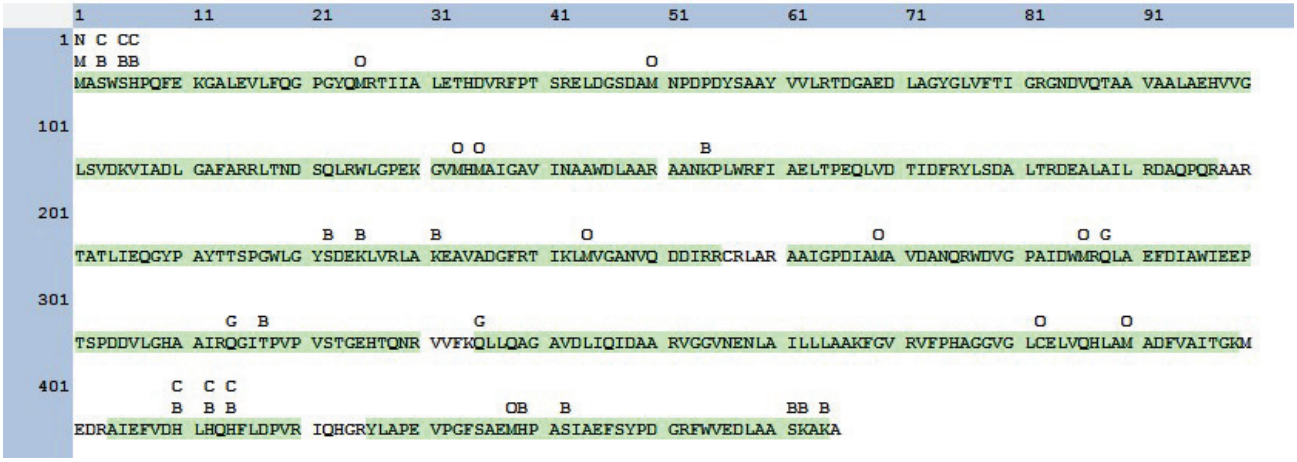

Figure 3.16 K220M FucD treated with 3-HP gives adducts similar to WT FucD. Adducts corresponding to 58-Da (B) and 86-Da (C) were found in K220M FucD samples (100 µg/mL, 1.97 µM) treated with 50 mM 3-HP FucD. (O = oxidation, M = N-terminal Met loss, N = N-terminal methionine loss +acetyl, G = Gln to pyro-Glu). The distribution of 58-Da adducts is 5 His, 5 Ser, 5 Lys and 1 Thr. The distribution of 86-Da adducts is 4 His and 2 Ser. Sequence coverage was 95.27%.

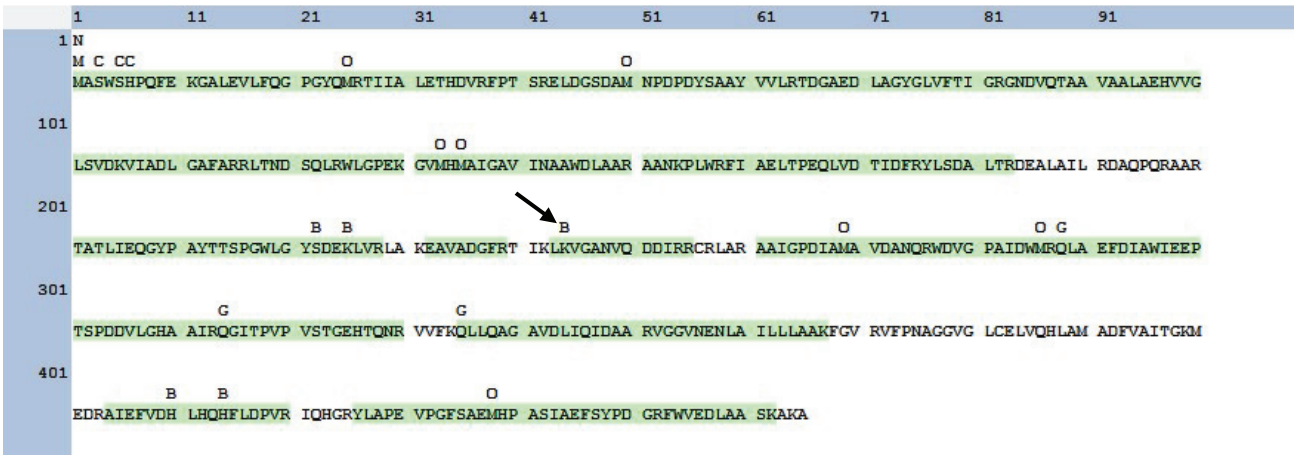

Figure 3.17 H351N FucD treated with 3-HP gives adducts similar to WT FucD without the 86-Da Lys 220 adduct. Adducts corresponding to 58-Da (B) were found in H351N FucD samples treated with 3-HP. A 58- Da adduct was observed on Lys 220 (indicated by the arrow) but no 86-Da adduct (would be labelled as a "C"). (O = oxidation, M = N-terminal Met loss, N = N-terminal methionine loss +acetyl, G = Gln to pyro-Glu). The distribution of 58-Da adducts is 2 His, 2 Lys and 1 Ser. The distribution of 86-Da adducts is 1 His and 2 Ser. Sequence coverage was 83.66 %.

To assess whether the alkylating agent could be GLH, generated by chemistry catalyzed by FucD as proposed in scheme 3.1 and then released from active site, WT FucD was treated with GLH until no activity was observed and then analyzed using LC-MS/MS. In this case, 58-Da adducts were observed, which was expected based on literature reports (Glomb & Monnier, 1995). However, there were no observed cases of modified His residues in the literature, which were common in the 3-HP treated samples. Residues modified by GLH were predominantly Lys and Arg residues which had been previously reported in the literature (Fig 3.16) (Acharya & Manning, 1983; Glomb &

Monnier, 1995). All modified residues from LC-MS/MS trials without reduction and alkylation are listed in Table 3.4.

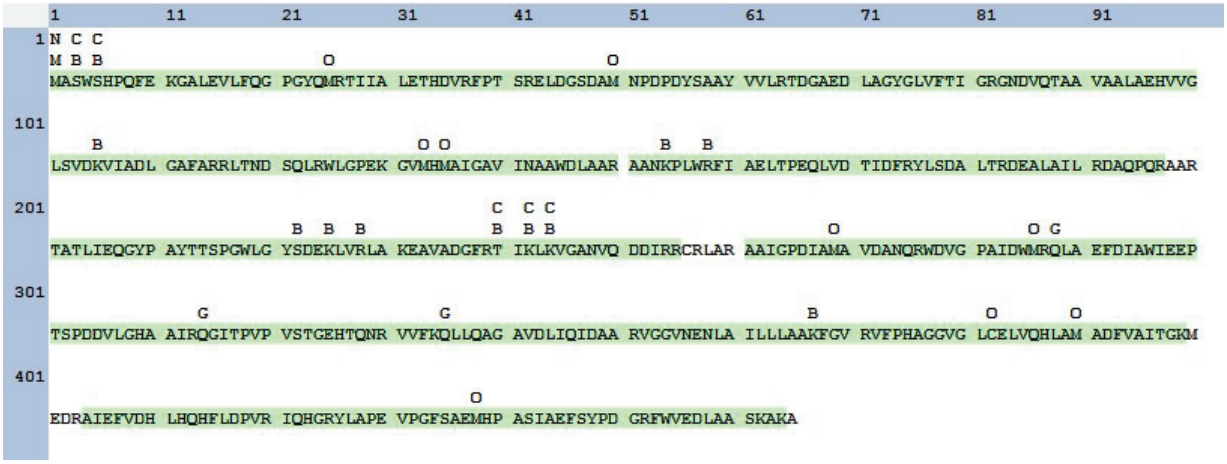

Figure 3.18 GLH treated FucD also gives 58-Da adducts. FucD samples treated with GLH until no activity was observed also displayed 58- and 86-Da adducts (B= 58 Da adduct, C = 86 Da adduct, O = oxidation, M = N-terminal Met loss, N = N-terminal Met loss + acetyl, G = Gln to pyro-Glu). The distribution of 58-Da adducts is 6 Lys, 2 Arg 3 Ser and 1 Thr. The distribution of 86-Da adducts is 2 Ser, 2 Lys and 1 Thr. Sequence coverage was 97.20%.

Table 3.4 Distribution of modifications caused by 3-HP and GLH

FucD Variant	Reagent	Modified Residues	
		58-Da Adduct	**86-Da Adduct**
WT	3-HP	H6*, K11*, H73, K220, H386, H388, H390, S411, H415, S418	S3*, S5*, H6*, K220
WT	GLH	S3*, S5*, K81, K130, R134, S198, K201, R204, T216, K218, K220, K343	S3*, S5*, T216, K218, K220
K220M	3-HP	S3*, S5*, H6*, K130, S198, K201, K207, T293, H386, H388, H390, H415, S418, S437, K438, K440	S3*, S5*, H6*, H386, H388, H390
H351N	3-HP	S198, K201, K220, H386, H390	S3*, S5*, H6*

* = N-terminal StrepII-tag and linker region

3.3.5 ^{1}H NMR SPECTRA OF 3-HP REACTION SOLUTIONS

After observing 58-Da adducts in the MS/MS spectra, ^{1}H NMR spectroscopy experiments were carried out on 3-HP solutions in assay buffer in the absence of enzyme with and without incubation at 25 °C for 6 h. Samples with WT and K220M FucD were also prepared where both solutions were incubated at 25 °C for 6 h (section 3.2.11). No visible changes to ^{1}H NMR spectra are apparent between both samples without enzyme and the sample incubated with K220M FucD. Three peaks are apparent in ^{1}H NMR spectra of 3-HP in assay buffer (50 mM Tris, 10 mM $MgCl_2$, pH 7.5) where the peak at 4.73 ppm corresponds to the 3-HP proton adjacent to an un-hydrated ketone, the peak at 3.69 corresponds to the 3-HP proton adjacent to the hydrated ketone, and the peak at 3.76 corresponds to Tris (Gottlieb *et al*., 1997). The peak corresponding to the proton adjacent to the 3-HP hydrated ketone at 3.69 ppm appears altered in intensity in the sample incubated with WT FucD (Fig 3.18D). The relative integration of the un-hydrated to hydrated 3-HP peaks were 1.00 to 0.79 for the 3-HP solution prepared fresh (Fig 3.18A), 1.00 to 0.83 for the 3-HP solution incubated for 6 h at 25 °C (Fig 3.18B), and 1.00 to 0.96 for the sample incubated with K220M FucD (Fig 3.18C).

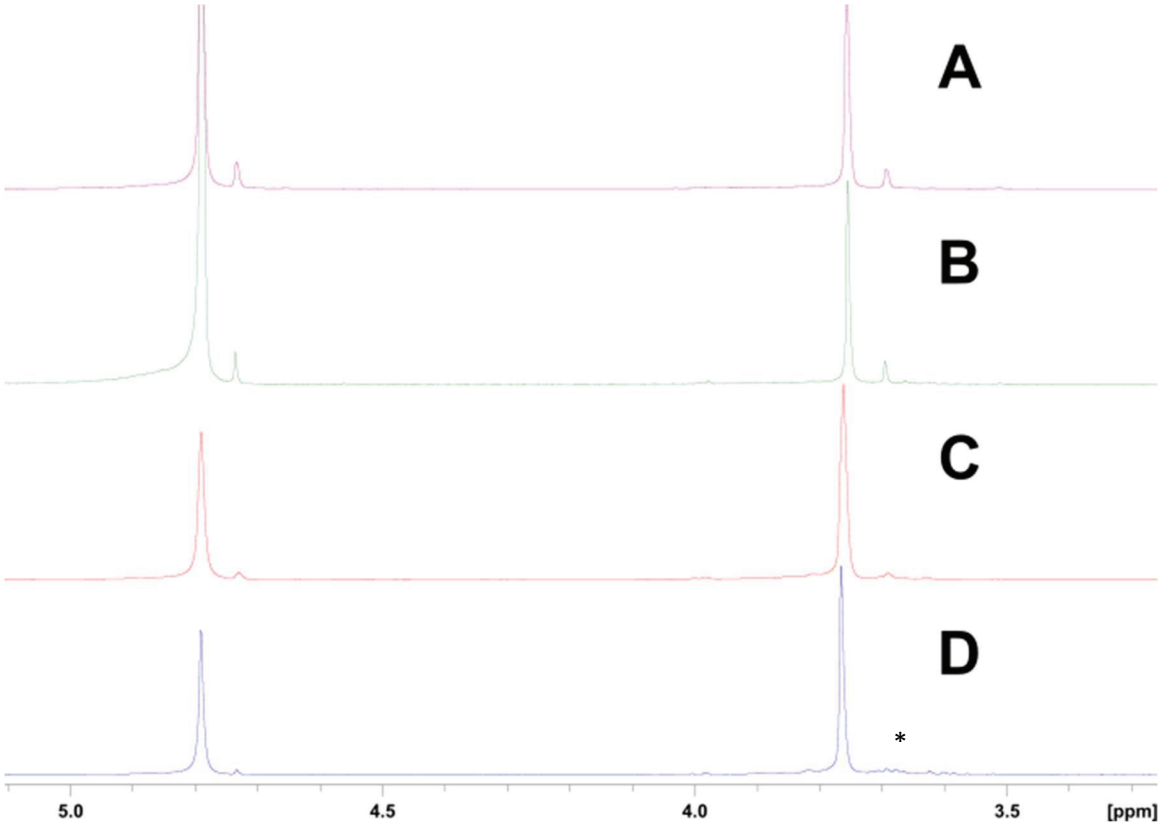

Figure 3.19 ^{1}H NMR spectra of 3-HP reaction solutions. Solutions of 100 mM 3-HP prepared fresh, hydrated to unhydrated = 1.00:0.79 (A), incubated for 6 h at 25 °C, hydrated to unhydrated = 1.00:0.83 (B), incubated for 6 h at 25 °C with K220M FucD, hydrated to unhydrated = 1.00:0.96 (C), and incubated for 6 h at 25 °C with WT FucD (D). The disturbed peak in D is highlighted with and asterisk.

3.3.6 ACTIVITY OF FucD VARIANTS

All Trp 101 FucD variants that were able to be purified in which the Trp residue at the tip of the interdigitating loop was replaced by Lys, Arg, Gln, or Glu did not display activity with L-fuconate using the CD-based assay up to enzyme concentrations well in excess of what is used for WT FucD assays (i.e., 300 μg/mL compared to 9.5 μg/mL). Also, no dehydration of *m*-galactarate by W101K, W101R, or WT FucD was observed using the CD-based assay developed for TGD (Easton *et al*., 2018). The K220M and H351N FucD variants were also assessed for activity and did not display measurable

velocity values even with high enzyme concentrations (100 μg/mL, 1.97 μM). All FucD variants were found to have overlapping CD spectra. Therefore, the loss of activity was likely not due to large scale protein folding differences relative to WT FucD (Fig 3.19). Also, all variants appeared identical by SDS-PAGE analysis with the exception of increased amounts of heat shock 70 protein in the K220M FucD preparation (Fig 3.20).

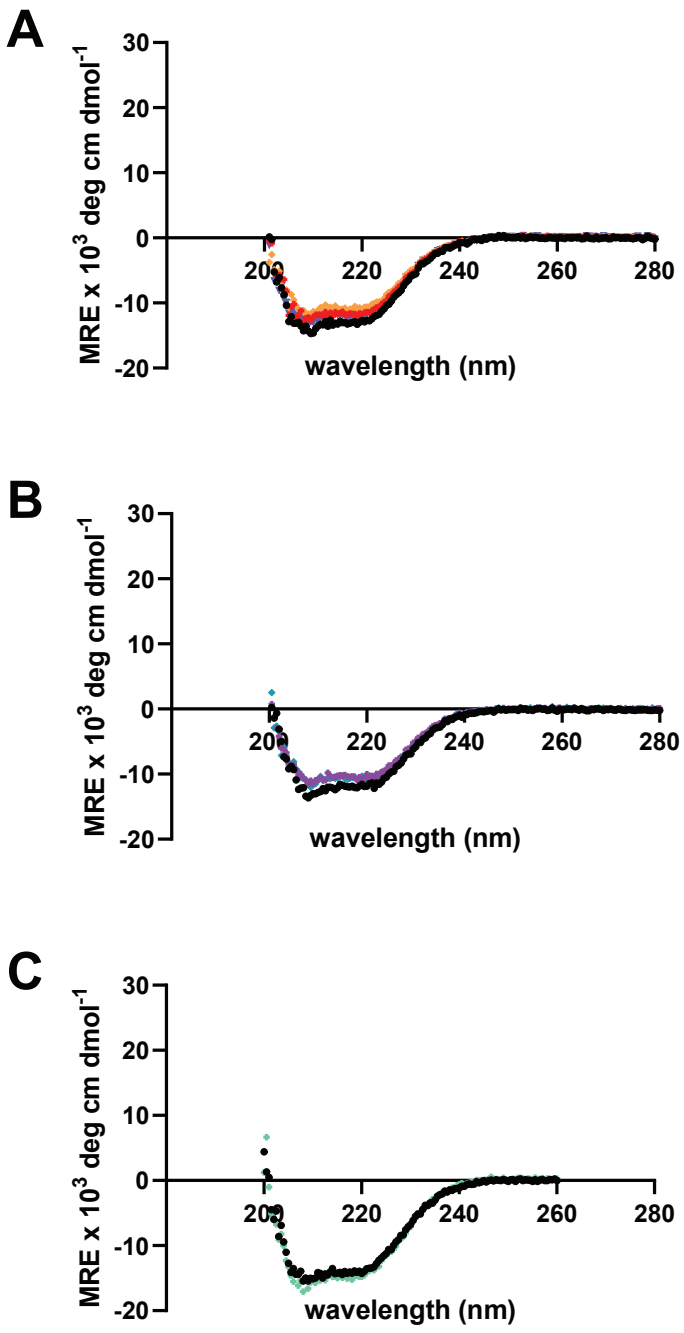

Figure 3.20 CD spectra of FucD variants. Overlaid CD spectra of WT, W101K, and W101R FucD variants (WT = ●, W101K = ■, W101R = ▲, K220M = ▼) (A). Overlaid CD spectra of WT, W101E, W101Q, and K220M FucD variants (WT = ● W101E = ✚, W101Q = ◆) (B). Overlaid CD spectra of WT and H351N FucD (WT = ●, H351N = ✚) (C). MRE = mean residue ellipticity.

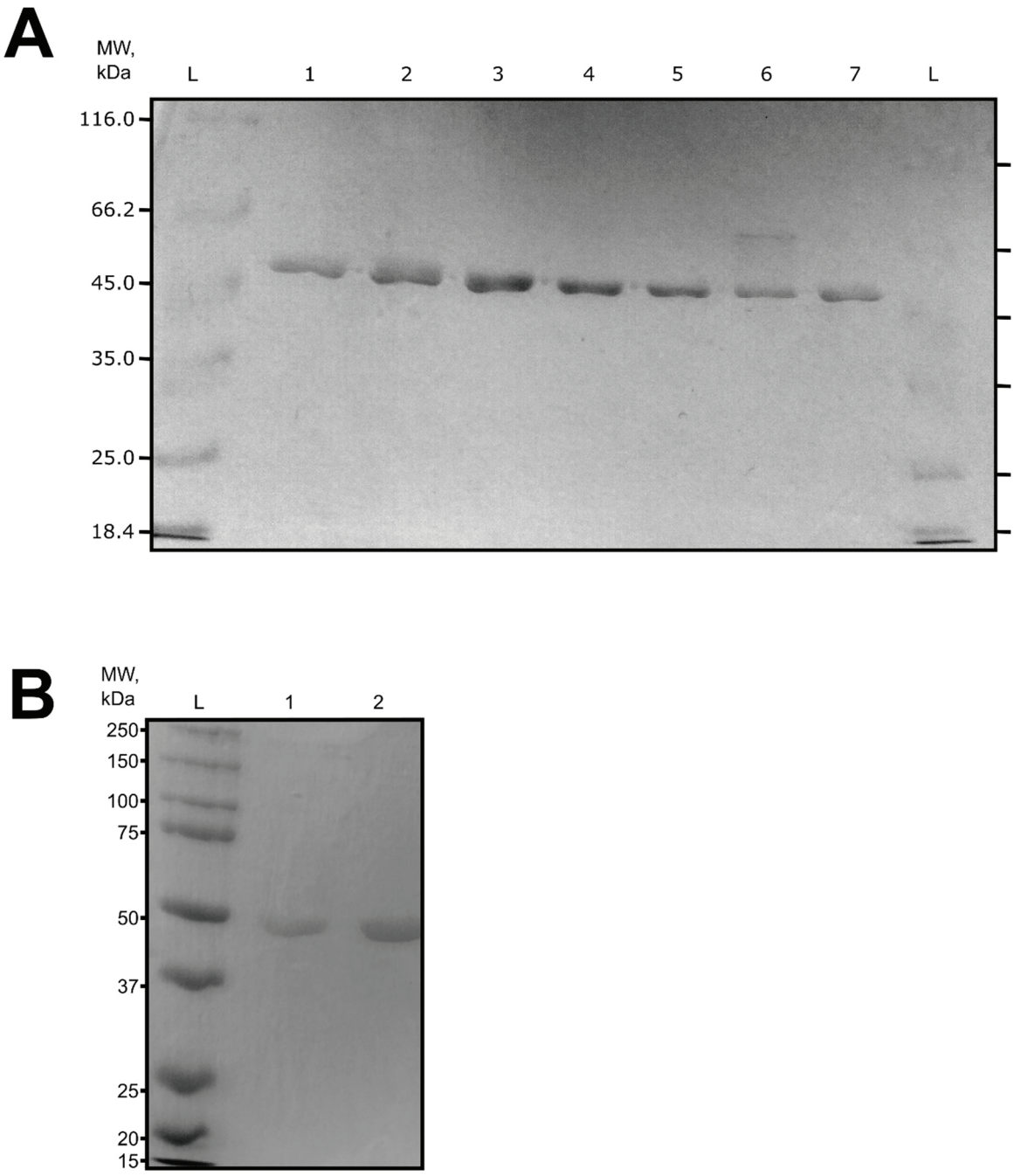

Figure 3.21 SDS-PAGE of FucD variants. Analysis of FucD variants by SDS-PAGE (10% SDS-polyacrylamide gel) found all to be the same estimated molecular weight and purity. Lanes are labelled as L = ladder, 1 and 7 = WT, 2 = W101K, 3 = W101R, 4 = W101Q, 5 = W101E, 6 = K220M (A). In B lanes are labelled as L = ladder, 1 = WT, 2 = H351N FucD. Calculated FucD variant MW: WT = 55.0 kDa, W101K = 53.1 kDa, W101R = 51.1 kDa, W101Q = 50.3 kDa, W101E = 49.6 kDa, K220M = 49.6 kDa (heat shock 70 = 63.5 kDa), H351N = 53.4 kDa.

3.3.7 DETERMINATION OF THE OLIGOMERIC STATE OF WT FucD AND ITS TRP 101 VARIANTS

Since 3-HP derived adducts appeared to be only on one side of the dimeric unit when mapped to the X-ray crystal structure (see discussion Fig 3.23 and 3.24), I hypothesized that FucD might exist in solution as a tetramer, such that one face of the dimer was protected from reaction with 3-HP or GLH. In addition, since Trp 101 is located at the tip of the interdigitating loop of FucD, it is possible that mutation of that residue could influence dimerization of FucD. Consequently, the oligomeric state of FucD was investigated using GF-HPLC and DLS.

GF-HPLC revealed that all FucD variants (WT, W101K, W101R, W101Q and W101E) were dimeric, comparing with MR as a control, which was found to be tetrameric (Fig 3.21, Table 3.5). DLS measurements revealed that FucD particles had a hydrodynamic diameter (d_H) of 6.4 ± 0.4 nm compared to MR, which had a d_H value of 9.6 ± 0.5 nm (Fig 3.22). These DLS results are also consistent with a dimeric structure of FucD and a higher oligomeric state of MR considering comparable monomeric molecular weights.

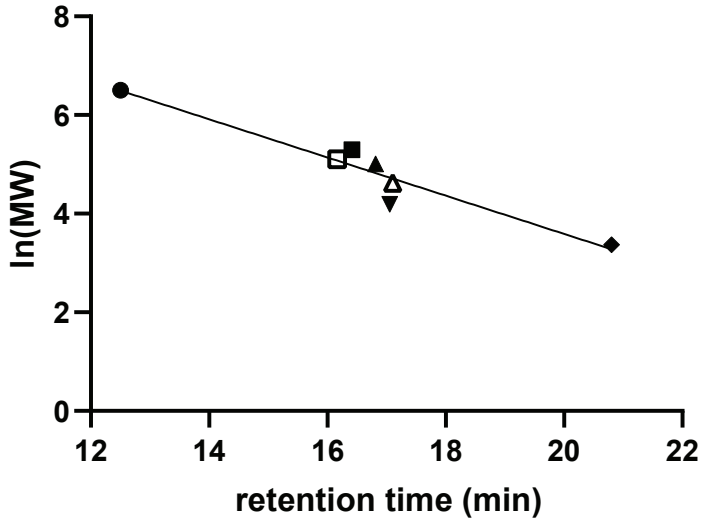

Figure 3.22 Representative standard curve for GF-HPLC. Shown is a representative plot of ln(MW) vs. retention time to determine the oligomeric state of FucD and MR (● = bovine thyroglobulin (669 kDa), □ = tetrameric MR, ■ = β-amylase (200 kDa), ▲ = alcohol dehydrogenase (150 kDa), △ = dimeric FucD, ▼ = bovine serum albumin (66 kDa), ◆ = carbonic anhydrase(29 kDa)). The linear equation used to calculate the MW of FucD and MR is ln(MW) = -0.38584(ret time in min) + 11.324 with an R value is 0.95998. The error on the slope and ordinal intercept from direct fitting of the data is ± 0.064991 and ± 1.0998 respectively using *KaleidaGraph* software (v. 4.02, Synergy Software, Reading, PA).

Table 3.5 GF-HPLC results for FucD variants compared to WT MR

Enzyme Variant	Retention Time (min)	Calculated Molecular Weight (kDa)	Monomer Molecular Weight (kDa)	Deduced Oligomeric State
WT FucD	17.15 ± 0.05	114.5 ± 1.3	50.8	dimer
W101K FucD	17.33 ± 0.05	106.9 ± 1.3	50.8	dimer
W101R FucD	17.29 ± 0.06	108.7 ± 1.2	50.8	dimer
W101Q FucD	17.14 ± 0.06	114.8 ± 0.9	50.8	dimer
W101E FucD	17.18 ± 0.05	113.1 ± 1.3	50.8	dimer
WT MR	16.19 ± 0.02	164.8 ± 3.1	41.3	tetramer

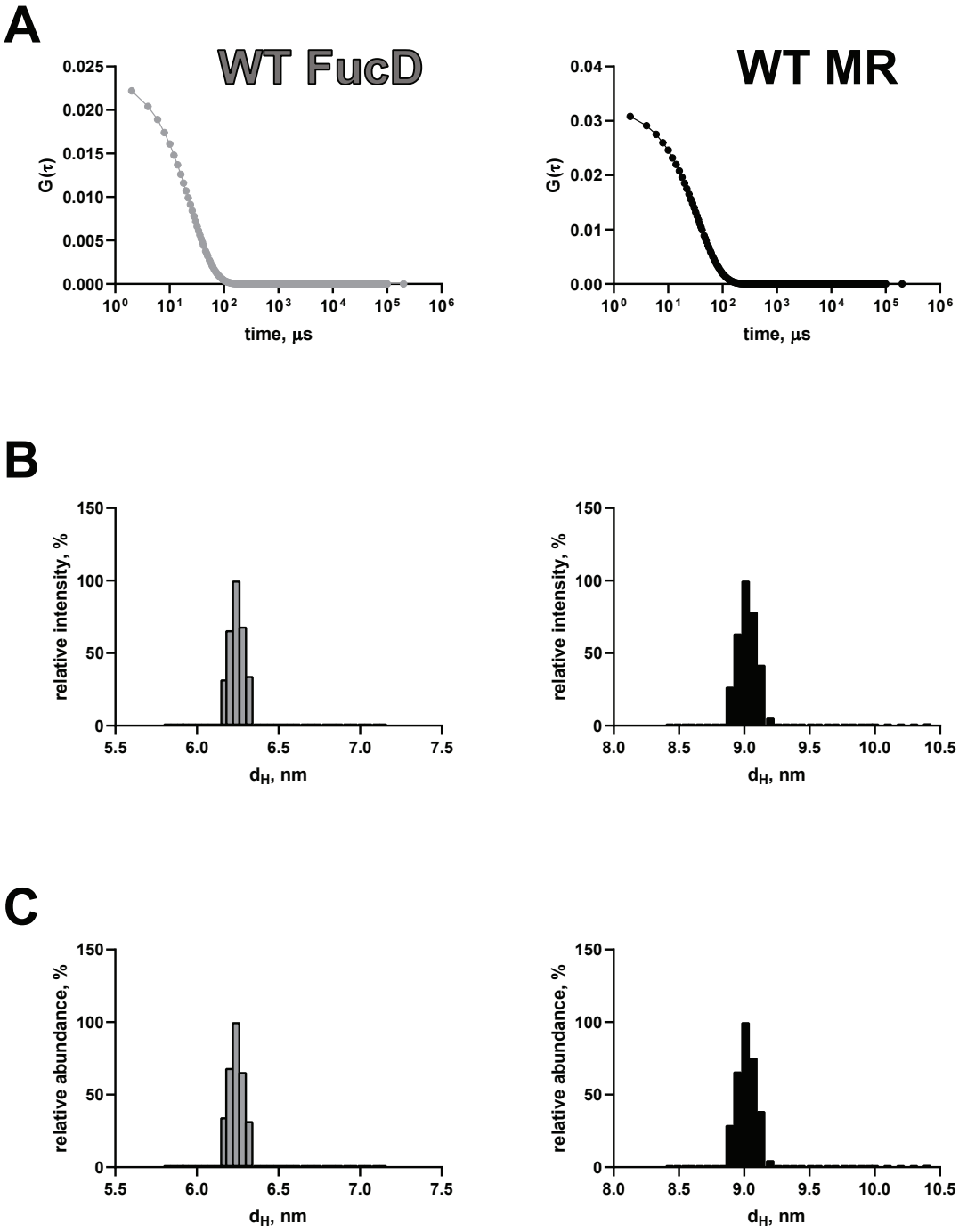

Figure 3.23 DLS results showing that MR is larger in solution than FucD. The d_H of FucD is smaller than MR, consistent with the GF-HPLC results that showed that FucD is a dimer. NNLS fits to the autocorrelation functions from DLS analysis of WT FucD (grey) or WT MR (black) (A). Intensity (B) and number (C) weighted populations of WT FucD and WT MR from the DLS analysis.

3.4 DISCUSSION

3.4.1 INHIBITION OF FucD BY TARTRONATE

Tartronate is an interesting inhibitor of MR since it interacts with binding determinants that are all components of the machinery used to catalyze the enolization reaction. These binding determinants are conserved for all subgroup members discovered so far (Bearne, S. L. & St. Maurice, 2017; Nagar, Mitesh et al., 2014). MR bound tartronate between His 297 and Lys 166 via a bridging carboxylate group while the opposite carboxylate group and hydroxyl group chelated the Mg^{2+} ion (Fig 1.6B). Therefore, these interactions might permit tartronate to bind to all MR subgroup enzymes, despite it's not sharing structural similarity to the enzyme's substrate, product, or proposed transition state.

Although X-ray crystal structures of MR subgroup enzymes (see Fig 1.7) show that the binding determinants are all located in roughly the same locations in the active sites, one variable that could impact the strength of tartronate binding to MR subgroup enzymes would be the pK_a of the catalytic His and Lys residues. That FucD binds tartronate more weakly than MR does, suggests that the pK_a of His 351 and/or Lys 220 of FucD may be lower than that for His 297 and Lys 166 in MR. A lower pK_a of the catalytic acid-base residues in FucD would result in less positive character of the active site components poised to interact with the negatively charged distal carboxylate group of tartronate via a salt bridge. Another possibility as to why FucD binds tartronate with less affinity than MR does may be because of differences in the positioning of these residues. When the enzymes are in solution they are conformationally flexible. Should the active site His and Lys residues be more flexible in FucD than MR, they may be less often in

the correct orientation to bind tartronate efficiently. These differences would not be able to be detected in X-ray crystal structures.

Previous members of the Bearne group have determined the K_i values of tartronate for the MR subgroup members L-talarate/galactarate dehydratase (TGD) (Easton *et al*., 2018) and D-tartrate dehydratase (TarD) (Aboushawareb and Bearne, unpublished) (Table 3.6). These results are part of a general study to determine whether a binding trend could be deduced for MR subgroup members that exhibited slightly different reactions (i.e., racemization/epimerization and/or dehydration). Since affinity for tartronate could be related to the positive character of the active site catalytic His and Lys residues, comparison of the K_i values might also help to delineate the relative basicity/acidity of active site residues required to carry out either racemization or dehydration reactions. Unfortunately, no clear trend emerged. In general, tartronate was an inhibitor exhibiting moderate affinity with MR and TarD, but of relatively weak affinity with FucD and TGD (Table 3.6). That said, tartronate certainly is recognized by all members of the MR subgroup examined.

Table 3.6 Comparison of tartronate binding to MR subgroup members MR, TarD, TGD, and FucD

	MR	TGD	TarD	FucD
K_i (mM)	1.8 ± 0.1[a]	10.7 ± 0.4[c]	0.5 ± 0.1[d]	8.4 ± 0.7
K_m (mM)	1.03 ± 0.05[b] (*R*)-mandelate	0.38 ± 0.05[c]	0.086 ± 0.007[e]	0.49 ± 0.02
K_i/K_m	1.8	28	5.8	17
Reaction	racemization	dehydration, ketonization, and epimerization	dehydration	dehydration and ketonization

[a] (Nagar, Mitesh *et al*., 2014)
[b] (Fetter *et al*., 2019)
[c] (Easton *et al*., 2018)
[d] Sarah Aboushawareb and Bearne, unpublished
[e] (Yew *et al*., 2006)

3.4.2 INACTIVATION OF FucD BY 3-HP

3-HP was found to be an active site-directed irreversible inactivator of MR (Nagar, Mitesh *et al*., 2015). MS/MS evidence showed that an 86-Da adduct with Lys 166 where in the proposed mechanism 3-HP forms a Schiff base with Lys 166 which is deprotonated by His 297 (Scheme 1.5). X-ray crystallography was employed to determine whether the Schiff base formation occurred at carbons 2 or 3, depending on whether 3-HP tautomerized to tartronate semialdehyde (Scheme 1.5). Electron density suggested two major conformations of the adduct in the active site of MR, both connected to Lys 166 at C-2 indicating no tautomerization to tartronate semialdehyde took place before adduct formation (Fig 1.8). In this thesis work, 3-HP was found also to be an irreversible inactivator of FucD. This is consistent with the identical positioning of FucD Lys 220 and MR Lys 166 in the active site as well as FucD His 351 and MR His

297. However, compared with other MR subgroup members tested for inactivation by 3-HP, FucD deviates from TGD and TarD, which were only reversibly inhibited by 3-HP.

3-HP-dependent inactivation of FucD was found to be much less efficient than inactivation of MR, suggesting either a different mechanism of inactivation occurred, or the reactivity of Lys 220 towards 3-HP was much reduced relative to Lys 166 of MR. There were no readily available competitive inhibitors of FucD available to test whether 3-HP inactivates FucD by modifying the active site or another area of the protein. However, given the very slow rate of inactivation, such that greater than 93% of protein in solution was estimated to still be active over a five-minute assay time span, conventional inhibition studies were conducted to determine the mode of inhibition. Consistent with previously studied MR subgroup members, where 3-HP was not an irreversible inactivator (Easton and Bearne, unpublished), 3-HP was found to be a competitive inhibitor of FucD of modest affinity (Fig 3.6).

LC-MS/MS analysis was conducted to determine if the mechanism of inactivation was the same as that described for MR (Nagar, Mitesh *et al*., 2015). An 86-Da adduct at Lys 220 was found, analogous to what was observed with MR, but surprisingly a 58-Da adduct was also observed at this residue. ^{1}H NMR experiments were conducted to potentially observe the presence of aldehyde (potentially tartronate semialdehyde or glycolaldehyde) generated non-enzymatically or by FucD. No aldehyde peak was apparent in any of the samples (i.e., ~10 ppm), although the peak corresponding to the proton adjacent to the hydrated ketone of 3-HP appeared altered in intensity in the 3-HP sample incubated with WT FucD (Fig 3.18D). Aldehyde species could be hydrated such

that no peak at ~10 would be observed and spectral changes could overlap with the hydrated 3-HP peak.

Furthermore, 58-Da adducts were found on polar residues on the exterior of the protein, seemingly localizing to one side of the dimer (Fig 3.23). This finding suggests the formation of a reactive intermediate that is either released from the active site or is formed non-enzymatically over the course of the reaction that then reacts to form 58-Da adducts.

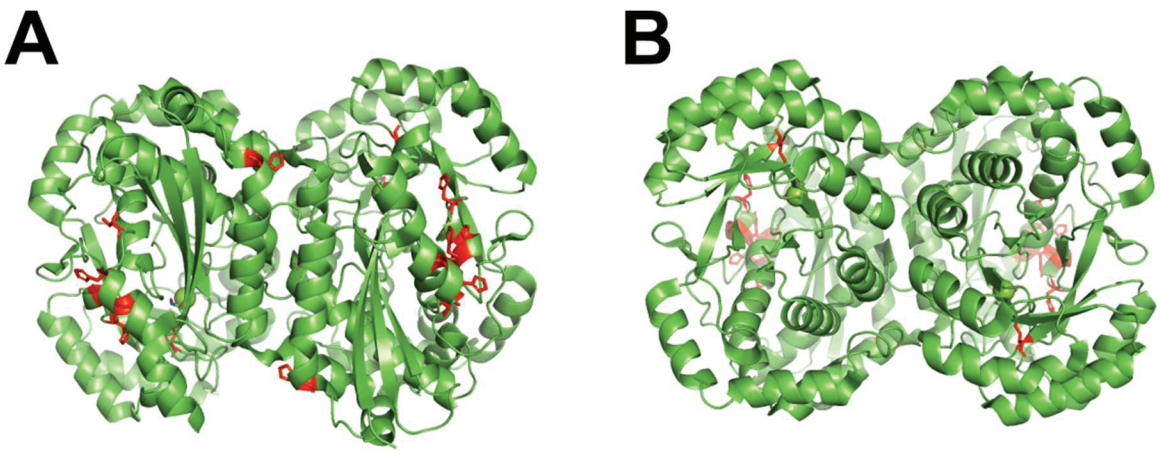

Figure 3.24 58-Da adducts arising from 3-HP treatment appear to be localized to one side of the FucD dimer. Shown in red are the residues modified by 58-Da adducts when WT FucD was treated with 3-HP. The dimer face with 58-Da adducts has modified residues shown in red (A). The opposite side of the dimer doesn't show the presence of 58-Da adducts (B).

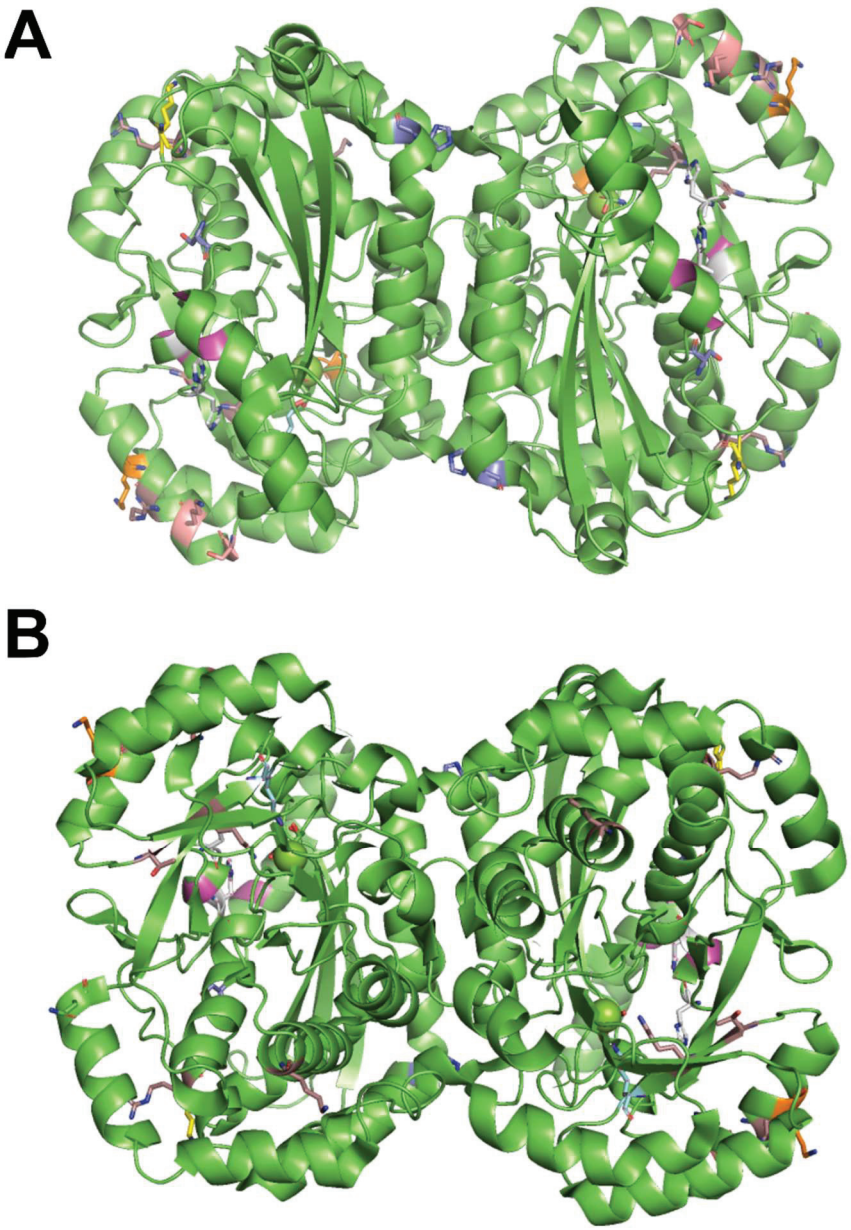

Figure 3.25 Residues modified with 58-Da adducts observed in all LC-MS/MS experiments. Shown are all modified residues from WT, K220M and H351N FucD variants treated with 3-HP and WT FucD treated with GLH (A and B are opposing faces of the dimer). Modified residues found in WT, WT-GLH, and H351N = Lys 220 (cyan), WT and K220M = H388, H415, S418 (magenta), WT-GLH and K220M = K130 (yellow), WT-GLH, K220M, and H351N = S198, K201 (salmon), All 3-HP treated samples = H386, H390 (gray), WT 3-HP = H73, S411 (purple), K220M 3-HP = K207, T293, S437, K438, K440 (orange), H351N 3-HP = none not shared, WT-GLH = R134, R204, T216, K218, K343 (brown).

A mechanism for formation of 58-Da adducts from 3-HP was proposed (Scheme 3.1), which included formation of the two-carbon reducing sugar glycolaldehyde, which has been shown previously to react with polar amino acids on proteins to form 58-Da adducts (Glomb & Monnier, 1995; Thorpe & Baynes, 2003). This reaction has been well-studied as a Maillard reaction pathway where carbohydrates modify proteins to create the brown color and influence the flavor of popular foods like steak, bacon and bread (van Boekel, 2006).

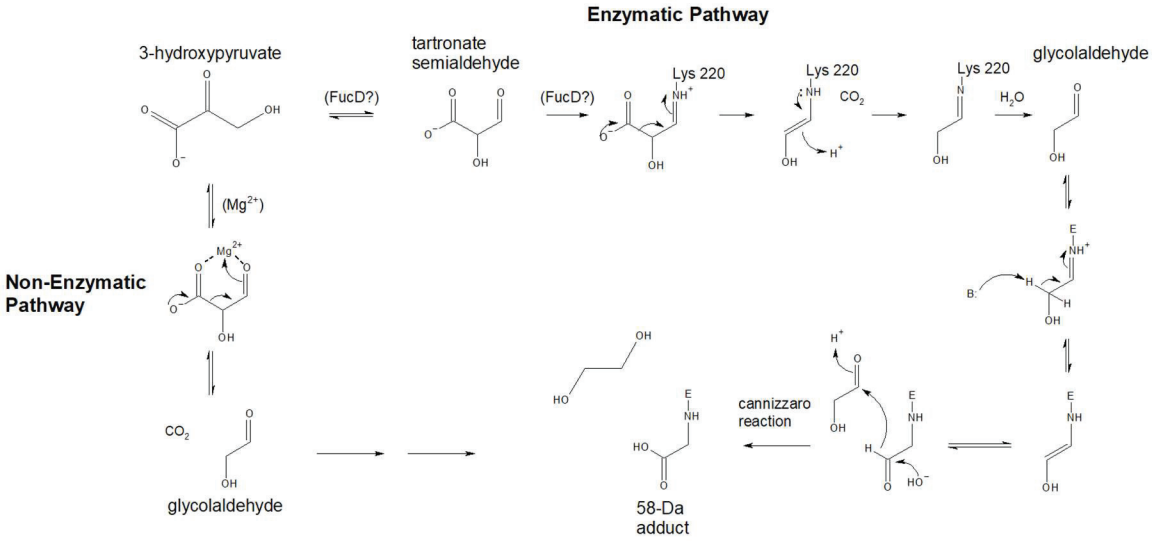

Scheme 3.1 Possible mechanism for formation of 58-Da adducts formed upon incubation of 3-HP with FucD

FucD is proposed to catalyze the tautomerization of 3-HP to tartronate semialdehyde, which then ether spontaneously decarboxylates to glycolaldehyde (GLH) or does so in a FucD-dependent manner as shown in scheme 3.1. GLH could add to reactive polar residues (e.g. Lys) to form a Schiff base and then undergo a Canizzaro reaction to form a 58-Da adduct with Lys 220 or other polar residues. This mechanism was tested in three ways: treatment of FucD with GLH, 3-HP incubation with K220M

and H351N FucD followed by MS/MS analysis, and determining if Mg^{2+} was required for FucD inactivation.

Incubation of FucD with GLH resulted in irreversible inactivation as expected for a known protein alkylating agent (Fig 3.10). Furthermore, MS/MS analysis revealed the presence of 58-Da adducts, but primarily on Lys and Arg residues on the protein surface, as opposed to on His residues which was typically observed in 3-HP-dependent inactivation experiments. It could be that exterior Lys residues are protected in 3-HP incubation experiments by hydrolysable Schiff base products with 3-HP considering the relatively large concentration of 3-HP in solution, where GLH is relegated to residues that form less stable Schiff base products and are thus more available for reaction and formation of stable 58-Da adducts.

Incubation of K220M FucD with 3-HP produced 58-Da adducts at surface residues (Ser, Lys, and His residues see Fig 3.15) in roughly the same proportions as WT FucD. This demonstrates that formation of a reactive alkylating intermediate for formation of 58-Da adducts (i.e., GLH) does not require Lys 220.

The H351N FucD variant was also assayed to determine what adducts form upon incubation with 3-HP given His 351 is also a reactive base in the FucD active site (Yew *et.al.,* 2006) that could be involved the tautomerization of 3-HP to tartronate semialdehyde. However, 58-Da adducts were observed on the surface of H351N FucD similar to WT and K220M variants, indicating His 351 is not required for formation of the alkylation reagent. However, interestingly no 86 Da adduct was found on Lys 220 of H351N FucD when it was treated with 3-HP (Fig 3.16). Formation of 86-Da adducts was dependent on His 297 in MR and did not form on Lys 166 when H297N MR was treated

with 3-HP (Nagar *et.al.,* 2015). Therefore, that an 86-Da adduct was not observed on Lys 220 in the H351N FucD variant (analogous to H297N MR) may suggest that the 86-Da Lys 220 adduct reaction pathway follows the same route as MR.

Literature reports indicated that Mg^{2+} catalyzes the tautomerization of 3-HP to tartronate semialdehyde (Hedrick & Sallach, 1961), which can be decarboxylated to give GLH. Therefore, experiments investigating the role of Mg^{2+} in 3-HP mediated inactivation of FucD were conducted. It was found that Mg^{2+} is essential for 3-HP-mediated inactivation of FucD. It is possible that the Mg^{2+} ion may be aiding formation of tartronate semialdehyde either in solution (i.e., non-enzymatically) or on the enzyme. Tautomerization of 3-HP to tartronate semialdehyde may be catalyzed by FucD, and not by MR, since FucD tautomerizes the enol product during its normal reaction with L-fuconate (Yew, W. *et al*., 2006). Therefore, the presence of this ketonization function may account for formation of the 58-Da adduct in FucD and not in MR.

Notably, the dependence on Mg^{2+} was also observed for inactivation of MR by D,L-α-phenylglycidate (α-PGA) (Fee, Hegeman, & Kenyon, 1974a). In the case of inactivation of MR by α-PGA, the mechanism involved opening an oxirane ring to form an adduct to Lys 166. Therefore, it could be that beyond potentially aiding the decarboxylation of 3-HP, the Mg^{2+} ion may be simply required to make the active site amino acids sufficiently reactive to catalyze the inactivation chemistry with whatever 3-HP derived species may be in the FucD active site. It would be of interest to determine whether 58-Da adducts are observed in Apo-FucD incubated with 3-HP in Mg^{2+}-free assay buffer.

3.4.3 OLIGOMERIC STATE OF FucD

As mentioned (Section 3.4.3, Fig 3.23), 58-Da adducts were found predominantly on one face of the FucD dimer. This finding led to suspicion that, in solution, FucD may not exist as a dimer but rather as a higher oligomeric state. MR crystallizes as an octamer and there is convincing crosslinking evidence that it is either a tetramer or octamer in solution (Fee *et al*., 1974b; Neidhart *et al*., 1991). GF-HPLC results suggested that FucD was a dimer compared to MR as a tetramer (Fig 3.21); however, these experiments are under non-equilibrium conditions. Therefore, DLS experiments were conducted to determine the size of FucD and MR in solution. FucD was found to be smaller than MR (Fig 3.14) with a hydrodynamic diameter consistent with a dimer structure (Fig 3.22). MR was not able to be confirmed as either a tetramer or an octamer given the high similarity of the hydrodynamic diameter for these two species (Fig 3.24). Possibly, small angle X-ray scattering would be a better technique for such an analysis given that a shape could be determined that could be modeled to a relatively cubic octamer or a rectangular prism tetramer.

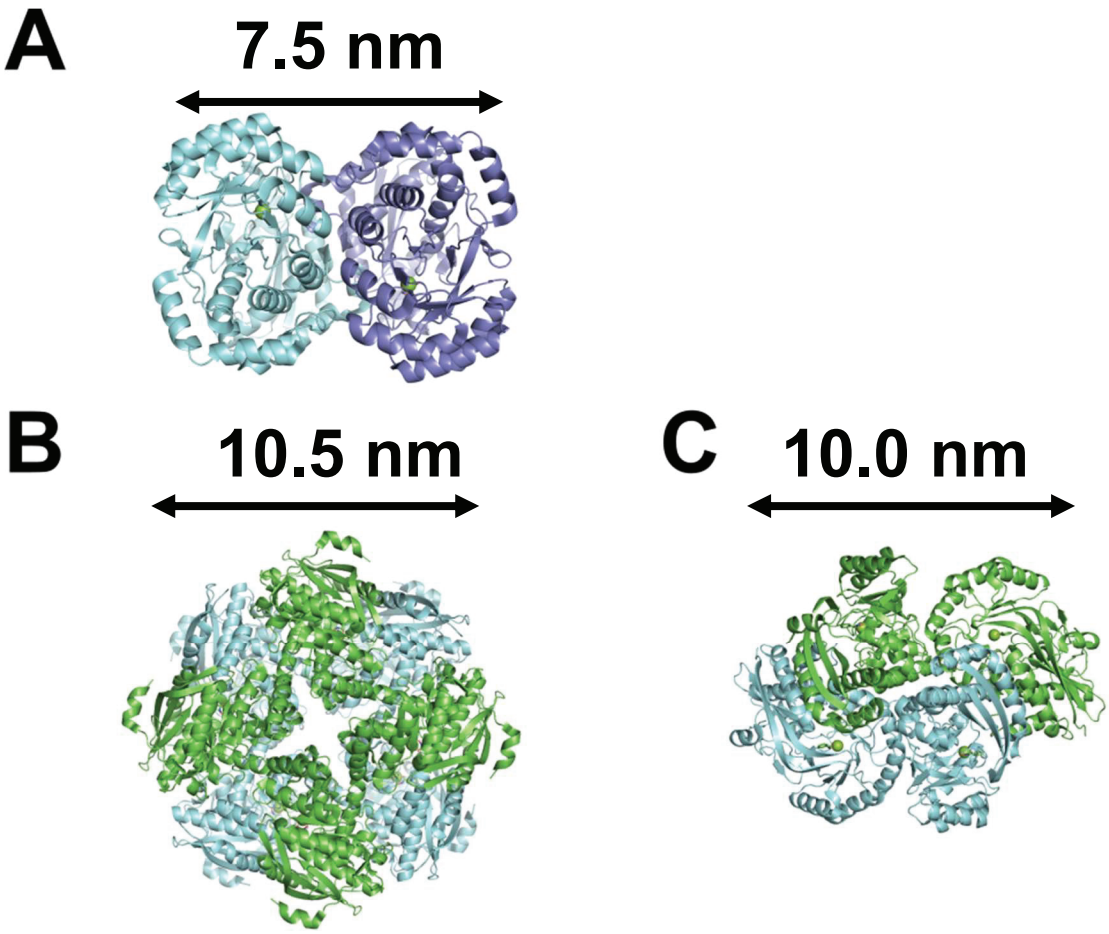

Figure 3.26 Oligomeric forms of FucD and MR. Distances were determined from the X-ray crystal structures of dimeric FucD (A)(pdb entry 2HXT), octameric MR (B) and, tetrameric MR (C) (pdb entry 3UXK).

The question that remains is, why are 58-Da adducts resulting from the treatment of FucD with 3-HP localized to one side of the dimer? Protection on one side of the oligomer by another dimer would be an intuitive solution to this problem. However, DLS and GF-HPLC experiments both show that FucD is a dimer in solution and do not support the presence of higher order species. Therefore, an alternative explanation must be presented. Interestingly, the 58-Da adducts are localized near the active site of FucD. Considering that 3-HP was found to be a competitive inhibitor of FucD it could be that GLH released from the active site is only able to react with residues close to the active site due to the competing reaction with water to form the hydrate (Collins & George, 1971). Alternatively; there are more His, Ser and Lys residues present on one face of the dimer and so the observed co-localization of adducts to one side could simply be explained by the higher concentration of residues able to form adducts.

3.4.4 THE ROLE OF TRP 101 IN FucD CATALYSIS

In FucD, as in other members of the MR subgroup of the ENS, a loop extends from the capping domain of one protomer into the active site of its neighboring protomer (Bearne, Stephen L., 2017). In crystal structures of FucD, this appears as a tight dimer where Trp 101 at the tip of the interdigitating loop interacts directly with the terminal methyl group of L-fuconate bound in the active site (Fig 3.25). Therefore, it was of interest to determine whether an enzyme variant where Trp 101 had been mutated to a positive residue (Lys or Arg) could interact with the distal carboxylate of *m*-galactarate and use *m*-galactarate as a substrate (the substrate of TGD). This interdigitating loop is a structural characteristic of the MR subgroup and previous work in the Bearne laboratory

has shown that mutating the analogous residue to Trp 101 in MR Leu 93 to a Lys allows the L93K MR variant to bind tartrate more tightly than the WT enzyme (unpublished).

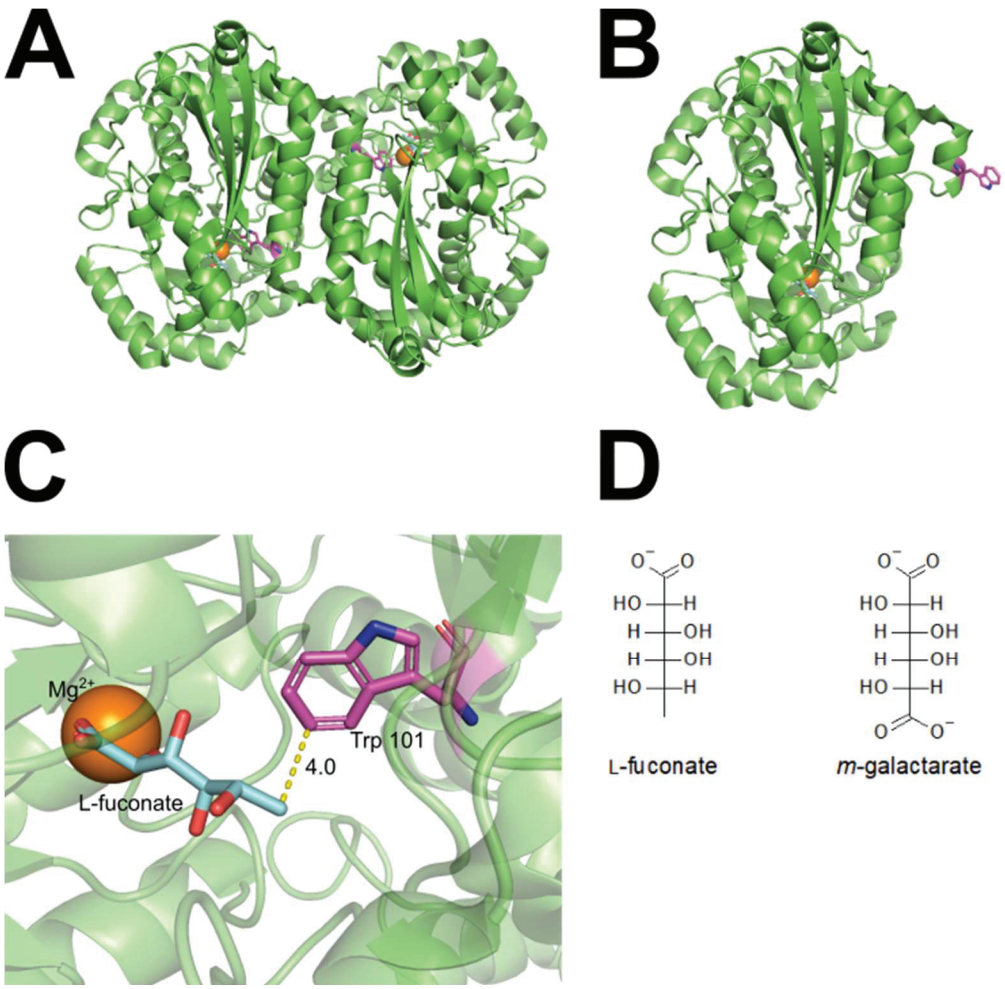

Figure 3.27 Trp 101 at the tip of the interdigitating loop of FucD. Dimeric FucD with Trp 101 in magenta and the Mg^{2+} ion in orange (A). One monomer of FucD and position of Trp 101 (magenta) in the interdigitating loop of FucD (B). Trp 101 is in position to interact with the methyl group of L-fuconate (cyan) (C). *m*-Galactarate is identical to L-fuconate save the terminal methyl is replaced by a carboxylate group (D) (pdb entry 2HXU).

Interestingly, despite an apparent significant similarity between the cases of W101K FucD and L93K MR, they presented significantly different catalytic activity. Namely, L93K MR is active with mandelate, while W101K and W101R FucD were both inactive with *m*-galactarate and L-fuconate. This led to the investigation of other Trp 101 substitutions. The W101Q and W101N variants were selected to mirror the neutral non-protic-polar and steric character of Trp 101. The W101E variant was also created to determine what effect a negative charge at this position might have. Notably, no Trp 101 FucD variants were able to catalyze dehydration of L-fuconate to a degree measurable by the CD-based assay.

An initial thought as to whether mutating the residue at the tip of the interdigitating loop might disrupt dimerization was investigated using GF-HPLC. However, all variants were found to be dimers in solution, discounting this hypothesis (Table 3.4). A more subtle explanation for the loss of dehydration activity in these variants might lie in the precise orientation of L-fuconate in the active site. A study of alternative substrates of FucD by Gerlt and colleagues showed that D-altronate was a weak dehydration substrate of FucD but displayed substantially higher rates of hydrogen-deuterium exchange (Fig 1.11 and 3.24) (Yew, W. *et al*., 2006). This indicates that deprotonation of the α-proton was much more efficient than β-elimination. D-Altronate is an epimer of L-galactonate at carbon 5, which is a much better dehydration substrate of FucD. This suggests that the substituent positions at carbon five are important for facilitating dehydration but are less important for initial abstraction of the α-proton. Binding the 5-OH of L-fuconate by Gly 22 and Tyr 32 appears to be important for dehydration of a substrate. Trp 101 is near both Gly 22 and Tyr 32 and therefore mutation

of Trp 101 might lead to disruption of the local structure such that binding of the 5-OH group is impaired (Fig 3.26), which may then obviate dehydration activity in the Trp 101 variants analogous to the case of D-altronate. To test this hypothesis, deuterium exchange studies would need to be conducted to ascertain whether efficient abstraction of the α-proton can still take place in the Trp 101 variants.

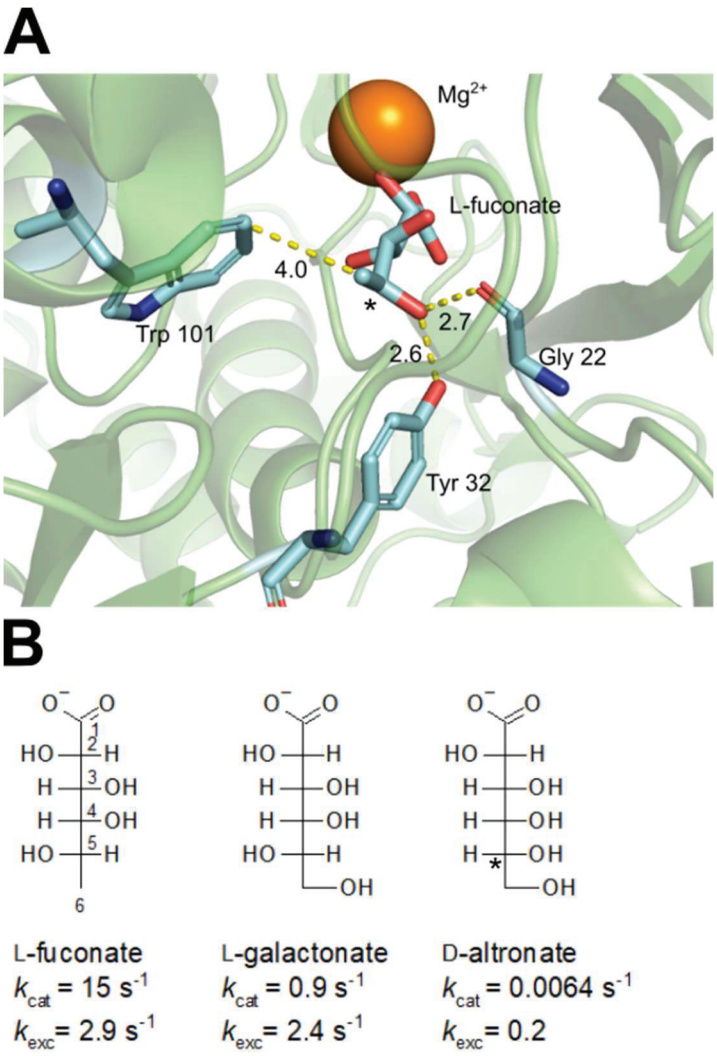

Figure 3.28 Gly 22 and Tyr 32 interacting with the 5-OH group of L-fuconate in FucD. Trp 101 is shown near the same area of L-fuconate binding in the active site, distances are in Å. The stereocenter altered in D-atronate is indicated by an asterisk (A) (pdb entry 2HXU). Structures of L-fuconate, L-galactonate, and D-altronate with FucD kinetic parameters (Yew, W. *et al*., 2006). The altered stereocenter in D-altronate is indicated with an asterisk (B).

3.5 CONCLUSIONS

A thorough study of FucD was undertaken investigating its affinity and reactivity to two catalytic residue targeting inhibitors, tartronate and 3-HP. Tartronate was found to be a modest linear mixed-type inhibitor of FucD. 3-HP was found to be an irreversible inhibitor of FucD with evidence to suggest it acts by a different mechanism than was found with MR. Trp 101 at the tip of the interdigitating loop was found to be essential for dehydration of L-fuconate and mutation to a Lys or Arg did not confer activity with *m*-galactarate. This loss of activity was not due to mutation of the loop adversely affecting the oligomeric state of FucD variants since FucD was found to be a dimer by both GF-HPLC and DLS experiments.

CHAPTER 4 CONCLUSION
4.1 CONCLUSION

Enzymes in the MR subgroup of the ENS possess conserved active site residues that catalyze the deprotonation of an α-carbon adjacent to a carboxylate group (Babbitt *et al*., 1996). In this thesis work I investigated the role of Tyr 137 in MR catalysis, FucD interactions with the inhibitors tartronate and 3-HP which target the catalytic machinery of the enzyme, and the role of Trp 101 in FucD catalysis.

The pK_a of Lys 166 was found to be 6.4 in the ground state by Gerlt and colleagues (Landro *et al*., 1991) which is ~4 pH units below the average pK_a of Lys residues in folded proteins (Grimsley *et al*., 2009). I investigated whether the Tyr 137-Lys 164-Lys 166 triad could be acting to reduce the pK_a of Lys 166. In this triad, Tyr 137 may hold Lys 164 in position to interact with Lys 166, promoting its deprotonation by electrostatic repulsion. Analysis of pH profiles for both the Y137F and WT MR variants showed that the pK_a of Lys 166 was increased in the Y137F variant (section 2.3.3). This is consistent with the model where the Tyr 137-Lys 164-Lys 166 triad helps to reduce the pK_a of Lys 166 by positioning a positively charged Lys 164 close to Lys 166 in order to promote its deprotonation. Unexpectedly, the pK_a of His 297 was also increased by a similar amount in the Y137F variant compared to WT MR. This was surprising and indicates that there are longer range effects involved in removing the hydroxyl of Tyr 137, potentially impacting the electrostatic character of the active site. Using the Y137L MR variant, it was also found that a cation-π interaction between Tyr 137 and Lys 164 is not crucial for catalysis. Lastly, a LFER was observed between enzymatic efficiency

(k_{cat}/K_m) of the Tyr 137 MR variants and their affinity for the transition state analogue inhibitor BzH ($1/K_i$), indicating Tyr 137 plays an indirect role in TS stabilization.

FucD was investigated as a member of the MR subgroup of the ENS which maintains the conserved positions of the catalytic machinery involved in abstracting the α-proton of its substrate but catalyzes β-elimination of an acid sugar and ketonization of the resulting enol product (Yew, W. *et al*., 2006). The catalytic residue targeting inhibitors of MR, tartronate and 3-HP, were investigated as inhibitors of FucD because of the conserved binding determinants shared with MR. Tartronate was found to be a linear mixed-type inhibitor of FucD, binding with a lower affinity than was found for MR. However, considering tartronate bears little structural resemblance to any known substrate, product, or transition state analogue inhibitor of FucD, it is impressive that it is recognized at all.

FucD was irreversibly inactivated by 3-HP, similar to MR (Nagar, Mitesh *et al*., 2015) but contrasting to other MR subgroup enzymes tested so far (TGD and TarD) (Easton, Aboushawareb & Bearne, unpublished). Inactivation was significantly less efficient than was observed for MR (~4400-fold) and 58- and 86-Da adducts were found on Lys 220 of FucD instead of only the 86-Da adduct found on Lys 166 of MR. Furthermore, 58-Da adducts were found on polar surface residues of FucD as well as the catalytic Brønsted acid-base residue Lys 220, which is analogous to Lys 166 of MR. These findings suggest a different mechanism of 3-HP-mediated inactivation in FucD than was observed for MR. A potential mechanism was proposed which involved either FucD-catalyzes glycolaldehyde (GLH) formation from 3-HP or non-enzymatic decarboxylation of 3-HP for formation of GLH catalyzed by Mg^{2+}. This mechanism was

tested by incubating WT FucD with GLH, K220M and H351N FucD with 3-HP followed by MS/MS analysis and determining whether Mg^{2+} is required for 3-HP-dependent FucD inactivation. These experiments revealed that GLH can form 58-Da adducts with FucD and that Lys 220 and His 351 are not essential for the formation of the 58-Da adducts on polar surface residues. It was further determined that Mg^{2+} was required for 3-HP-mediated inactivation of FucD. This indicates that Mg^{2+} is essential for inactivation either by promoting the non-enzymatic decarboxylation of 3-HP, or by contributing to the capability of FucD to catalyze the inactivation chemistry.

An interesting finding was that the 86-Da adduct did not form on Lys 220 when H351N FucD was treated with 3-HP as was found with WT FucD. Given that the corresponding residue His 297 is required for formation of 86-Da adducts on Lys 166 of MR (Nagar *et al*., 2015), this result indicates that formation of 86-Da adducts on Lys 220 of FucD may follow an analogous pathway.

Another observation was that 58-Da adducts appeared only on surface residues on one face of the FucD dimer. This led to investigation of the oligomeric state of FucD by GF-HPLC and DLS given a tetrameric state would account for protection of this surface in solution such that no adducts would be observed. Supporting this hypothesis was that other enzymes of the MR subgroup display higher oligomeric states where crystal structure tetramer or octamer structures, if replicated with FucD, would afford the required protection of the unmodified surface area (Fee et al., 1974b; Neidhart et al., 1991). However, FucD was found to be a dimer with no evidence for higher order species and so an alternate hypothesis for why 58-Da co-localize to one face of the dimer was required. It was interesting to note that all 58-Da adducts were near the active site of

FucD. This observation, along with experiments that found 3-HP to exhibit competitive inhibition of FucD, lead to the hypothesis that 58-Da adducts are formed on surface residues by the intermediate GLH released from the active site of FucD. The competing hydration reaction would relegate reaction of surface residues to those nearby the active site given that released GLH would be hydrated rapidly and thus made unreactive. A simpler hypothesis is that there are more His, Ser and Lys residues on one face of the dimer compared to the other, which indicates that the co-localizing of adducts to one side may be more indicative of which residues can be modified than any protection of the opposite face of FucD.

Lastly, the role of Trp 101 in FucD catalysis was investigated. Trp 101 is the residue at the tip of the interdigitating loop of FucD and interacts directly with the terminal methyl group of L-fuconate. Initially, W101K and W101R FucD variants were assayed for their ability to dehydrate *m*-galactarate which is identical to L-fuconate save the terminal methyl group is replaced by a carboxylate. Both W101K and W101R variants were unable to catalyze the dehydration of *m*-galactarate or L-fuconate. Therefore, the W101E and W101Q FucD variants were assayed to probe whether a negatively or polar-neutral amino acid could be tolerated at this position. However, both W101E and W101Q FucD variants were found to be similarly inactive. Given that Trp 101 is located at the tip of the interdigitating loop and its mutation could potentially disrupt the oligomeric state of the enzyme, the oligomeric state of FucD was investigated by GF-HPLC. All Trp 101 variants were found to be dimers, the same as WT FucD. Therefore, an alternative hypothesis was proposed that the Trp 101 variants are unable to dehydrate L-fuconate due to disruption of the hydrogen bonding network that binds the

distal end of L-fuconate. The basis for this hypothesis stems from the finding by Gerlt and colleagues that L-galactonate and D-altronate (epimers at C-5) display vastly different rate of dehydration but similar rates of deuterium exchange at the α-carbon (Yew, W. *et al*., 2006). This hypothesis could be tested by using hydrogen-deuterium exchange experiments with the Trp 101 variants.

In summary, I investigated various functional aspects of the active sites of MR and FucD by using pH, inhibition, and mutational studies. I found that Tyr 137 acts to reduce the pK_a of the catalytic Brønsted acid-base residues Lys 166 and His 297 in MR, supporting a catalytic role for the Tyr 137-Lys 164-Lys 166 triad. A LFER was also found between the enzyme efficiency (k_{cat}/K_m) and BzH affinity ($1/K_i$) of Tyr 137 MR variants (slope = 1.31 ± 0.13, r = 0.985) which indicates an indirect role for Tyr 137 in TS stabilization. I also found that although the active site of FucD may appear similar to MR in X-ray crystal structures, it binds tartronate more weakly and interacts differently with 3-HP. The oligomeric state of FucD was also determined to be a dimer by GF-HPLC and DLS. Lastly, Trp 101 was found to be critical for FucD catalysis but not essential for dimerization.

4.2 FUTURE WORK

As stated, many enzymes in the MR subgroup of the ENS encode an analogous residue to Tyr 137 (section 2.1) although it is not entirely conserved. It would be interesting to determine if a Tyr-Lys-Lys triad works similarly in other MR subgroup enzymes to decrease the pK_a of the catalytic Lys residue. Also, determination of whether there is any difference in the pK_a of the Lys and His residues of the subgroup members that do not have an analogous Tyr-Lys-Lys triad may furnish more insights into the catalytic role of this residue.

There is more work to do to finish the story of FucD inactivation by 3-HP. It would be interesting to determine if His 351 plays the same role in 3-HP-dependent formation of the 86-Da adduct to Lys 220 of FucD as His 297 does in MR (Scheme 1.5). Therefore, a LC-MS/MS experiment could be conducted where H351N FucD is incubated with 3-HP and then reduced with sodium cyanoborohydride to determine if an 88 Da adduct is observed as was found for H297N MR (Nagar *et. al*, 2015). Also, while all samples analyzed by LC-MS/MS for MR were completed in HEPES assay buffer, FucD samples were prepared in Tris buffer. Given different adducts were found in MR and FucD a MS/MS experiment of FucD in HEPES assay buffer would be a good control experiment to ensure the adduct differences are solely due to the different enzyme. In addition, whether 3-HP-dependent inactivation relies on access to the active site should be determined by use of a competitive inhibitor such as D-erythronohydroxamate (Yew, W. *et al*., 2006). The chemical mechanism of inactivation must also be more thoroughly investigated. These experiments could take the form of using ^{13}C- or ^{14}C- labelled 3-HP to show which carbons are attaching to FucD during inactivation. The role of the Mg^{2+}

ion should also be investigated in potentially catalyzing the decarboxylation reaction. These experiments could begin with determining the metal binding affinity of FucD but also determining if metal ions that MR can accommodate (Mn^{2+}, Ni^{2+} etc.) (Fee *et al*., 1974b) could also be used for FucD catalysis given literature indicates they catalyze the rate of 3-HP decarboxylation at different rates than Mg^{2+} in solution (Hedrick & Sallach, 1961) and may be able to furnish insights into the role of the metal ion in 3-HP-mediated inactivation of FucD.

Lastly, whether a replacement residue for Trp 101 can be found that is able to maintain dehydration activity should be determined. Also, whether the Trp 101 variants can catalyze hydrogen-deuterium exchange should be investigated as part of the story of what makes some MR-subgroup enzymes racemases/epimerases and others dehydratases.

REFERENCES

Acharya, A. S., & Manning, J. M. (1983). Reaction of glycolaldehyde with proteins: Latent crosslinking potential of α-hydroxyaldehydes. *Proceedings of the National Academy of Sciences, 80*(12), 3590-3594. doi:10.1073/pnas.80.12.3590

Akiva, E., Brown, S., Almonacid, D. E., Barber, A. E., Custer, A. F., Hicks, M. A., . . . Babbitt, P. C. (2014). The structure-function linkage database. *Nucleic Acids Research, 42*(D1), D521-D530. doi:10.1093/nar/gkt1130

Babbitt, P. C., Hasson, M. S., Wedekind, J. E., Palmer, D. R., Barrett, W. C., Reed, G. H., . . . Gerlt, J. A. (1996). The enolase superfamily: A general strategy for enzyme-catalyzed abstraction of the alpha-protons of carboxylic acids. *Biochemistry, 35*(51), 16489-16501. doi:10.1021/bi9616413

Bearne, S. L., & Wolfenden, R. (1997). Mandelate racemase in pieces: Effective concentrations of enzyme functional groups in the transition state. *Biochemistry, 36*(7), 1646-1656. doi:10.1021/bi9620722

Bearne, S. L., & St. Maurice, M. S. (2017). A paradigm for C–H bond cleavage: Structural and functional aspects of transition state stabilization by mandelate racemase. In *Advances in protein chemistry and structural biology* (Vol. 109, pp. 113-160) Academic Press. doi:10.1016/bs.apcsb.2017.04.007

Bearne, S. L. (2017). The interdigitating loop of the enolase superfamily as a specificity binding determinant or 'flying buttress'. *Biochimica Biophysica Acta - Proteins and Proteomics, 1865*(5), 619-630. doi:10.1016/j.bbapap.2017.02.006

Bernasconi, C. F. (1992). The principle of non-perfect synchronization. In *Advances in physical organic chemistry,* (Vol. 27, pp. 119-238). Academic Press doi.org/10.1016/S0065-3160(08)60065-9

Bourque, J. R., Burley, R. K. M., & Bearne, S. L. (2007). Intermediate analogue inhibitors of mandelate racemase: *N*-hydroxyformanilide and cupferron. *Bioorganic & Medicinal Chemistry Letters, 17*(1), 105-108. doi:10.1016/j.bmcl.2006.09.079

Burley, R. K. M., & Bearne, S. L. (2005). Inhibition of mandelate racemase by the substrate–intermediate–product analogue 1,1-diphenyl-1-hydroxymethylphosphonate. *Bioorganic & Medicinal Chemistry Letters, 15*(19), 4342-4344. doi:10.1016/j.bmcl.2005.06.060

Buschiazzo, A., Goytia, M., Schaeffer, F., Degrave, W., Shepard, W., Grégoire, C., . . . Minoprio, P. (2006). Crystal structure, catalytic mechanism, and mitogenic properties of *Trypanosoma cruzi* proline racemase. *Proceedings of the National Academy of Sciences, 103*(6), 1705-1710. doi:www.pnas.org/cgi/doi/10.1073/pnas.0509010103

Chiang, Y., Kresge, A. J., Pruszynski, P., Schepp, N. P., & Wirz, J. (1990). The enol of mandelic acid, detection, acidity in aqueous solution, and estimation of the keto-enol equilibrium constant and carbon acidity of mandelic acid. *Angewandte Chemie International Edition in English, 29*(7), 792-794. doi:10.1002/anie.199007921

Collins, G. C. S., & George, W. O. (1971). Nuclear magnetic resonance spectra of glycolaldehyde. *Journal of the Chemical Society B: Physical Organic,* 1352-1355. doi:10.1039/J29710001352

Cornish-Bowden, A. (1976). Estimation of the dissociation constants of enzyme-substrate complexes from steady-state measurements. Interpretation of pH-independence of K_m. *The Biochemical Journal, 153*(2), 455-461. doi:10.1042/bj1530455

Easton, N. M., Aboushawareb, S. A. E., & Bearne, S. L. (2018). A continuous assay for L-talarate/galactarate dehydratase using circular dichroism. *Analytical Biochemistry, 544*, 80-86. doi:10.1016/j.ab.2017.12.015

Eigen, M. (1964). Proton transfer, acid-base catalysis, and enzymatic hydrolysis. Part I: Elementary processes. *Angewandte Chemie International Edition in English, 3*(1), 1-19.

Fee, J. A., Hegeman, G. D., & Kenyon, G. L. (1974a). Mandelate racemase from *Pseudomonas putida*. Affinity labeling of the enzyme by D,L-α-phenylglycidate in the presence of magnesium ion. *Biochemistry, 13*(12), 2533-2538. doi:10.1021/bi00709a009

Fee, J. A., Hegeman, G. D., & Kenyon, G. L. (1974b). Mandelate racemase from *Pseudomonas putida*. Subunit composition and absolute divalent metal ion requirement. *Biochemistry, 13*(12), 2528-2532. doi:10.1021/bi00709a008

Felfer, U., Strauss, U. T., Kroutil, W., Fabian, W. M. F., & Faber, K. (2001). Substrate spectrum of mandelate racemase: Part 2. (hetero)-aryl-substituted mandelate derivatives and modulation of activity. *Journal of Molecular Catalysis.B, Enzymatic, 15*(4-6), 213-222. doi:10.1016/S1381-1177(01)00035-2

Fersht, A. (1985). Chapter 2: Chemical Catalysis. In *Enzyme structure and mechanism* (pp. 33) W. H. Freeman and Company.

Fetter, C. M., Morrison, Z. A., Nagar, M., Douglas, C. D., & Bearne, S. L. (2019). Altering the Y137-K164-K166 triad of mandelate racemase and its effect on the observed pK_a of the Brønsted base catalysts. *Archives of Biochemistry and Biophysics, 666*, 116-126. doi:10.1016/j.abb.2019.03.011

Gasteiger, E., Gattiker, A., Hoogland, C., Ivanyi, I., Appel, R. D., & Bairoch, A. (2003). ExPASy: The proteomics server for in-depth protein knowledge and analysis. *Nucleic Acids Research, 31*(13), 3784-3788. doi:10.1093/nar/gkg563

Gerlt, J. A., & Gassman, P. G. (1993). An explanation for rapid enzyme-catalyzed proton abstraction from carbon acids: Importance of late transition states in concerted mechanisms. *Journal of the American Chemical Society, 115*(24), 11552-11568.

Gerlt, J. A., & Gassman, P. G. (1993). Understanding the rates of certain enzyme-catalyzed reactions: Proton abstraction from carbon acids, acyl-transfer reactions, and displacement reactions of phosphodiesters. *Biochemistry, 32*(45), 11943-11952. doi:10.1021/bi00096a001

Gerlt, J. A., & Gassman, P. G. (1992). Understanding enzyme-catalyzed proton abstraction from carbon acids: Details of stepwise mechanisms for β-elimination reactions. *Journal of the American Chemical Society, 114*(15), 5928-5934.

Gerlt, J. A., Babbitt, P. C., Jacobson, M. P., & Almo, S. C. (2012). Divergent evolution in enolase superfamily: Strategies for assigning functions. *The Journal of Biological Chemistry, 287*(1), 29-34. doi:10.1074/jbc.R111.240945

Gerlt, J. A., Kreevoy, M. M., Cleland, W. W., & Frey, P. A. (1997). Understanding enzymic catalysis: The importance of short, strong hydrogen bonds. *Chemistry & Biology, 4*(4), 259-267. doi:10.1016/S1074-5521(97)90069-7

Glomb, M. A., & Monnier, V. M. (1995). Mechanism of protein modification by glyoxal and glycolaldehyde, reactive intermediates of the Maillard reaction. *The Journal of Biological Chemistry, 270*(17), 10017-10026. doi:10.1074/jbc.270.17.10017

Gottlieb, H. E., Kotlyar, V., & Nudelman, A. (1997). NMR chemical shifts of common laboratory solvents as trace impurities. *The Journal of Organic Chemistry, 62*(21), 7512-7515. doi:10.1021/jo971176v

Grimsley, G. R., Scholtz, J. M., & Pace, C. N. (2009). A summary of the measured p*K* values of the ionizable groups in folded proteins. *Protein Science, 18*(1), 247-251. doi:10.1002/pro.19

Gunsalus, C. F., Stanier, R. Y., & Gunsalus, I. C. (1953). The enzymatic conversion of mandelic acid to benzoic acid III. Fractionation and properties of the soluble enzymes. *The Journal of Bacteriology, 66*(5), 548-553.

Guthrie, J. P. (1998). Predicting the rates of proton transfer reactions: A simple model using equilibrium constants and distortion energies. *Journal of Physical Organic Chemistry, 11*(8-9), 632-641.

Guthrie, J. P., & Kluger, R. (1993). Electrostatic stabilization can explain the unexpected acidity of carbon acids in enzyme-catalyzed reactions. *Journal of the American Chemical Society, 115*(24), 11569-11572.

Hedrick, J. L., & Sallach, H. L. (1961). The metabolism of hydroxypyruvate I. The nonenzymatic decarboxylation and autoxidation of hydroxypyruvate. *The Journal of Biological Chemistry, 236*(7), 1867-1871.

Hegeman, G. D., Rosenberg, E. Y., & Kenyon, G. L. (1970). Mandelic acid racemase from pseudomonas putida. Purification and properties of the enzyme. *Biochemistry, 9*(21), 4029-4036. doi:10.1021/bi00823a001

Ho, M., Menetret, J., Tsuruta, H., & Allen, K. (2009). The origin of the electrostatic perturbation in acetoacetate decarboxylase. *Nature, 459*(7245), 393-397. doi:10.1038/nature07938

Hornback, J. M. (2006). Chapter 4: The acid-base reaction. In S. Kiselica, S. Lowe & S. Harkrader (Eds.), *Organic chemistry* (2nd ed., pp. 103) Thomson Brooks/Cole.

Jencks, W., & Regenstein, J. (1968). Ionization constants of acids and bases. In H. Sober (Ed.), *Handbook of Biochemistry* (pp. J150-J189) CRC Press.

Kallarakal, A., Mitra, B., Kozarich, J., Gerlt, J., Clifton, J., Petsko, G., & Kenyon, G. (1995). Mechanism of the reaction catalyzed by mandelate racemase: Structure and mechanistic properties of the K166R mutant. *Biochemistry, 34*(9), 2788-2797.

Kenyon, G., Gerlt, J., Petsko, G., & Kozarich, J. W. (1995). Mandelate racemase - structure-function studies of a pseudosymmetric enzyme. *Accounts of Chemical Research, 28*(4), 178-186. doi:10.1021/ar00052a003

Knowles, J. R., & Jencks, W. P. (1976). The intrinsic pK_a-values of functional groups in enzymes: Improper deductions from the pH-dependence of steady-state parameter. *CRC Critical Reviews in Biochemistry, 4*(2), 165-173. doi:10.3109/10409237609105457

Kokesh, F. C., & Westheimer, F. H. (1971). A reporter group at the active site of acetoacetate decarboxylase. II. Ionization constant of the amino group. *Journal of the American Chemical Society, 93*(26), 7270-7274. doi:10.1021/ja00755a025

Landro, J. A., Kenyon, G. L., & Kozarich, J. W. (1992). Mechanism-based inactivation of mandelate racemase by propargylglycolate. *Bioorganic & Medicinal Chemistry Letters, 2*(11), 1411-1418.

Landro, J. A., Gerlt, J. A., Kozarich, J. W., Koo, C. W., Shah, V. J., Kenyon, G. L., . . . Petsko, G. A. (1994). The role of lysine 166 in the mechanism of mandelate racemase from pseudomonas putida: Mechanistic and crystallographic evidence for stereospecific alkylation by (*R*)-α-phenylglycidate. *Biochemistry, 33*(3), 635-643. doi:10.1021/bi00169a003

Landro, J. A., Kallarakal, A. T., Ransom, S. C., Gerlt, J. A., & Kozarich, J. W. (1991). Mechanism of the reaction catalyzed by mandelate racemase. 3. Asymmetry in reactions catalyzed by the H297N mutant. *Biochemistry, 30*(38), 9274-9281. doi:10.1021/bi00102a020

Li, R., Powers, V. M., Kozarich, J. W., & Kenyon, G. L. (1995). Racemization of vinylglycolate catalyzed by mandelate racemase. *The Journal of Organic Chemistry, 60*(11), 3347-3351.

Lietzan, A. D., Nagar, M., Pellmann, E. A., Bourque, J. R., Bearne, S. L., & Maurice, M. S. (2012). Structure of mandelate racemase with bound intermediate analogues benzohydroxamate and cupferron. *Biochemistry, 51*(6), 1160-1170. doi:10.1021/bi2018514

Maurice, M. S., Bearne, S. L., Lu, W., & Taylor, S. D. (2003). Inhibition of mandelate racemase by α-fluorobenzylphosphonates. *Bioorganic & Medicinal Chemistry Letters, 13*(12), 2041-2044. doi:10.1016/S0960-894X(03)00311-1

Mitra, B., Kallarakal, A. T., Kozarich, J. W., Gerlt, J. A., Clifton, J. G., Petsko, G. A., & Kenyon, G. L. (1995). Mechanism of the reaction catalyzed by mandelate racemase: Importance of electrophilic catalysis by glutamic acid 317. *Biochemistry, 34*(9), 2777-2787. doi:10.1021/bi00009a006

Mozzarelli, A., & Bettati, S. (2006). Exploring the pyridoxal 5′-phosphate-dependent enzymes. *Chemical Record, 6*(5), 275-287. doi:10.1002/tcr.20094

Nagar, M., Narmandakh, A., Khalak, Y., & Bearne, S. (2011). Redefining the minimal substrate tolerance of mandelate racemase. Racemization of trifluorolactate. *Biochemistry, 50*(41), 8846-8852. doi:10.1021/bi201188j

Nagar, M., & Bearne, S. L. (2015). An additional role for the Brønsted acid-base catalysts of mandelate racemase in transition state stabilization. *Biochemistry, 54*(44), 6743-6752. doi:10.1021/acs.biochem.5b00982

Nagar, M., Kumar, H., & Bearne, S. L. (2018). A platform for chemical modification of mandelate racemase: Characterization of the C92S/C264S and γ-thialysine 166 variants. *Protein Engineering, Design and Selection, 31*(4), 135-145. doi:10.1093/protein/gzy011

Nagar, M., Lietzan, A. D., St. Maurice, M., & Bearne, S. L. (2014). Potent inhibition of mandelate racemase by a fluorinated substrate-product analogue with a novel binding mode. *Biochemistry, 53*(7). 1169-1178. doi:10.1021/bi401703h

Nagar, M., Wyatt, B. N., St. Maurice, M., & Bearne, S. L. (2015). Inactivation of mandelate racemase by 3-hydroxypyruvate reveals a potential mechanistic link between enzyme superfamilies. *Biochemistry, 54*(17), 2747-2757. doi:10.1021/acs.biochem.5b00221

Narmandakh, A., & Bearne, S. L. (2010). Purification of recombinant mandelate racemase: Improved catalytic activity. *Protein Expression and Purification, 69*(1), 39-46. doi:10.1016/j.pep.2009.06.022

Neidhart, D. J., Howell, P. L., Petsko, G. A., Powers, V. M., Li, R. S., Kenyon, G. L., & Gerlt, J. A. (1991). Mechanism of the reaction catalyzed by mandelate racemase. 2. Crystal structure of mandelate racemase at 2.5-Å resolution: Identification of the active site and possible catalytic residues. *Biochemistry, 30*(38), 9264-9273. doi:10.1021/bi00102a019

Powers, V. M., Koo, C. W., & Kenyon, G. L. (1991). Mechanism of the reaction catalyzed by mandelate racemase. 1. Chemical and kinetic evidence for a two-base mechanism. *Biochemistry, 30*(38), 9255-9263. doi:10.1021/bi00102a018

Schafer, S. L., Barrett, W. C., Kallarakal, A. T., Mitra, B., Kozarich, J. W., Gerlt, J. A., . . . Kenyon, G. L. (1996). Mechanism of the reaction catalyzed by mandelate racemase: Structure and mechanistic properties of the D270N mutant. *Biochemistry, 35*(18), 5662-5669. doi:10.1021/bi960174m

Segel, I. H. (1975). *Enzyme kinetics*. New York: John Wiley & Sons, Inc.

Sharp, T. R., Hegeman, G. D., & Kenyon, G. L. (1979). A direct kinetic assay for mandelate racemase using circular dichroic measurements. *Analytical Biochemistry., 94*(2), 329-334. doi:https://doi.org/10.1016/0003-2697(79)90368-3

St Maurice, M., & Bearne, S. L. (2000). Reaction intermediate analogues for mandelate racemase: Interaction between Asn 197 and the α-hydroxyl of the substrate promotes catalysis. *Biochemistry, 39*(44), 13324-13335. doi:10.1021/bi001144t

St Maurice, M., & Bearne, S. L. (2002). Kinetics and thermodynamics of mandelate racemase catalysis. *Biochemistry, 41*(12), 4048-4058. doi:10.1021/bi016044h

Thorpe, S. R., & Baynes, J. W. (2003). Maillard reaction products in tissue proteins: New products and new perspectives. *Amino Acids, 25*(3), 275-281. doi:10.1007/s00726-003-0017-9

Toney, M. D. (2019). Carbon acidity in enzyme active sites. *Frontiers in Bioengineering and Biotechnology, 7*, 25-25. doi:10.3389/fbioe.2019.00025

Tsou, A. Y., Ransom, S. C., Gerlt, J. A., Powers, V. M., & Kenyon, G. L. (1989). Selection and characterization of a mutant of the cloned gene for mandelate racemase that confers resistance to an affinity label by greatly enhanced production of enzyme. *Biochemistry, 28*(3), 969-975. doi:10.1021/bi00429a008

Van Boekel, M. A. J. S. (2006). Formation of flavour compounds in the Maillard reaction. *Biotechnology Advances, 24*(2), 230-233. doi:10.1016/j.biotechadv.2005.11.004

Wierenga, R. K. (2001). The TIM-barrel fold: A versatile framework for efficient enzymes. *FEBS Letters, 492*(3), 193-198. doi:10.1016/S0014-5793(01)02236-0

Wolfenden, R. (1972). Analog approaches to the structure of the transition state in enzyme reactions. *Accounts of Chemical Research, 5*(1), 10-18. doi:10.1021/ar50049a002

Yew, W., Fedorov, A., Fedorov, E., Rakus, J., Pierce, R., Almo, S., & Gerlt, J. (2006). Evolution of enzymatic activities in the enolase superfamily: L-Fuconate dehydratase from *Xanthomonas campestris*. *Biochemistry, 45*(49), 14582-14597. doi:10.1021/bi061687o

Yew, W., Fedorov, A., Fedorov, E., Wood, B., Almo, S., & Gerlt, J. (2006). Evolution of enzymatic activities in the enolase superfamily: D-Tartrate dehydratase from *Bradyrhizobium japonicum*. *Biochemistry, 45*(49), 14598-14608. doi:10.1021/bi061688g

Yew, W., Fedorov, A. A., Fedorov, E., Almo, S. C., & Gerlt, J. (2007). Evolution of enzymatic activities in the enolase superfamily: L-Talarate/galactarate dehydratase from *Salmonella typhimurium. Biochemistry, 46*(33), 9564-9577. doi:10.1021/bi7008882

Yoshimura, T., & Esaki, N. (2003). Amino acid racemases: Functions and mechanisms. *Journal of Bioscience and Bioengineering, 96*(2), 103-109.

Yung-Chi, C., & Prusoff, W. H. (1973). Relationship between the inhibition constant (KI) and the concentration of inhibitor which causes 50 per cent inhibition (I50) of an enzymatic reaction. *Biochemical Pharmacology., 22*(23), 3099-3108. doi:https://doi.org/10.1016/0006-2952(73)90196-2

Zhai, X., Reinhardt, C. J., Malabanan, M. M., Amyes, T. L., & Richard, J. P. (2018). Enzyme architecture: Amino acid side-chains that function to optimize the basicity of the active site glutamate of triosephosphate isomerase. *Journal of the American Chemical Society, 140*(26), 8277-8286. doi:10.1021/jacs.8b04367

Zheng, J., Kwak, K., Xie, J., & Fayer, M. D. (2006). Ultrafast carbon-carbon single-bond rotational isomerization in room-temperature solution. *Science (New York, N.Y.), 313*(5795), 1951-1955. doi:10.1126/science.1132178

APPENDIX

COPYRIGHT PERMISSION

Title: Altering the Y137-K164-K166 triad of mandelate racemase and its effect on the observed pK a of the Brønsted base catalysts

Author: Christopher M. Fetter,Zachary A. Morrison,Mitesh Nagar,Colin D. Douglas,Stephen L. Bearne

Publication: Archives of Biochemistry and Biophysics

Publisher: Elsevier

Date: 15 May 2019

Please note that, as the author of this Elsevier article, you retain the right to include it in a thesis or dissertation, provided it is not published commercially. Permission is not required, but please ensure that you reference the journal as the original source. For more information on this and on your other retained rights, please visit: https://www.elsevier.com/about/our-business/policies/copyright#Author-rights

Dear Chris Fetter,

We hereby grant you permission to reprint the material below at no charge **in your thesis** subject to the following conditions:

1. If any part of the material to be used (for example, figures) has appeared in our publication with credit or acknowledgement to another source, permission must also be sought from that source. If such permission is not obtained then that material may not be included in your publication/copies.

2. Suitable acknowledgment to the source must be made, either as a footnote or in a reference list at the end of your publication, as follows:
"This article was published in Publication title, Vol number, Author(s), Title of article, Page Nos, Copyright Elsevier (or appropriate Society name) (Year)."

3. Your thesis may be submitted to your institution in either print or electronic form.

4. Reproduction of this material is confined to the purpose for which permission is hereby given

5. This permission is granted for non-exclusive world **English** rights only. For other languages please reapply separately for each one required. Permission excludes use in an electronic form other than submission. Should you have a

specific electronic project in mind please reapply for permission.

6. Should your thesis be published commercially, please reapply for permission.

This includes permission for the Library and Archives of Canada to supply single copies, on demand, of the complete thesis. Should your thesis be published commercially, please reapply for permission- Canada
This includes permission for UMI to supply single copies, on demand, of the complete thesis. Should your thesis be published commercially, please reapply for permission-ROW

7. Posting of the full article online is not permitted. You may post an abstract with a link to the Elsevier website www.elsevier.com , or to the article on ScienceDirect if it is available on that platform.

8. Article can used be in the University library if it is embedded in the thesis and not used commercially.

Permissions Helpdesk
ELSEVIER |Operations
permissionshelpdesk@elsevier.com